GEOPHYSICAL INVESTIGATION OF THE TECTONIC AND VOLCANIC HISTORY OF THE NAURU BASIN, WESTERN PACIFIC

Michael J. Murphy

A Thesis Submitted to the
University of North Carolina Wilmington in Partial Fulfillment
Of the Requirements for the Degree of
Master of Science

Center for Marine Science

University of North Carolina Wilmington

2004

Approved by

Advisory Committee

Dr. Nancy Grindlay

Dr. Frederick Bingham

Dr. Lewis Abrams
Chair

Accepted by

Dean, Graduate School

TABLE OF CONTENTS

ABSTRACT

In the western Pacific, oceanic crust is Jurassic in age based on magnetic anomaly lineations. However, drilling expeditions have instead recovered mid-Cretaceous age basalts in deep, supposedly Jurassic age basins such as the Nauru, East Mariana, and Pigafetta. In the southern Nauru Basin, mulitchannel seismic reflection and sonobuoy refraction data support an off-ridge tectonic setting for the emplacement of mid-Cretaceous flood basalts over original Late Jurassic-Early Cretaceous oceanic crust. Forward modeling of refraction data provide velocity structure for coincident seismic reflection data to determine the types and thickness of materials overlying oceanic crust in the southern Nauru Basin. From these models the detection of thin, high velocity sills/flows within a thick, lower velocity layer are evident over a rough reflection surface interpreted as oceanic crust, with an age given by Mesozoic magnetic anomaly lineations. Oceanic crust clearly exists in the southernmost Nauru Basin without the overburden of high velocity sills/flows. Observations of thin sills/flows and oceanic crust beneath reflections from the mid-Cretaceous material cored at Deep Sea Drilling Project Site 462 indicate the presence of previously unsampled lithologic units in the Nauru Basin, notably oceanic crust.

ACKNOWLEDGEMENTS

I would like to foremost thank my parents for their support throughout my long tenure as a student, and their patience with me along the way.

As well, thanks go to the entire Earth Science Department and Center for Marine Science Research for their contribution to my education and research. I would especially like to thank my committee members, Dr. Lewis Abrams and Dr. Nancy Grindlay for providing me with opportunities that led to my participation on two oceanographic research cruises, and Dr. Fred Bingham for his support in preparing this thesis.

I would also like to give thanks to Dr. Deping Chian for all of his assistance with software updates and support throughout the modeling process of this thesis.

LIST OF TABLES

LIST OF FIGURES

INTRODUCTION

Oceanic crust is created at mid-ocean ridges. As older oceanic lithosphere spreads laterally apart along divergent plate margins, young crust forms through decompression melting of upwelling mantle material (White et al., 1992). The new crust demonstrates both physical and chemical characteristics that are evident across entire ocean basins. As the newly formed seafloor cools, the remnant geomagnetic polarity is recorded within the crustal rocks at the time of formation, with polarity reversals of the Earth's geomagnetic field recorded as linear magnetic anomaly stripes (Vine and Matthews, 1963). Correlating well-documented lineations serve as an indirect, yet accurate technique for measuring seafloor spreading rates and direction. More importantly, correct age estimates of ocean basins can be derived when correlating magnetic reversals and stable polarity intervals from land magnetic data to polarities identified on the seafloor.

An area of the western Pacific larger than the continental United States is thought to be Jurassic in age based on correlated magnetic anomaly lineations (Larson and Chase, 1972; Larson and Hilde, 1975; Larson, 1976). However, drilling during the Deep Sea Drilling Project (DSDP) and during the Ocean Drilling Program (ODP) has instead recovered mid-Cretaceous basalt in deep, supposedly Jurassic-age basins such as the East Mariana, Pigafetta and Nauru (Figure 1).

As a result, two competing hypotheses have been proposed to explain those observations:

1.) The lineated magnetic anomalies are formed at Jurassic spreading centers. Subsequently, this oceanic crust was overprinted by widespread emplacement of volcanic material produced in an off-ridge setting (Larson and Schlanger et al., 1981).

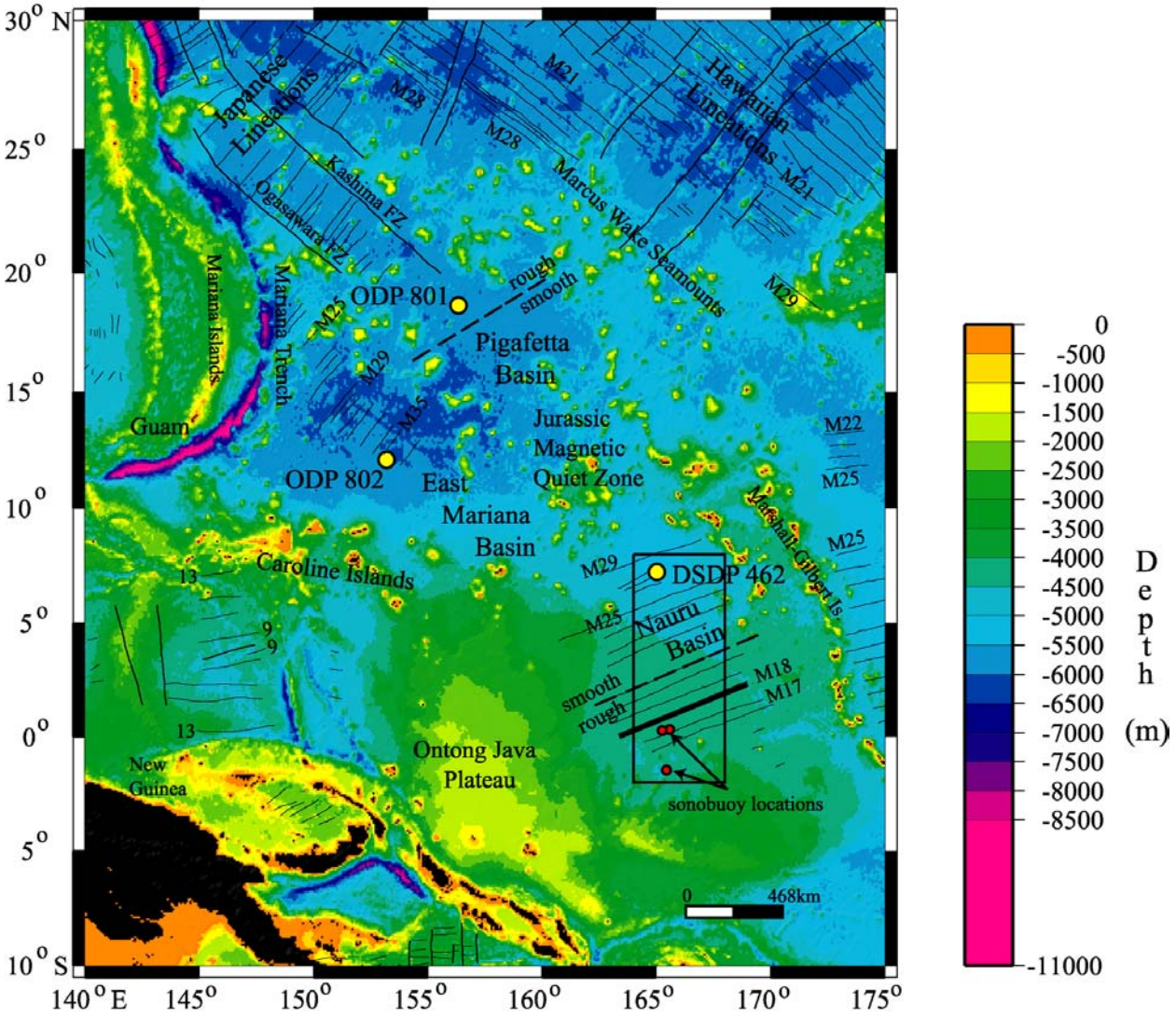

Figure 1. A bathymetric map of the western Pacific. Numbered black lines are magnetic anomaly lineations indicating Early Cretaceous-Late Jurassic oceanic crust in the region, with the thick black line M18 representing the Jurassic-Cretaceous boundary. The dashed black line denotes the rough/smooth boundary marking the approximate extent of the mid-Cretaceous igneous complex overlying Jurassic oceanic crust (Abrams et al., 1993). Yellow circles denote DSDP and ODP drill sites where mid-Cretaceous basalts (ODP 802, DSDP 462) and Late Jurassic basalts (ODP 801) were recovered. Red circles mark sonobuoy locations examined in this paper. The boxed region is shown in figure 2. The map was created with The Generic Mapping Tools, with bathymetry data provided from the predicted topography database (Sandwell and Smith, 1997; Wessel and Smith, 1995).

2.) The igneous material recovered is mid-ocean ridge basalt (MORB) created at mid-Cretaceous age spreading centers, and the magnetic lineations in the region are incorrectly identified (Castillo et al., 1986; 1991).

This paper examines multichannel seismic reflection (MCS) and sonobuoy refraction data acquired from the southern Nauru Basin in 1998 during cruise KH98-1 of the R/V Hakuho Maru (Eldholm et al., 1998). These data are used primarily to constrain the interpretations of MCS data collected between 1986 and 1988 in the Nauru Basin by Shipley et al., [1993] by adding sub-surface velocity structure. The MCS data from the 1998 cruise are correlated to the Shipley et al. [1993] MCS data and used to determine sub-seafloor structure in a portion of the southern Nauru Basin. Observations from reflection character and interval velocity structure from the combined data sets provide constraints on the validity of the two competing hypothesis and insight concerning the origin and tectonic/volcanic history of the Nauru Basin.

TECTONIC SETTING

The Nauru Basin covers more than 1.7 million km^2 in the western Pacific, reaching depths greater than 4000 m (Figures 1 & 2). A ridge at 4200 meters below seafloor (mbsf) trending WNW at 2° to 4°N, divides the Nauru region into respective northern and southern sub-basins (Shipley et al., 1993). The Nauru basin is bounded to the west and south by the Earth's largest igneous province, the Ontong-Java Plateau. To the east and west, chains of linear seamounts comprise the Marshall-Gilbert Islands and the Caroline Islands. The East Mariana and Pigafetta Basins lie to the north and northwest.

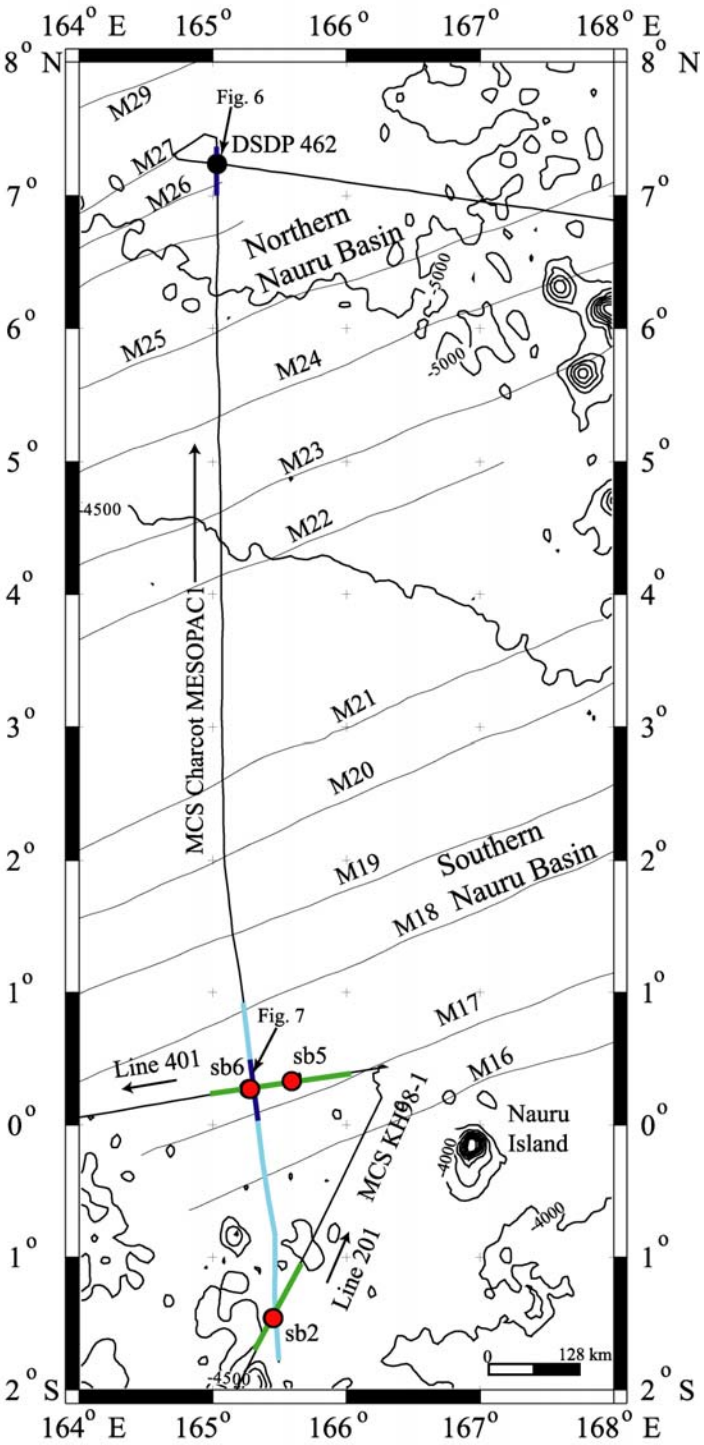

Figure 2. A bathymetric map of the Nauru Basin (boxed region of Figure 1). MCS track lines from MESOPAC I and KH98-1 are shown as colored lines. The black dot denotes the location of DSDP drill site 462. The colored lines are sections of seismic reflection data used in the paper. Red dots indicate the location where sonobuoys were deployed during the KH98-1 cruise. Black lines are correlated magnetic anomaly lineations.

In this paper, seafloor age is assigned according to the Gradstein et al. [1994] geologic time scale. In the Nauru basin, ENE trending magnetic anomaly lineations indicate the oldest oceanic crust is located in the northern Nauru Basin where igneous basement is inferred to be Oxfordian in age (M29, ~160 Ma; Figure 2; Cande et al, 1978). The younger parts of the Nauru Basin, to the southeast, are predicted to be Berriasian (M15, ~137 Ma; Figures 2 & 3; Larson et al., 1976). Magnetic anomaly M18, in the southern Nauru Basin is the approximate location of the Cretaceous-Jurassic boundary, that is, oceanic basement north of this location should be Jurassic. Similarly, oceanic crust in the East Mariana and Pigafetta basins to the north are inferred to be Jurassic based on magnetic lineations mapped in these basins. The oldest in-situ oceanic crust on Earth (~ 180 Ma) is predicted to lie north of the Nauru Basin in an area of low-amplitude, uncorrelated magnetic anomalies, called the Jurassic Magnetic Quiet Zone (JQZ) (Figure 1) (Handschumacher et al., 1988). Oceanic crust in the Nauru basin was produced at half-spreading rates of 4.7 cm/yr assuming constant seafloor spreading and correct age estimates of correlated magnetic anomalies. This spreading rate is comparable to those on spreading ridges intermediate between the fast (10-12 cm/yr) spreading rates on the modern EPR, and the slower spreading of ~2 cm/yr at the Mid-Atlantic Ridge (Kennett, 1982).

This study is focused on the southern Nauru Basin, where magnetic anomalies (M21 to M15, ~146.5 to 137 Ma; Figure 3) indicate the presence of late Jurassic to early Cretaceous oceanic crust. Results from DSDP and ODP drilling and previous multichannel seismic studies indicate that the Nauru, East Mariana and Pigafetta basins

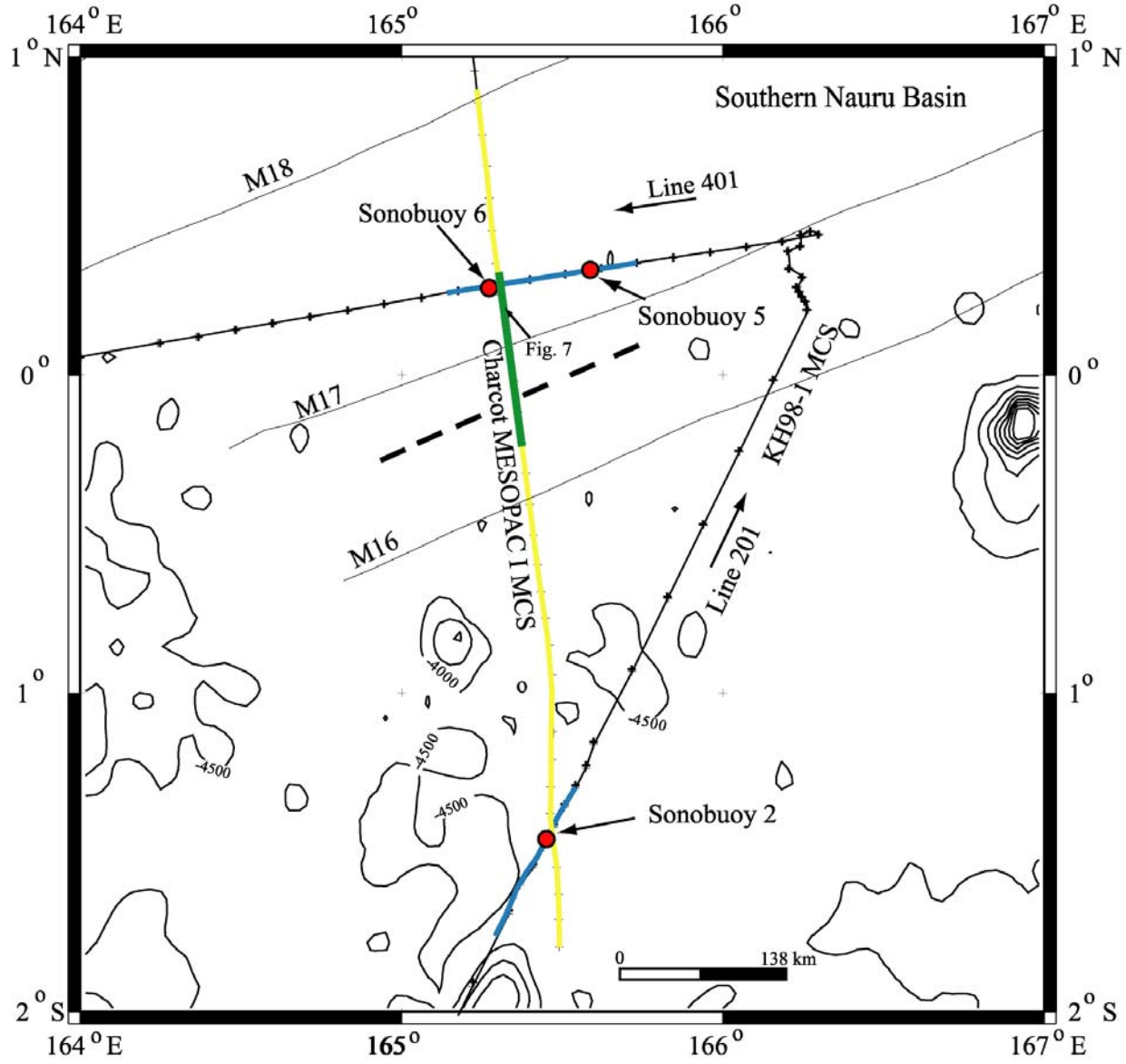

Figure 3. A bathymetric map of the southern Nauru Basin with portions of KH98-1 MCS data used in this paper labeled in blue and MESOPAC I data labeled in yellow. The green line indicates the section of MCS data displayed in figure 7. The thick dashed line marks the extent to which the sill/flow complex extends in the study area. South of this line, oceanic crust is imaged without overlying sills/flows. Sonobuoy 5 and 6 lie within anomalies M17-M18 (Early Cretaceous), with Sonobuoy 6 strategically located at the intersection of MCS Line 401 with MESOPAC 1. Sonobuoy 2 lies over Early Cretaceous oceanic crust close to the intersection of MCS Line 201 with MESOPAC 1.

all contain basalt that appears to be related geochemically and chronologically to the largest outpouring of igneous material in the last 200 m.y. that resulted in the construction of the Ontong-Java plateau at 120 Ma (Tarduno et al., 1991; Shipley et al., 1993; Castillo et al., 1994; Janney et al., 1996).

PREVIOUS STUDIES

Magnetic lineations M29 to M17 indicate oceanic crust in the Nauru Basin should be ~156 Ma to 140 Ma (Larson, 1976; Cande et al., 1978; Gradstein et al., 1994). DSDP Site 462, the only drill site in the entire Nauru Basin, lies between magnetic anomalies M-26 and M-27 (~155 Ma) in an area of low topographic relief in the northern Nauru Basin (Figures 1 & 2; Wipperman et al., 1981). DSDP Site 462 penetrated to 1068.5 meters below seafloor (mbsf) and recovered Berremian to upper Eocene and younger sedimentary rocks. However, instead of recovering Jurassic (>144 Ma) basalt, the deepest/oldest materials cored were Albian (~110 Ma) sills and flows. These basalts are geochemically similar to moderately enriched MORB (Batiza, 1981) and to basalt cored from the Ontong-Java Plateau (Scheka, 1981).

In the East Mariana Basin to the north, ODP Site 802 is the only site to reach massive igneous basement in that basin. Again, the basalt recovered is much younger (~ 114 Ma, Aptian) than the mid-Jurassic age predicted from magnetic lineations and geochemically similar to moderately enriched MORB (Castillo and Pringle, 1991). Based on seismic reflection character of MCS data, Abrams et al., [1993] hypothesize that Aptian age basalt sills/flows exist in the southeast Pigafetta basin within the JQZ. Thus the controversy: were these basalts formed at a mid-Cretaceous spreading center or are these flood basalts that overlie a deeper, unsampled, Jurassic age oceanic basement?

During ODP Leg 129 at Site 801, in the JQZ of the Pigafetta Basin, upper Jurassic (Bathonian, ~166.8 +/- 4.5 Ma) basalts were recovered for the first time (Figure 1; Lancelot, Larson et al., 1990; Larson, Lancelot et al., 1992). This site remains the only location on the entire Pacific plate where in-situ Jurassic age MORB and overlying sediments unequivocally exist. Abrams et al. [1993] describe the acoustic basement reflector over this site as an undulating, low amplitude, hyperbolic surface with a relief of 100-200 m. This rough reflection surface correlates to the Jurassic basalts and appears morphologically similar to oceanic crust produced at modern, fast- spreading centers (Figure 4). Supporting refraction data indicate a shallow crustal arrival tangent to the acoustic basement reflector with a velocity of ~4 km/s that increases monotonically with depth. This is analogous to normal oceanic crust where velocities invariably increase rapidly with depth (White et al., 1992; Figure 5).

In the northwest Pigafetta and East Mariana Basin, mid-Cretaceous basalts were recovered at Sites 800 and 802 where Jurassic oceanic crust is predicted from magnetic anomaly lineations (Figure 1). Regional seismic studies indicate the acoustic basement reflection over these two drill sites corresponds to a flat-lying, high-amplitude reflection surface with a relief of less than 100 m, unlike any basement surfaces adjacent to present-day spreading centers (Abrams et al., 1993) (Figure 4). Refraction data show a refracted arrival with a higher velocity of 5.3 km/s preceding a lower velocity (~2 km/s) sedimentary section and main crustal arrivals in sonobuoy records (Figure 5). Combining

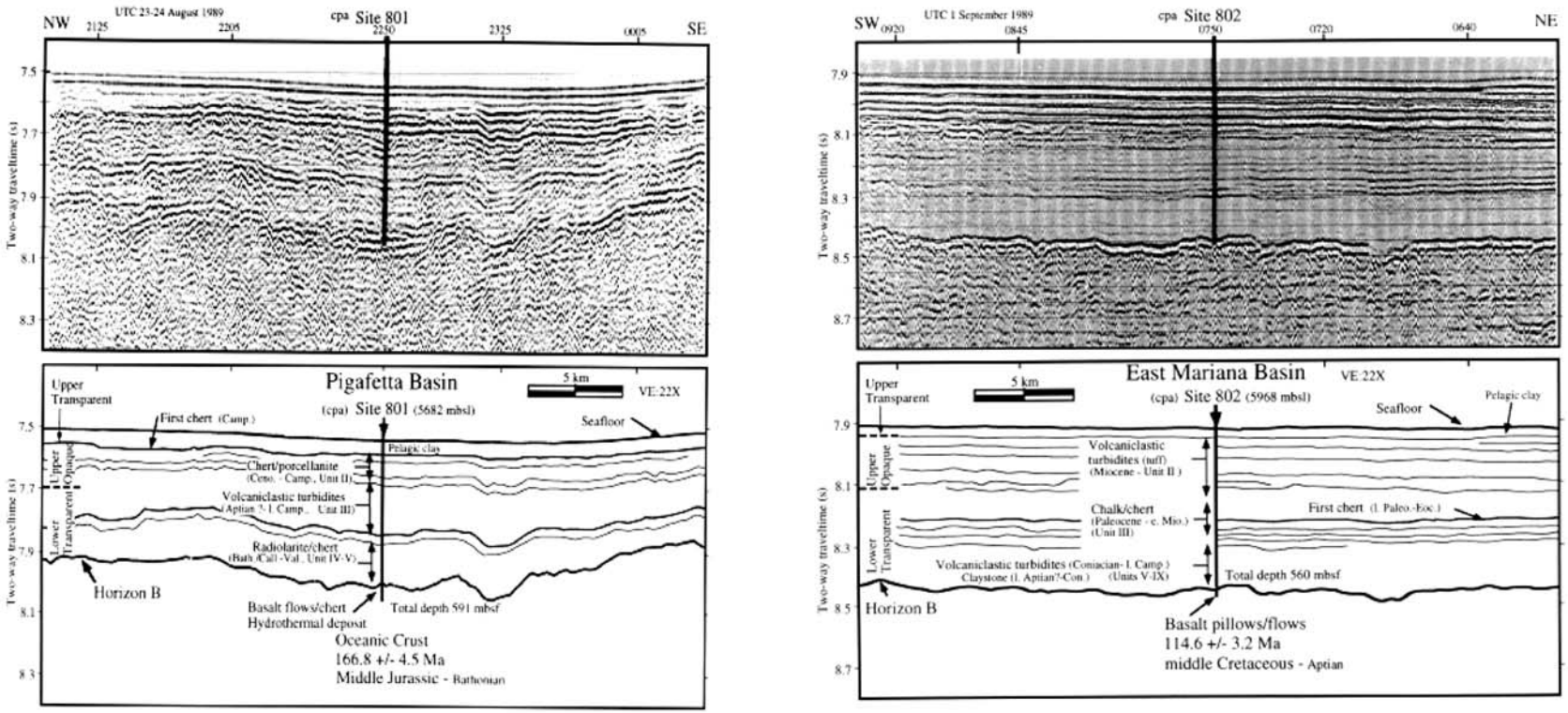

Figure 4. Seismic stratigraphy over ODP Site 801 (left) and 802 (right) and interpretation based on cored sediments from the Pigafetta and East Mariana Basin. Site 801 reached Jurassic oceanic crust in the Pigafetta Basin, with acoustic basement interpreted as a "rough", high-relief, low-amplitude reflection in MCS reflection profiles. Acoustic basement in the East Mariana Basin is depicted as a "smooth", low-relief, high-amplitude reflection in MCS reflection profiles, corresponding to recovered mid-Cretaceous basalts drilled at Site 802 that overlay a deeper, unsampled oceanic crust (From Abrams et al., 1993).

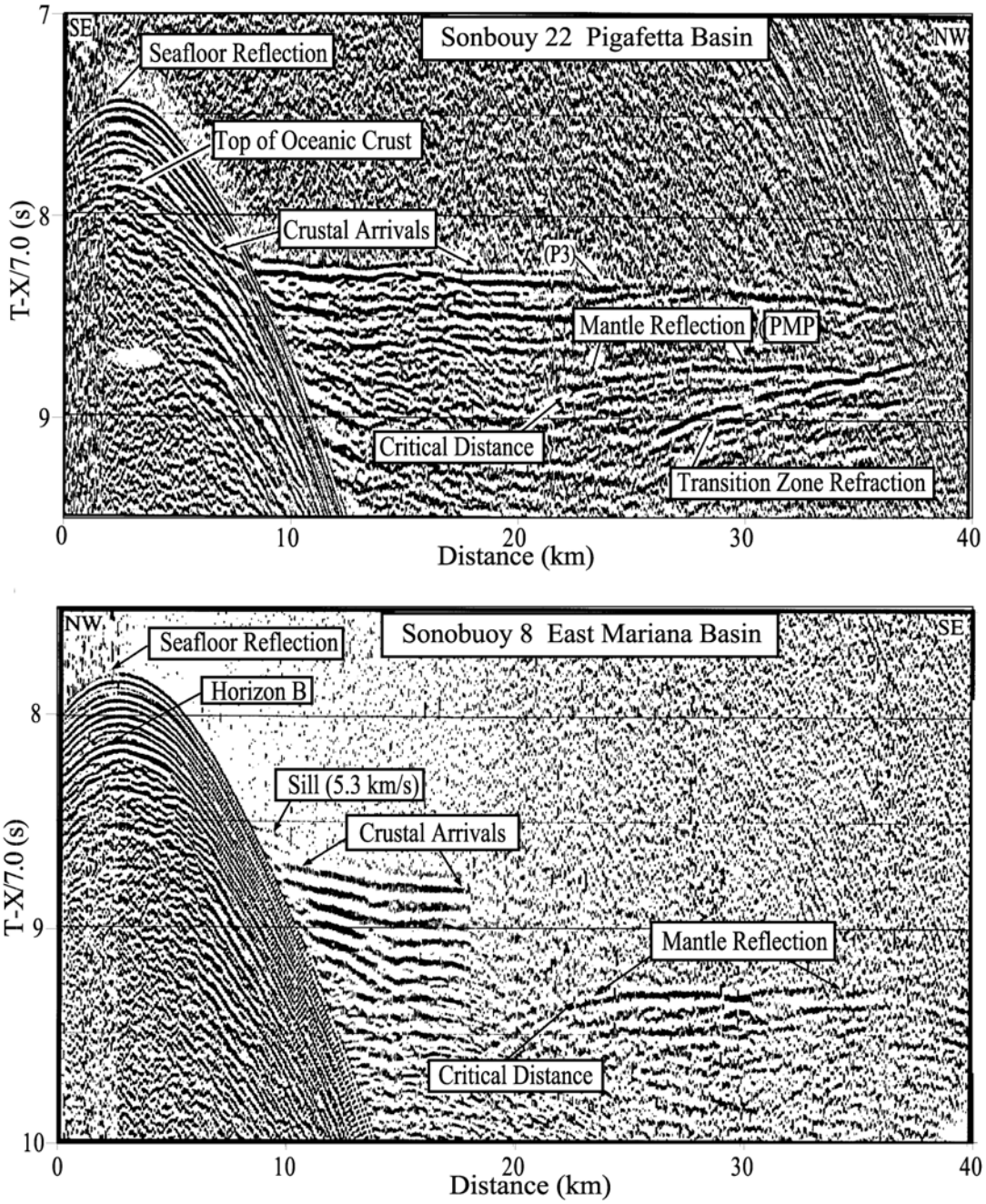

Figure 5. (Top) Sonobuoy 22 travel time-range (T/X) data from the Pigafetta Basin in the Jurassic Magnetic Quiet Zone. Crustal arrivals are tangent to acoustic basement with a velocity of 3.98 km/s and increasing rapidly with depth. Located near ODP Site 801, the T/X record shows no indication of shallow, high velocity refracted arrival preceding the main crustal arrivals. (Bottom) Sonobuoy 8 T/X data from the East Mariana Basin. The high-velocity, short-range refraction has been interpreted as a thin sill overlying a lower velocity sediment package and Jurassic oceanic crust (Modified from Abrams et al., 1993).

seismic reflection character with velocity structure in the East Mariana, it is likely that the sequence of a thin, high-velocity layer and an underlying low-velocity section corresponds to mid-Cretaceous basalts and sediments overlying Early Cretaceous-Late Jurassic oceanic crust.

Likewise, modeling of ocean bottom seismometer (OBS) refraction data at DSDP Site 462 in the Nauru Basin, requires a low velocity layer beneath the observed sill horizon, which may indicate a layer of sedimentary rocks "sandwiched" between the sills and an un-imaged oceanic crustal section (Wipperman et al., 1981).

The deepest recovered materials are 649 m of mid-Cretaceous volcanic sills and flows, with interbedded volcanogenic turbidites, labeled Kv in the figures. Subsequently deposited were 112 m of Albian to Maestrictian age volcaniclastic sediments and zeolitic sandstone, mudstone and limestone. Above this unit, lie 150 m of cherts, chalks and limestones of middle Maestrichtian to middle Eocene age, the top of which is label mE in the figures. The uppermost units combined are ~297 m thick, and are mostly turbidite deposits composed of calcareous and radiolarian oozes and chalks. These units of late Eocene age and younger are labeled eM (early Miocene) and mM (middle Miocene) in the figures (Figure 6; Larson et al., 1981; Shipley et al. 1993).

The Cretaceous volcanics recovered at DSDP Site 462 are comprised entirely of tholeiitic basalts and dolerites compositionally indistinguishable from normal MORB based on major element chemistry (Janney and Castillo, 1986). The recovered basalt is, however, more enriched in highly incompatible elements than those in normal-MORB (Saunders, 1985; Batiza, 1980; Castillo et al., 1996). The Nauru Basin sills/flows are also

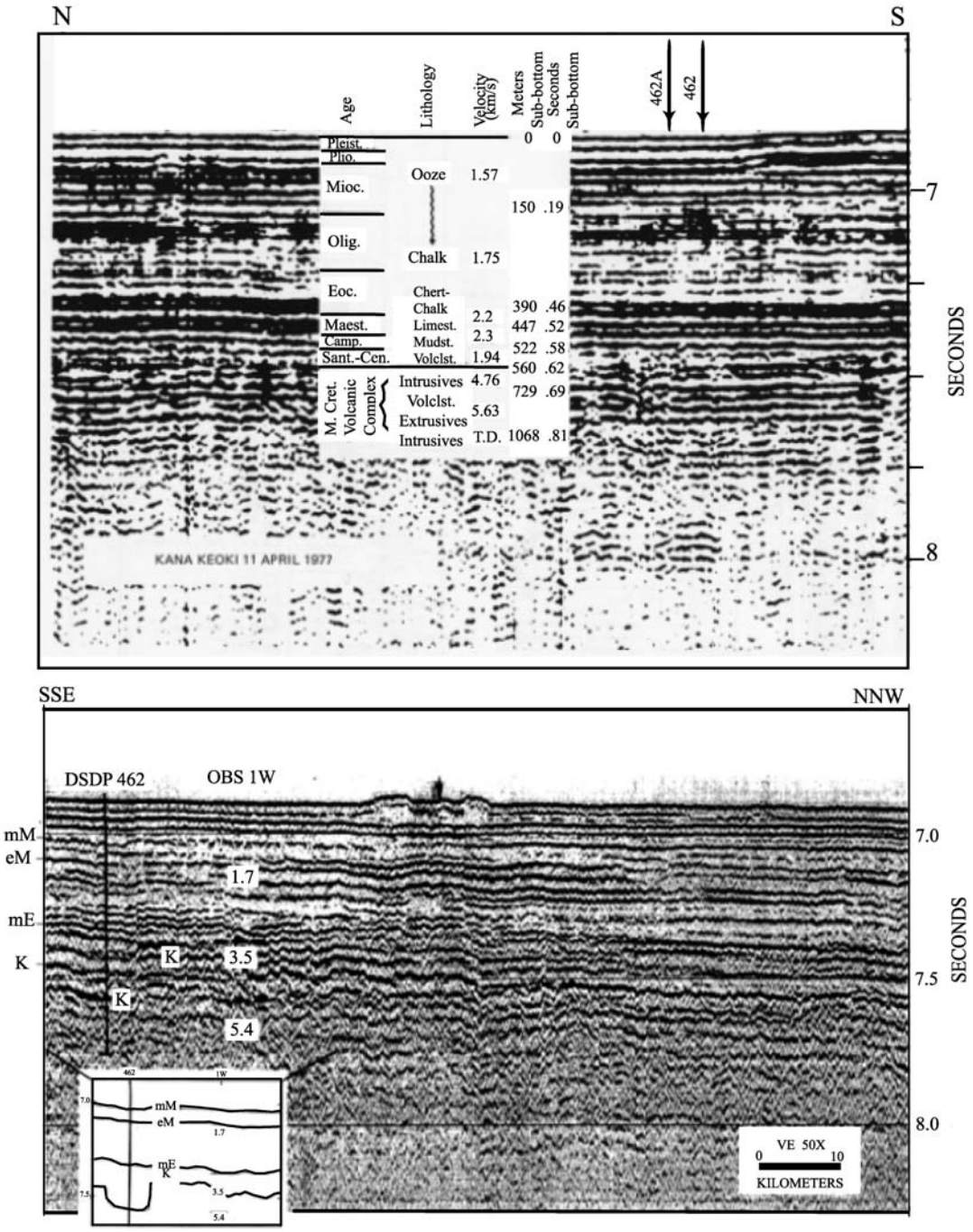

Figure 6. (Top; from Larson and Schlanger, 1981) Interpreted seismic reflection profile acquired during DSDP Leg 61 site survey along with drilling results showing age, lithology, velocities, and depths to recovered strata. (Bottom; from Shipley et al., 1993) A seismic section from Roundabout 12 near DSDP Site 462. Lithologies cored at DSDP Site 462 were correlated based on seismic reflection character. The top of the cored Cretaceous volcanics corresponds to a flat-lying high-amplitude reflection, labeled K. Oceanic crust was not reached at DSDP Site 462, nor imaged in seismic reflection profiles.

similar, geochemically and isotopically, to lavas from the Manihiki and Ontong-Java Plateau, which are believed to be intraplate, mantle plume-derived basalts (Shcheka, 1981; Tokuyama and Batiza, 1981). Unfortunately, isotopic and trace element data alone are not definitive as to whether or not basalt recovered at DSDP site 462 was formed at a mid-Cretaceous spreading center or emplaced in an intraplate environment on top of pre-existing Jurassic basement.

Acoustic basement is noted as having a distinctly different seismic reflection character in both the northern and southern sub-basins of the Nauru region (Shipley et al., 1993). In the northern Nauru Basin, a flat-lying, high-amplitude reflection corresponds to the top of Cretaceous volcanics drilled at DSDP Site 462 (Figure 6). Oceanic crust is not imaged in seismic reflection profiles, however, magnetic anomalies M29 to M21 indicate its existence beneath the thick Cretaceous igneous complex in the northern sub-basin.

In the southern Nauru Basin, an undulating, low-amplitude reflective surface with 150 m to 300 m of relief has been interpreted as the top of M21 to M15 oceanic crust (Shipley et al., 1993; Figure 7). The diagnostic reflection character is imaged beneath a shallow, high-amplitude reflection that has been interpreted as a thin volcanic layer within a thick sedimentary package. Thus, reflection character serves as one attribute distinguishing oceanic crust from overlying volcanic sills and flows.

STATEMENT OF THE PROBLEM

From seismic, magnetic, and geochemical studies, two competing hypotheses have been proposed as to the origin of the widespread Cretaceous igneous complex:

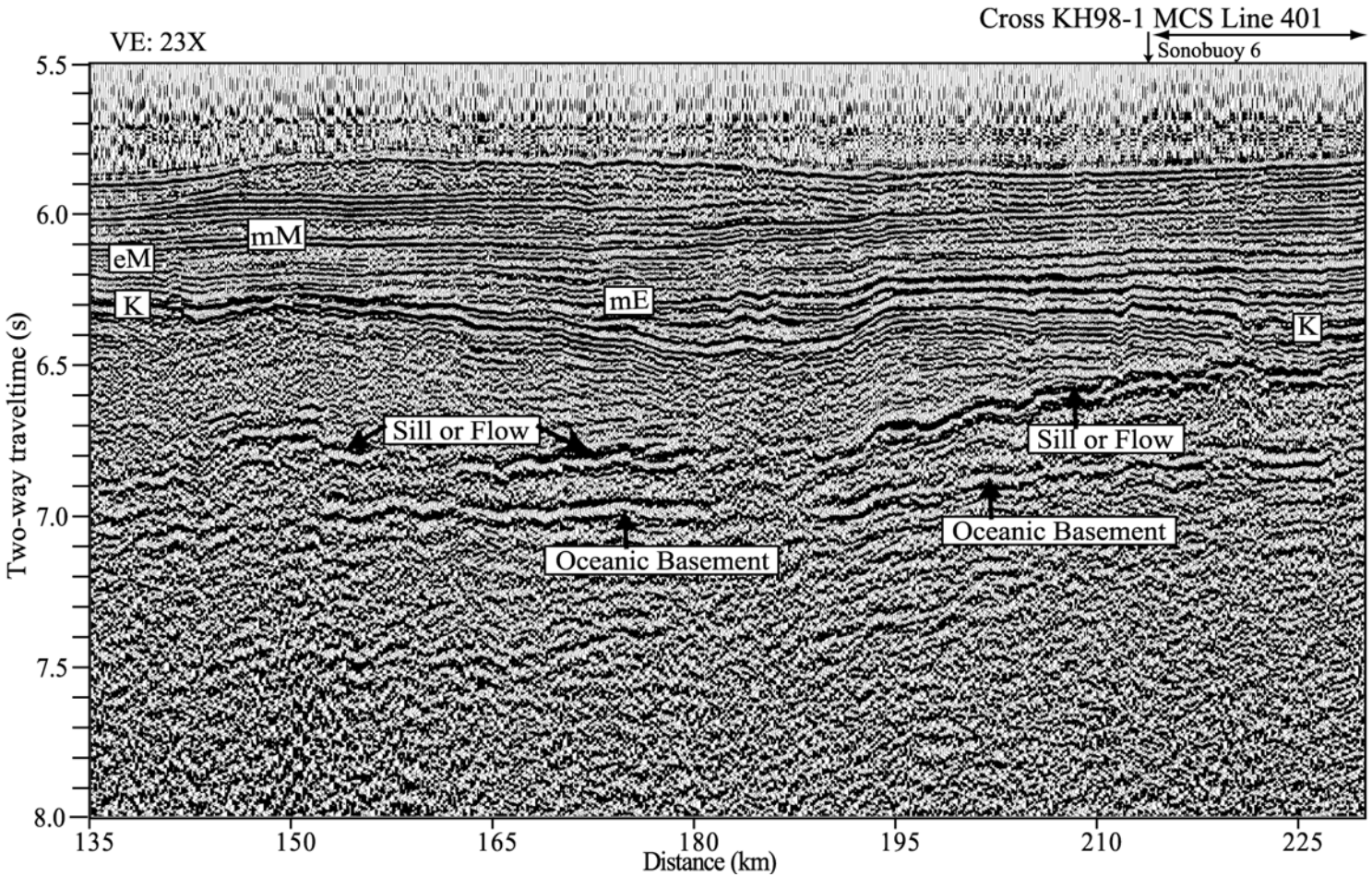

Figure 7. A portion of MESOPAC I MCS data collected in the southern Nauru Basin. Labeled seismic facies were correlated from material recovered at DSDP Site 462 (mM-K). Based on reflection character, Shipley et al. [1993] hypothesize the presence of thin sills/flows overlying Late Jurassic-Early Cretaceous oceanic crust and sediments beneath the unit cored at DSDP Site 462 (From Shipley et al., 1993).

Intraplate Model

1) The "intraplate" model predicts the lineated magnetic anomalies are indeed formed at Jurassic spreading centers. Subsequently, oceanic crust was overprinted by widespread emplacement of volcanic sills or flows produced in an off-ridge setting (Figure 8). The igneous materials are thought to have intruded along the pre-existing Jurassic crust as intraplate flood basalts along tension cracks and fractures associated with thermal uplift and/or mantle wedging. Seawater admitted into numerous fissures would minimize any potential reheating of the adjacent magnetic crust, thus preserving the Late Jurassic to Early Cretaceous anomaly lineations in the Nauru Basin (Larson and Schlanger, 1981). In addition, the normally magnetized Cretaceous basalts are an indication of rapid cooling during the Cretaceous magnetic quiet event, and act as a magnetic annihilator with respect to the underlying crust and not contributing to the crustal magnetic signature measured at the sea surface (Larson and Schlanger, 1981; Parker and Heustis, 1974).

Furthermore, the Cretaceous basalt recovered in the Nauru Basin is similar to lavas collected from proximal, mantle plume-derived oceanic plateaus (e.g. Manihiki and Ontong Java Plateau). The basalts vary slightly from the geochemically depleted type of MORB, and are thus interpreted as ocean-plateau tholeiites, deposited via intraplate eruptions (Tokuyama and Batiza, 1981). As a result, the intraplate hypothesis predicts the thick, widespread igneous complex erupted through numerous fissures intruding the pre-existing Jurassic crust, most likely associated with the formation of the Ontong Java Plateau approximately 120 Ma during the mid-Cretaceous.

It is the presence of this massive igneous complex, along with resistant sedimentary strata, that impede both seismic and drilling objectives designed to image and recover

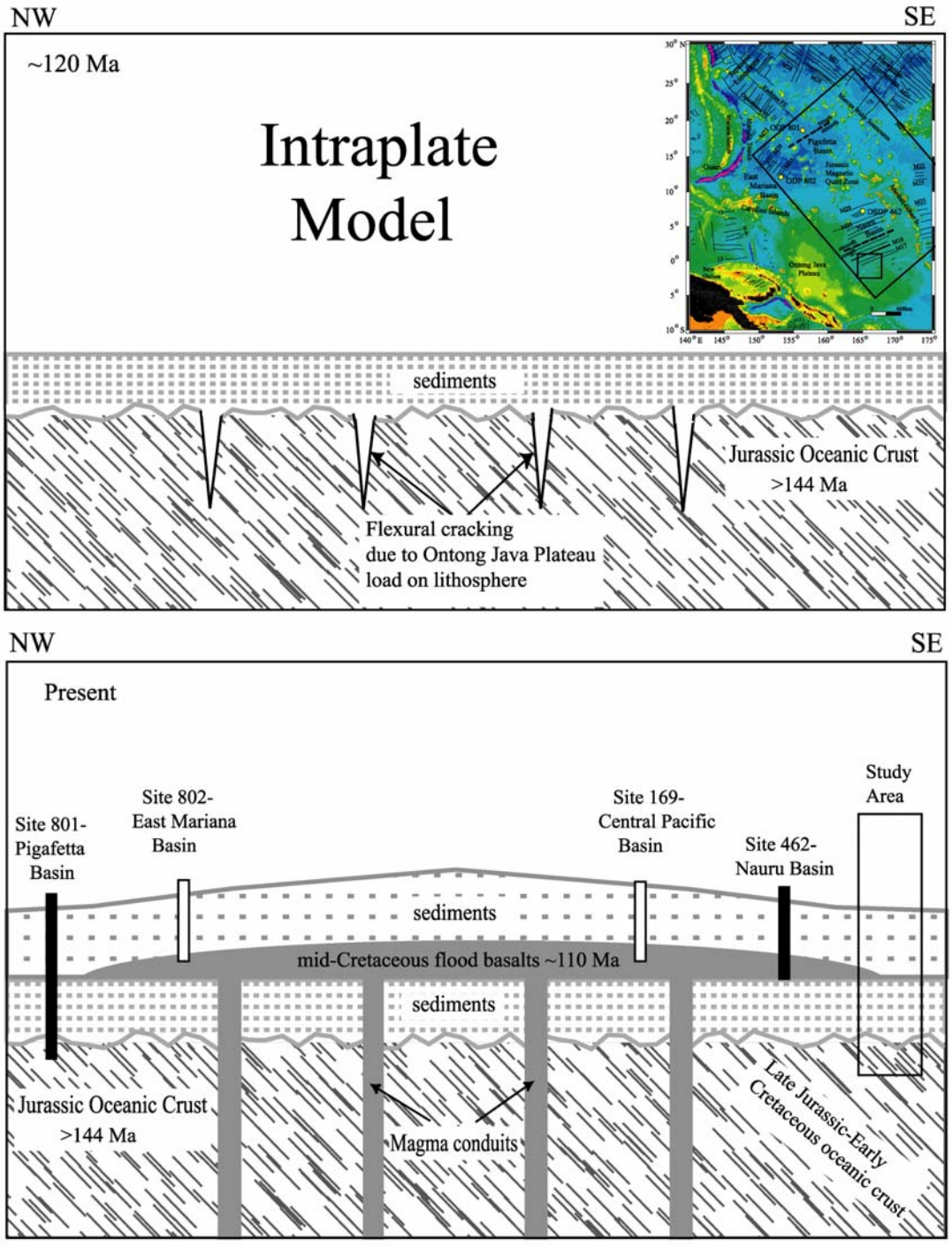

Figure 8. The intraplate model for emplacement of mid-Cretaceous basalts. Approximately 120 Ma Jurassic oceanic crust fractured from the formation of the Ontong-Java Plateau. Magmas then erupted along new fractures to form the mid-Cretaceous flood basalts over Late Jurassic-Early Cretaceous oceanic crust and sediments. The large box within the index map shows the NW-SE cross sectional extent of the model. The small box marks the study area at the feather edge of the mid-Cretaceous igneous complex. DSDP Site 169 is located just off to the east on the index map (Modified from Larson and Schlanger, 1981). oceanic crust in an area where obvious Jurassic magnetic anomalies exist.

Ocean Ridge Model

2) Based on the fairly homogenous petrology, geochemistry, and isotopic composition of the igneous complex, the "ocean ridge" model claims that Jurassic basement does not exist beneath the mid-Cretaceous complex. Instead, the igneous material is MORB created at mid-Cretaceous age spreading centers and the Ontong-Java Plateau was created at or near a spreading ridge environment (Janney and Castillo, 1996) (Figure 9).

Basalts analyzed from the Nauru Basin are geochemically similar to normal MORB (Batiza et al., 1980, Castillo et al., 1986; Janney and Castillo, 1996). The tholeiites are generally unfractionated with slight chemical variations falling within the trends observed in fractionated suites of global MORB. Trace element analyses of the sills and flows show similarities to MORB as well, both being depleted in light rare earth elements (Batiza, 1981; Castillo et al., 1991).

In the Central Pacific Basin, DSDP Leg 17 recovered Late Albian (100-105 Ma) tholeiitic pillow basalts and Late Cretaceous dolerite sills having trace element ratios similar to MORB emplaced near plume-derived hot spots (Winterer et al., 1973; Janney and Castillo, 1996). The homogenous petrology of the basalts is practically indistinguishable from Cretaceous basalts recovered from the East Mariana (ODP Site 802) and northern Nauru Basin (DSDP Site 462). The basalt samples are virtually free of any shallow-level contamination from pre-existing Jurassic crust. This argues against the interpretation of intrusion of the basalts through pre-existing Jurassic crust, where contamination would likely be evident (Castillo et al., 1991).

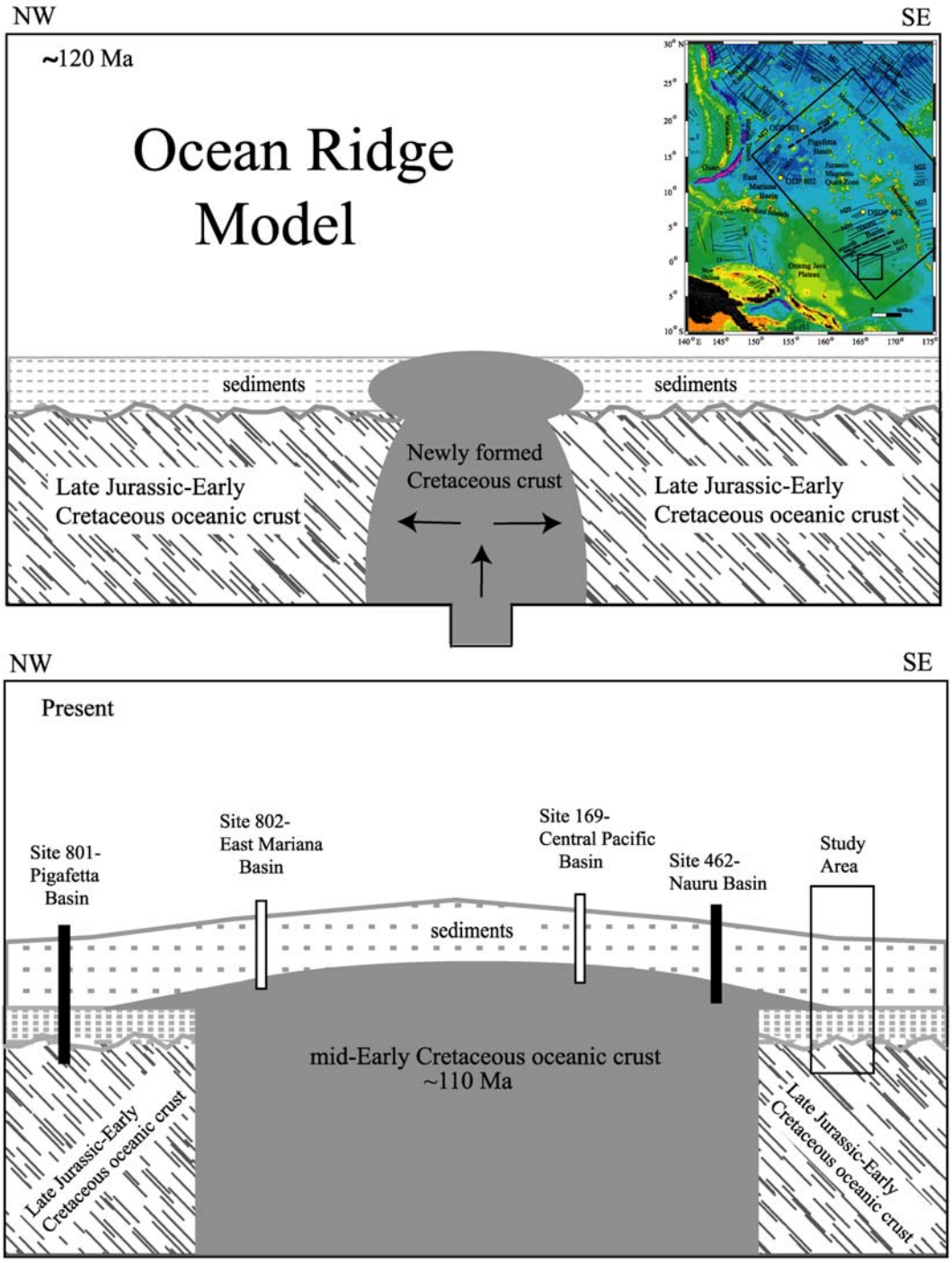

Figure 9. The ocean ridge model for the origin of the Cretaceous igneous complex. Rifting of Late Jurassic oceanic crust is initiated with the formation of the Ontong- Java Plateau at ~122 Ma. This model relies highly on geochemical analyses of basalt similar to MORB-like basalts, indicating the presence of mid-Early Cretaceous oceanic crust. The large box on the index map shows the NW-SE cross sectional extent of the model. The small box marks the study area at the feather edge of the mid-Cretaceous igneous complex. DSDP Site 169 is located just off to the east on the index map (Modified from Janney and Castillo, 1996).

Geochemical data suggest the basalts from three separate basins (East Mariana, ODP Site 802; Nauru, DSDP Site 462, and Central Pacific, DSDP Leg 17) were derived from the same mantle source. In addition, the similar seismic reflection character of the mid-Cretaceous basalts in each basin implies their emplacement under the same tectonic conditions (Janney and Castillo, 1996).

Thus, the "ocean ridge" model is consistent with geochemical data similar to MORB. In addition, the extensive coverage of the vast igneous complex throughout the western Pacific supports the emplacement of Cretaceous basalts through continuous eruption along large rifts or an ocean ridge system. However, the model is in clear conflict with the Late Jurassic-Early Cretaceous magnetic data and seismic results from proximal basins.

Correlating regional MCS stratigraphy throughout the Nauru Basin to the lithostratigraphy from material recovered at DSDP Site 462 in the northern Nauru Basin, Shipley et al. [1993] were able to extend seismic facies well into the southern Nauru Basin (Figure 7). One of the primary results of this study is the interpretation of Early Cretaceous to Jurassic oceanic crust with little (thin sills) or no mid-Cretaceous age massive igneous overburden in the southern Nauru Basin. If this is true, then the proposed mid-Cretaceous spreading ridge origin for the Nauru Basin cannot be correct, and an intraplate mode of emplacement for the mid-Cretaceous igneous complex is supported.

DATA ACQUISITION AND PROCESSING

Multichannel Seismic Reflection Data

The MCS reflection lines in this study were collected on two cruises. Data along MCS line MESOPAC I were collected in 1986 on a cruise of the N/O Charcot, using a high resolution,

implosive source sound (flexichoc) and a 24-channel receiving array (Shipley et al., 1993). The MESOPAC 1 line runs North-South, nearly perpendicular to Mesozoic magnetic anomaly lineations across the entire Nauru Basin (Figures 2 and 3). This orientation will maximize any basement roughness due to abyssal hills imaged in reflection data. Interpretations from this data are given in Shipley et al. [1993].

In February 1998, the KH98-1 cruise onboard the R/V Hakuho Maru acquired MCS reflection lines 201 and 401 that are interpreted in this study (Figures 2 and 3) **(**Eldholm et al., 1998**).** The seismic source on the Hakuo Maru consisted of one to three 17 and 20- liter airguns operating at approximately 1600 psi, with a shot spacing of 50-80 m. MCS Line 401 was acquired with a 1200-meter long solid-state streamer comprised of a 48-channel receiving array each spaced 25 m apart. The seismic data were sampled at 2 ms with a total record length of 16 s. MCS Line 401 intersects MESOPAC 1 in the Early Cretaceous section of the study area between M17 and M18.

A 300-meter long solid-state streamer comprised of a 24-channel receiving array, each spaced 12.5 m apart, was used to collect data along the SW-NE MCS Line 201. The source along this line was the same used on MCS Line 401. The seismic data were sampled at 2 ms with a full record length of 8 s. The shot spacing along MCS Line 201 ranged from 40-80 m. This line lies at an oblique angle to Early Cretaceous magnetic anomalies and intersects MESOPAC I in the southernmost Nauru Basin (Figure 3).

Processing of the KH98-1 MCS data were performed by the University of Texas Institute for Geophysics. Display parameter processing and interpretation of the MCS and refraction data were performed at UNCW using the commercial software package Seismic Processing Workshop and the freeware SeisWide. All MCS displays in the text are digitally stacked, band

pass filtered to 15-50 hertz, with an automatic gain control (AGC) of 200 millisecond time gates applied, and shown in relative amplitude to image both strong and weak amplitude signals adequately.

Sonobuoy Refraction Data

Sonobuoys are free floating expendable devices that are used to acquire seismic refraction and wide-angle seismic data up to 50 km from the seismic source. The three sonobuoys (2, 5, & 6) used in this study were collected during the KH98-1 cruise while shooting the MCS data (Figure 3). In order to calculate correct ranges, shot spacing for each sonobuoy were determined from direct wave arrivals and assuming a water velocity of 1.54 km/s. Initial processing was performed in Seismic Processing Workshop, with the SEG-Y data then entered into SeisWide for efficient forward modeling. Processing of sonobuoy data included application of a band pass filter 5-20 hertz and an AGC of 100 milliseconds to provide the best display for imaging both reflected and refracted arrivals.

METHODOLOGY

Research Design

The primary goal of this research is to determine sub-surface velocity structure from seismic refraction data that will provide the most definitive constraints on the interpretations of Shipley et al., [1993] short of direct sampling by deep-sea drilling. In addition, the new MCS data from the KH98-1 cruise will be correlated to the Shipley et al., [1993] data set to extend the coverage area of sub-surface structure and to compare/contrast reflection characteristics. The basic

premise is that sub-surface structure predicted by the two models can be compared to actual sub-surface structure obtained through analysis of seismic reflection and refraction data.

Oceanic crust has certain structural and chemical characteristics, distinguished by a well-established range of seismic wave velocities, velocity gradients, and thickness. From seismic refraction studies and synthetic seismogram modeling, White et al. [1992] estimated the average igneous section of oceanic crust to be 7.1+/-0.8 km thick, with variations seen as a result of mantle dynamics beneath spreading ridges, increasing age away from the ridge axis, and irregular spreading rates.

Seismic Refraction Data

Seismic refraction observations subdivide oceanic crust into three distinct layers based on velocity and velocity gradients. Layer 1 consists of sedimentary strata with variable thickness and relatively low velocities. Layers 2 and 3 comprise the igneous section of oceanic crust. Layer 2 is composed of basaltic lavas and dykes with high velocity gradients. Due to an increase in fracture porosity and weathering toward the surface, and more homogenous basalts with depth, primary wave velocities traveling within layer 2 range from as low as 2.5 km/s, to as high as 6.6 km/s, with a mean thickness of 2.11 +/- 0.55 km (White, 1992; Carlson, 1998). Making up over sixty-six percent of the igneous crustal section, layer 3 is over twice as thick as layer 2 (approximately 4.97 +/- 0.90 km). Layer three is characterized by gabbroic rocks, with primary wave velocities in this layer ranging from 6.7 km/s at the top, increasing to approximately 7.2 km/s at the base (White et al., 1992). Layer 3 is also distinguished from layer 2 by having relatively low velocity gradients.

Sills or flows within a sedimentary sequence overlying oceanic crust are characterized by high seismic, low gradient velocities, relative to Layer 2 in normal MORB, and have a limited thickness (Figure 10).

Seismic Reflection Data

Adjacent to modern spreading ridges (e.g. East Pacific Rise), the top of normal oceanic crust appears rough, undulating, and diffractive on seismic reflection profiles. The top of a sill/flow imaged with reflection data will appear smooth and flat relative to the basalt surface created at mid-ocean ridges (i.e. no abyssal hills).

Thus, seismic velocities obtained from refraction data and seismic reflection data can distinguish between basalts formed at a mid-ocean ridge and basalt sills/flows emplaced off-ridge. The detection of a high velocity sill/flow within the sedimentary sequence would be a clear indication of an off-ridge volcanic event (presumably mid-Cretaceous) and would be consistent with a model of MORB overprinted by later volcanism ("intraplate" hypothesis). A smooth, high-velocity structure would be consistent with off-ridge volcanism (sill), but could not completely eliminate a fast-spreading mid-ocean ridge origin. In addition, identification of a rough-undulating high-velocity surface beneath the sedimentary section would be consistent with the top of normal oceanic crust, with an age depending on correlated magnetic lineations..

If the southern Nauru Basin is similar in seismic reflection character to surrounding basins where sediments and high-velocity mid-Cretaceous basalts overly lower velocity sediments and original oceanic crust (i.e., East Mariana), and where oceanic crust unequivocally exists (i.e., Pigafetta Basin), an intraplate origin for mid-Cretaceous flood basalts and Jurassic aged normal oceanic crust is supported. If it is dissimilar in structure, then possibly a near-ridge Cretaceous

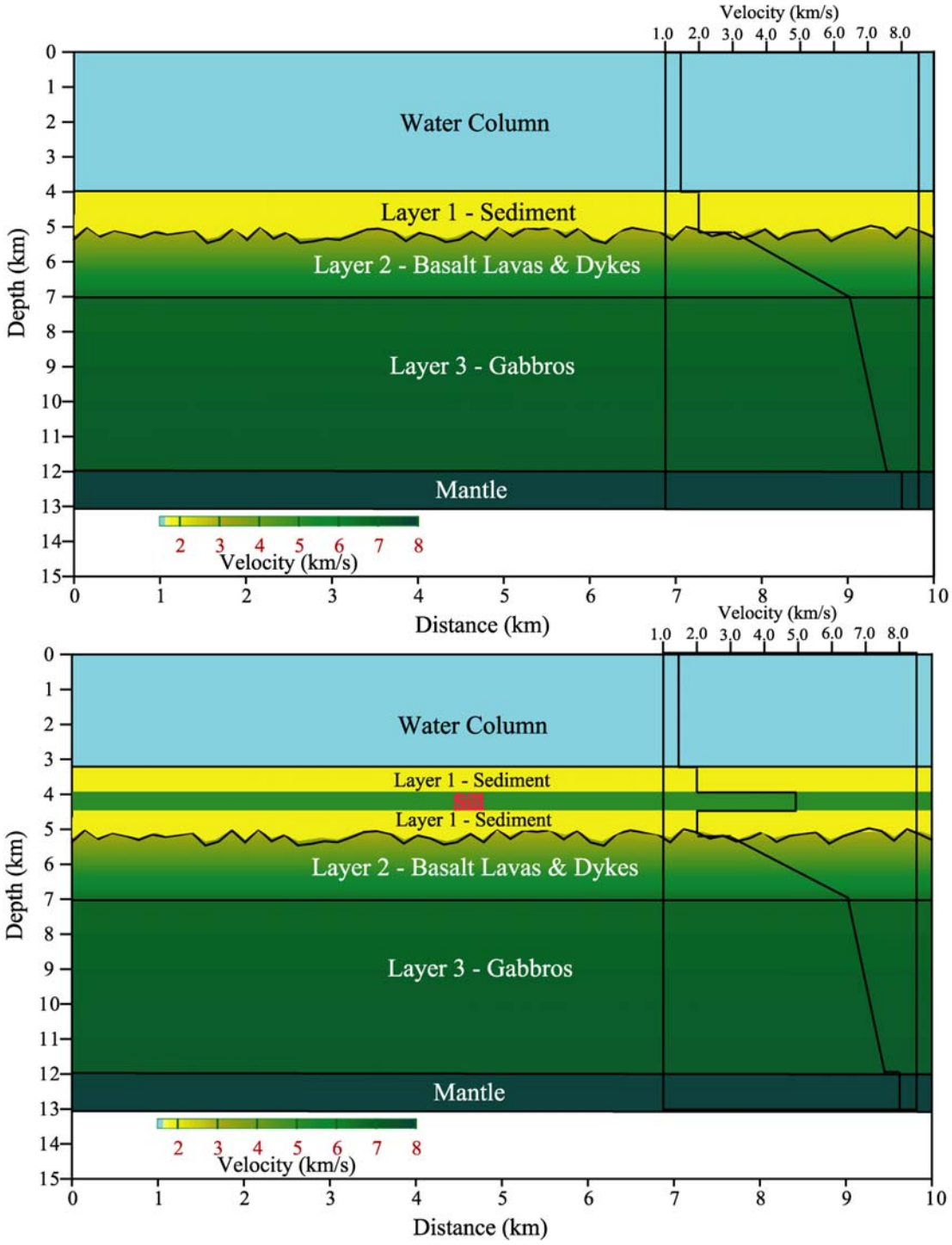

Figure 10. Simple subsurface models depicting the two end-member scenarios. (Top) The two models show typical structural, lithologic and primary seismic wave velocities associated with normal oceanic crust and a sill/flow within a sedimentary sequence overlying oceanic crust (bottom).

source for the Ontong-Java Plateau formation and normal oceanic crust is supported.

MODELING STRATEGY

Inverse Modeling

Initially, using coincident MCS data as a guide for reflection arrival picking, the T^2-X^2 method was applied to determine seismic velocity (Vrms) (Green, 1938). Digitized travel time and range values (T/X) from selected reflections and refractions were used to construct a sub-surface model consisting of layers with constant velocity and uniform thickness (Appendix D) (Dix, 1955). These velocity-depth models served as a starting point for ray-traced forward modeling of observed sonobuoy data (Table 1). The models are composed of individual layers with distinct velocities, velocity gradients and variation in layer thickness. The models are essentially one-dimensional in that they do not include horizontal variation in structure. This does not greatly affect the modeling process, in that the seafloor and sub-bottom reflections in the study area are essentially flat-lying with little relief. Amplitudes were not modeled in the T/X data, but were critical in making accurate first arrival picks with coincident MCS data, and in turn, useful in developing preliminary models for each sonobuoy.

Table 1. Velocity – Depth functions below seafloor for each sonobuoy analyzed in this paper. Primary wave velocities were determine from the T^2-X^2 method and are given in column 3. Dashed lines indicate layers with velocity gradients. The thickness of each layer is given in column 4 in seconds and in column 5 in kilometers.

Sonobuoy #	Layer	Water Depth (m)	Vp (km/s)	Two-Way Travel time (s)	Thickness (km)
6		4534	1.54		
	1		1.66	5.88	0.0896
	2		2.33	5.996	0.217
	3		1.80	6.182	0.0627
	4		1.85	6.28	0.1
	5		3.65	6.388	0.298
	6		5.709-	6.551	0.111
	7		4.07	6.59	0.497
	8		6.2305-	6.834	
5		4390	1.495		
	1		1.62	5.873	0.129
	2		1.60	6.032	0.034
	3		2.027	6.169	0.15
	4		3.207	6.317	0.21
	5		2.65	6.448	0.427
	6		5.189-	6.609	0.135
	7		1.98	6.661	0.224
	8		5.394-	6.887	
2		4489	1.513		
	1		2.553	5.934	0.227
	2		2.247	6.112	1.081
	3		6.101-	6.593	

Forward Modeling

The final goal of the modeling was to produce accurate velocity versus depth profiles over the range of the sonobuoy data. This enables conversion of MCS reflection travel time data to accurate depth models, constraining the type and thickness of material throughout the study area.

Forward models were created using SeisWide, a software developed by Dr. Deping Chian, which utilizes the ray tracing algorithm written by Zelt and Ellis [1988]. In the modeling process, the effects of varying layer thickness, velocity and/or velocity gradient to observe changes produced in arrival time, hyperbolic shape from reflected arrivals, as well as the slope and length of refracted arrivals through layers with a velocity gradient were evaluated.

Primary limitations in the iterative forward modeling process include: (1) it cannot provide the sense of non-uniqueness of any best-fit model, (2) trial-and-error modeling is a time consuming process, and (3) the modelers' predisposition to fit the data to meet a specific subsurface setting (Zelt and Smith, 1992; Zelt, 1999). SeisWide allowed for manipulation of the velocity-depth models to produce a variety of travel time curves. Ray tracing of models could be performed and modeled T/X curves were compared to observed data to allow model adjustment to fit the data. Model layer boundaries could be fine-tuned to a 1 m scale allowing arrival picking and ray tracing to +/- .01 s accuracy.

Sonobuoy Forward Models

The first task of this study was to construct two end-member models and compare the ray traced travel time-range results to observed sonobuoy records in the East Mariana and Pigafetta Basins where drilling results provide "ground-truth" constraints. The first end-member model corresponds to low-velocity sediments on top of normal oceanic crust (Figure 11). The second

model has a thin, high-velocity layer within sediment Layer 1 (a sill), overlying low-velocity sediments and normal oceanic crust (Figure 12). Subsequently, modeled travel times from respective models were compared to sonobuoy data in the Pigafetta Basin where sediments and oceanic crust were recovered at ODP Site 801, and East Mariana Basin where Abrams et al. [1993] interpret a high velocity sill overlying low-velocity sediments and normal oceanic crust (Figure 13). The successful modeling of a "known" sub-surface structure that is analogous to structure predicted by two competing tectonic models sets the stage for forward modeling of data in the southern Nauru Basin.

SEISMIC OBSERVATIONS AND RESULTS

Sonobuoy Analyses

Reflections in MCS data can be correlated to reflections from each of the three sonobuoys examined in this paper. The reflection horizons identified by Shipley et al., [1993] and interpreted in terms of the lithostratigraphy at DSDP Site 462 are included in the forward models.

Sonobuoy 6 displays the most detailed information with reflection data that can easily be compared to MCS data (Figures 14 and 15). Iterative forward modeling produced arrivals matching the observed T/X data (Figure 16). All reflections identified by Shipley et al., [1993] are matched by model reflections and the resulting subsurface-velocity structure is consistent with relatively low-velocities expected from the Shipley et al.,

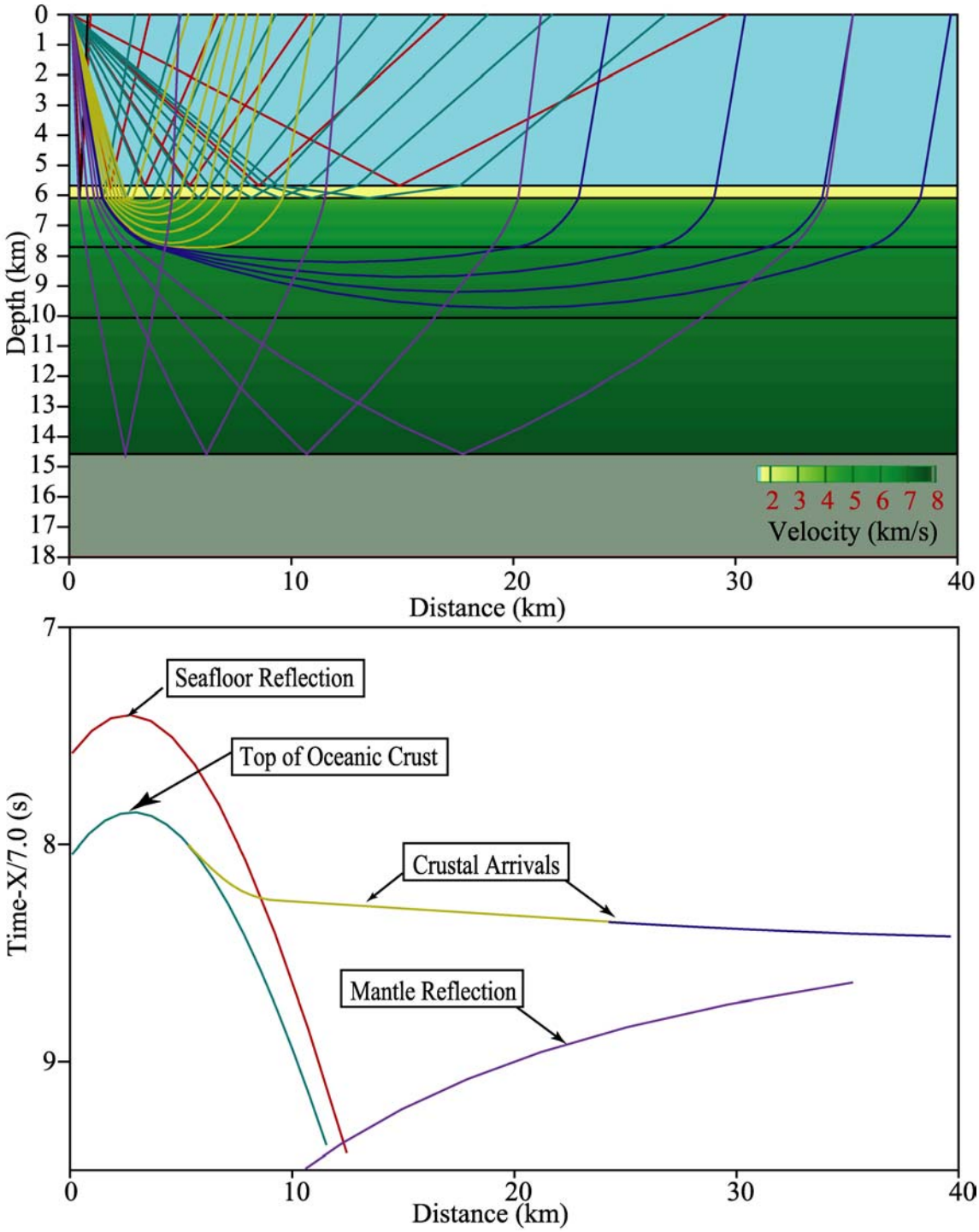

Figure 11. (Top) End-member forward model depicting the structure of oceanic crust. Sediment and crustal layer thickness and velocities are based on average results from White et al. [1992]. (Below) Observed travel time-range data depicting arrivals reflected off the seafloor, the top of oceanic crust and the MOHO. The travel times are colored according to their specific ray group. Refracted crustal arrivals are modeled tangent to reflected arrivals off the top off oceanic crust.

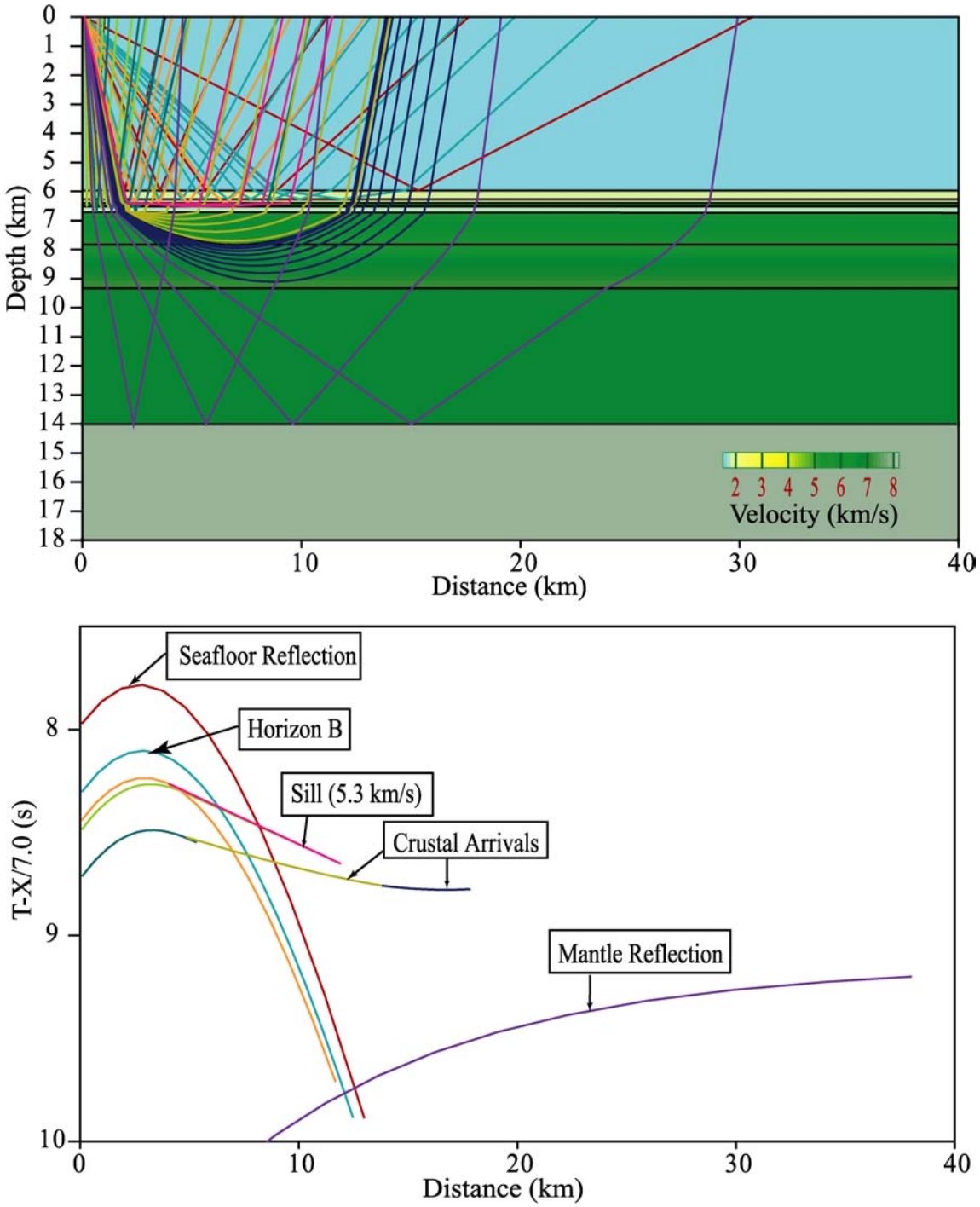

Figure 12. (Above) End-member forward model showing thin, high velocity layer within sedimentary Layer 1. (Below) Observed travel time-range plot with travel times are colored according to their specific ray group. Note the high velocity refraction tangent to a shallow reflection from the top of the high velocity layer. Both arrivals precede deeper crustal reflected and refracted arrivals from normal oceanic crust.

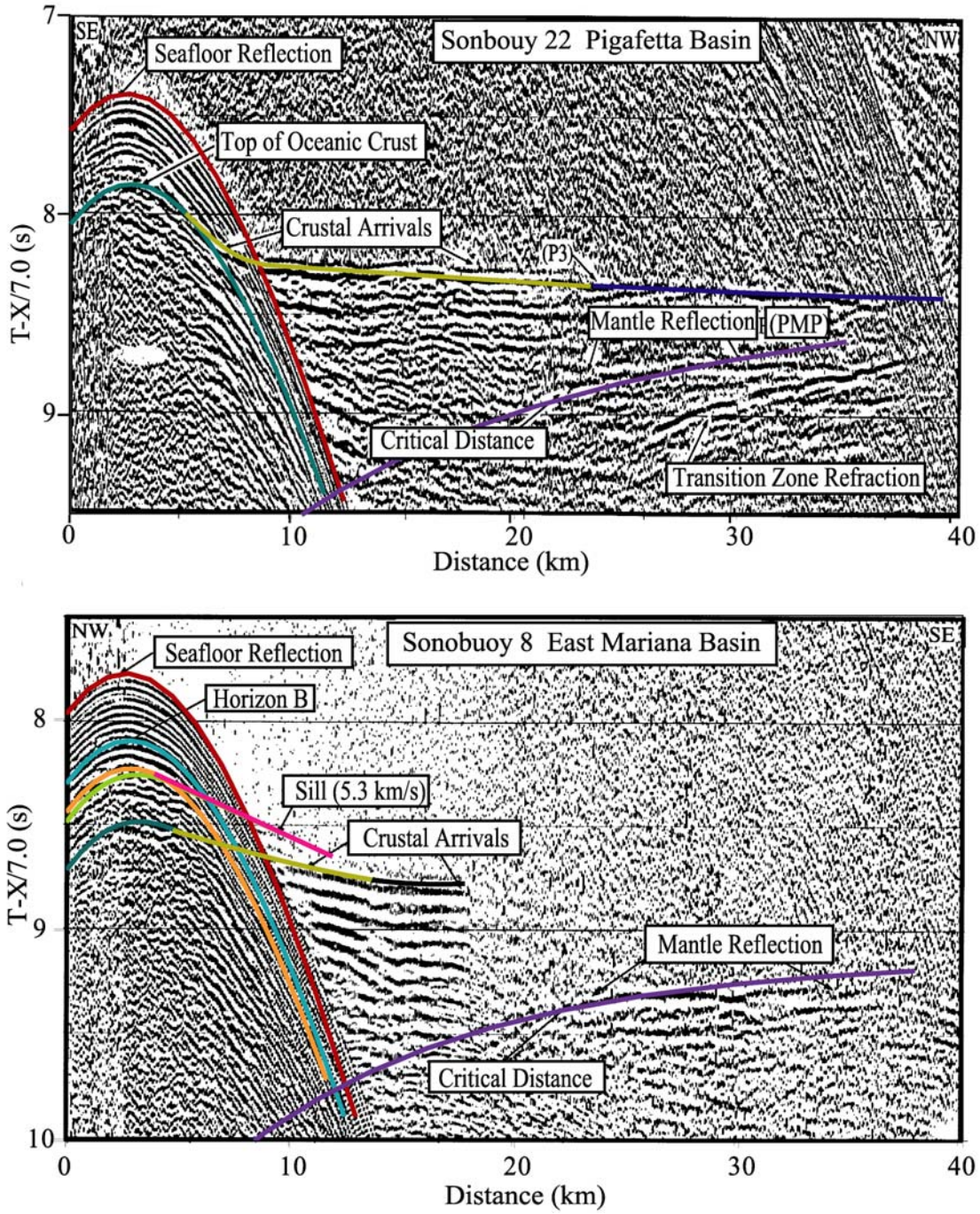

Figure 13. Modeled versus observed travel times from sonobuoy data acquired in the Pigafetta and East Mariana Basins. (Top) Modeled travel times compare well with Sonobuoy 22 data over normal oceanic crust. (Bottom) In order to match the observed data, modeled travel times require a thin sill within a sedimentary section overlying oceanic crust.

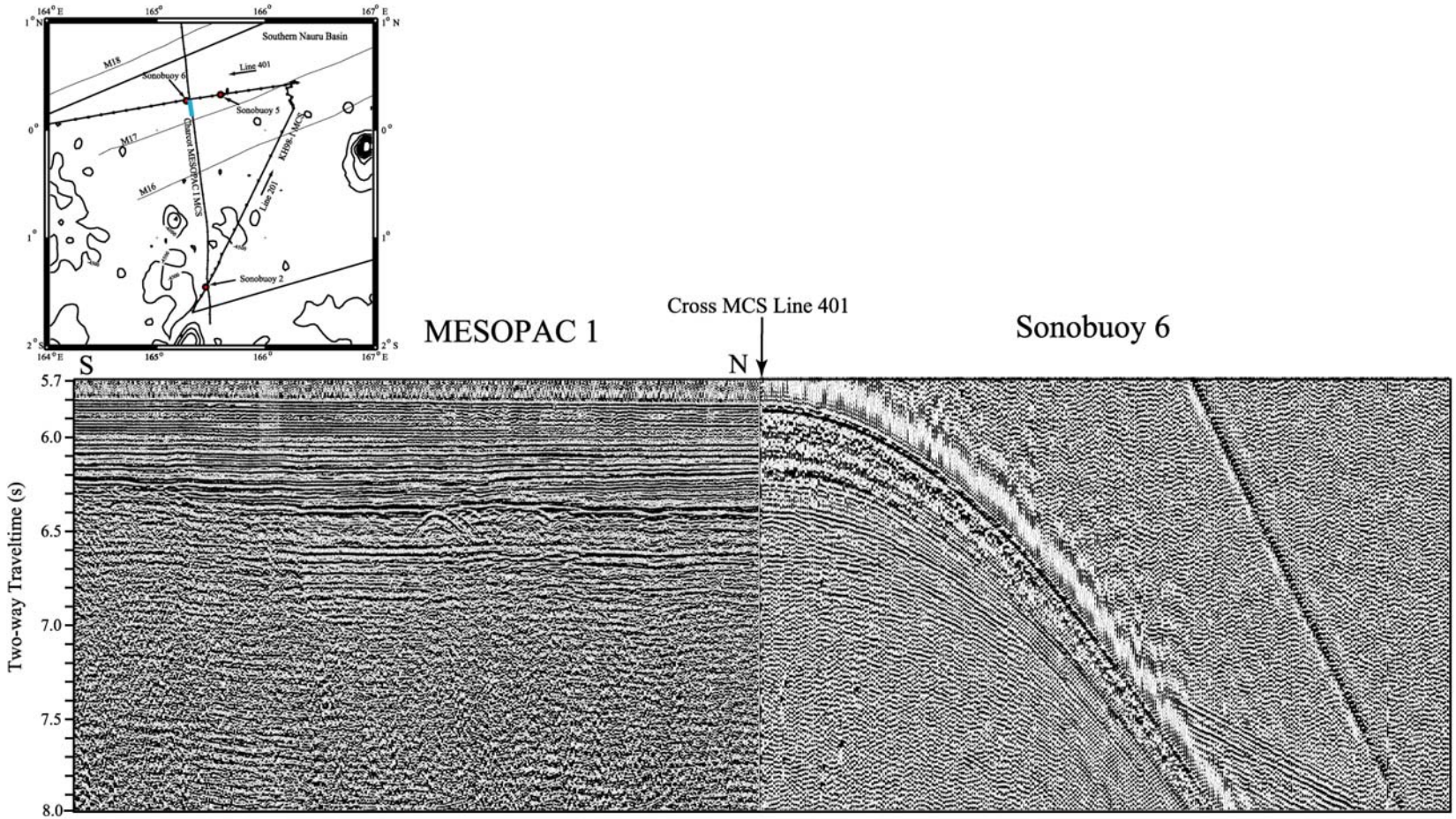

Figure 14. Merged reflection profiles of Sonobuoy 6 and its range over MCS MESOPAC I. An index map shows the location of MCS data (thick blue line) coincident with Sonobuoy 6. Significant reflections can be seen both in the sonobuoy record and coincident reflection profile initially interpreted by Shipley et al. [1993] based on reflection character. A refracted arrival is tangent to a reflection

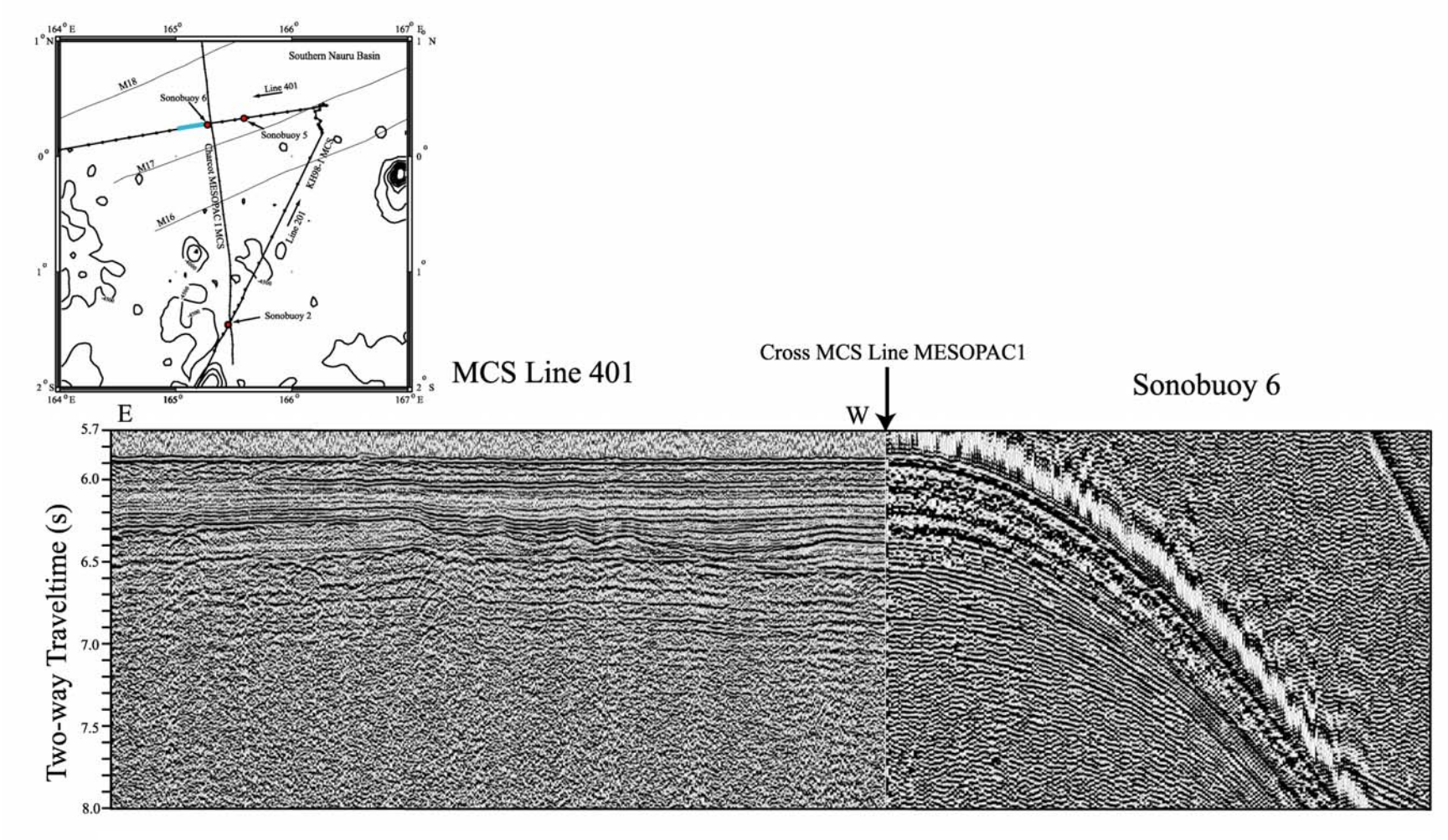

Figure 15. Merged reflection profiles of Sonobuoy 6 and its range over MCS Line 401. An index map shows the location of MCS data (thick blue line) coincident with Sonobuoy 6. Significant reflections can be seen both in the sonobuoy record and coincident reflection profile where Line 401 intersects MESOPAC 1. A refracted arrival is tangent to a reflection (~6.55 stwt) interpreted as a sill/flow.

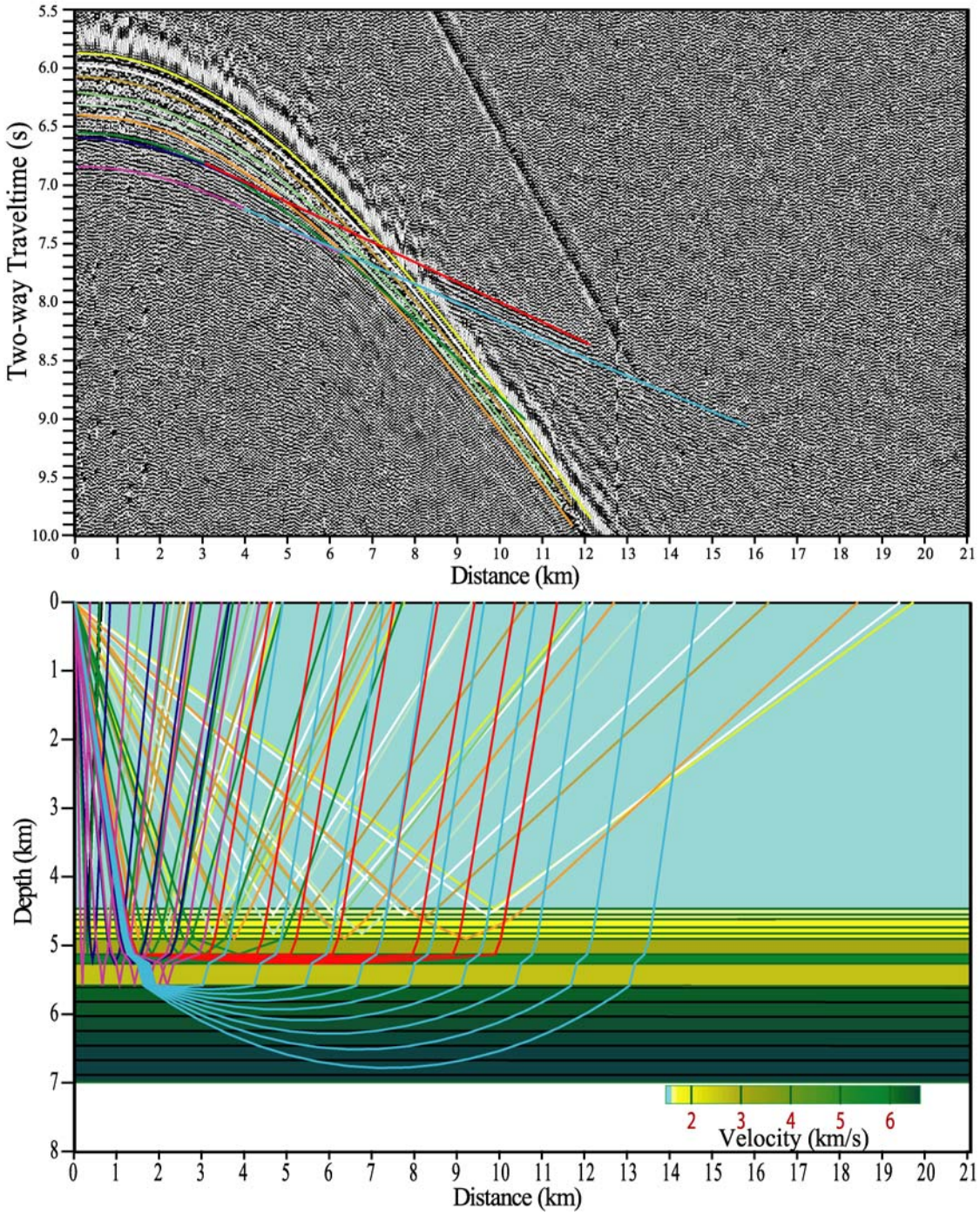

Figure 16. (Top) A comparison of modeled versus observed travel time-range data from Sonobuoy 6. Note the refraction arrives later than the high amplitude reflection corresponding to the top of the Cretaceous volcanic unit (~6.3 stwt) correlated from DSDP Site 462. (Bottom) Ray traced forward model of Sonobuoy 6 deployed at the intersection of MCS Line 401 and MESOPAC I while shooting the MCS data. The forward model requires unusually high velocity, low gradients in upper oceanic crust.

[1993] interpretation (Figure 17). The Cretaceous volcanic unit Kv is modeled with low velocities and is interpreted as a thin volcaniclastic unit.

A prominent refraction is observed as a first arrival beginning at ~ 8 km range and extending to 12 range (Figure 16). This refraction requires a relatively thin (0.133 km thick), high velocity (5.830 km/s), and low-velocity gradient layer (i.e., a nearly constant high velocity layer) inserted between two layers of relatively low velocity (3.0 km/s). This prominent refraction is observed to be tangent to a high amplitude reflection at ~6.564 stwt on both MCS and sonobuoy records. This distinct reflection was interpreted as a sill/flow (Figure 7) based only on its very high reflection amplitude (Shipley et al., 1993). The results of forward modeling provide velocity structure confirming this interpretation

In addition, a refraction was observed and modeled in the sonobuoy record tangent to a rough reflection at ~6.840 stwt in the MCS data. The refraction was modeled out to ~16.0 km range with high seismic velocities (~6.190 km/s) and with a velocity gradient smaller than Layer 2 oceanic crust. Thus, the Sonobuoy 6 data further support the Shipley et al., [1993] interpretation of a thin sill/flow within low velocity sediments, however the velocity data poorly constrain the presence of oceanic crust (Figure 18).

Reflections facies and interval velocities modeled from Sonobuoy 6 can be correlated along MESOPAC I coincident MCS reflection data along Line 401 to the location where Sonobuoy 5 was deployed (Figure 19-21). The major difference between Sonobuoy 5 and Sonobuoy 6 data are slightly lower interval velocities for each layer in the sonobuoy 5 model, but still well within the range of sedimentary strata and high velocity volcanic intrusion (Figure 22). The refracted first arrival in this data set is shorter (out to ~10.458

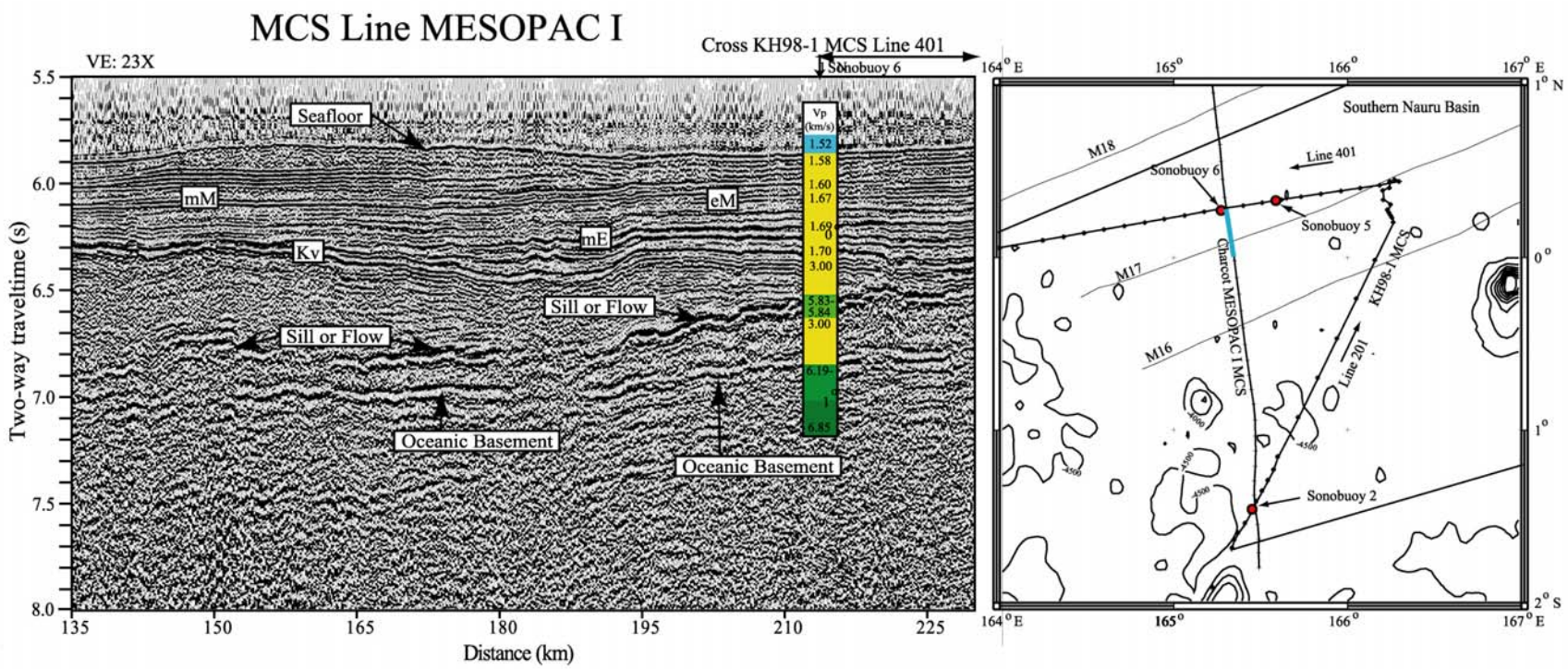

Figure 17. A section of the MESOPAC I MCS data (thick blue line) with the velocities obtained from modeling Sonobuoy 6 shown in the colored column. Velocity data support the Shipley et al. [1993] interpretation of thin sills/flows within sediments overlying oceanic crust.

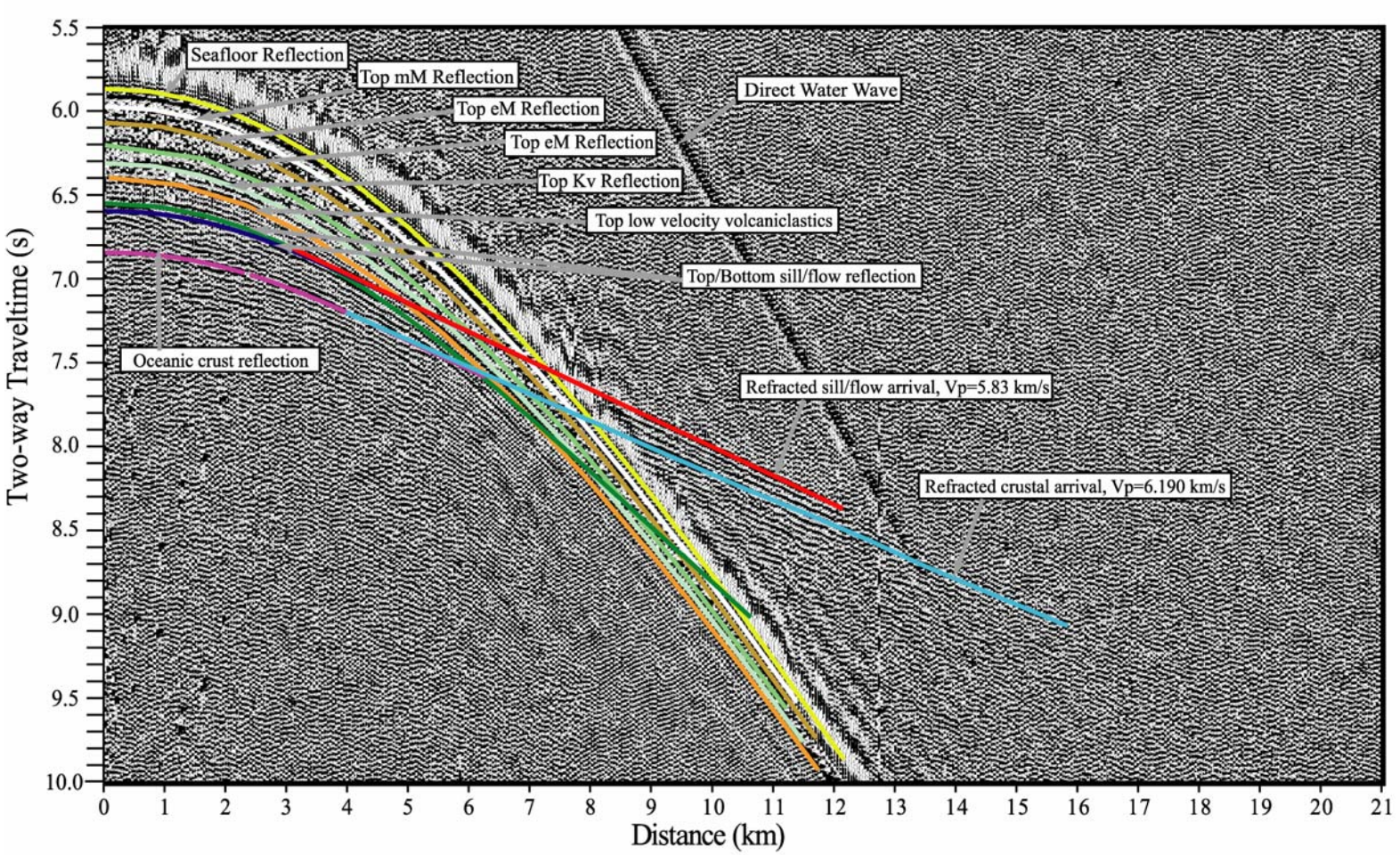

Figure 18. Modeled travel time-range curves on observed data from Sonobuoy 6. Significant reflections identified in MCS data by Shipley et al., [1993] are labeled. Note that refracted arrivals are tangent to reflections identified as sill/flow and oceanic crust.

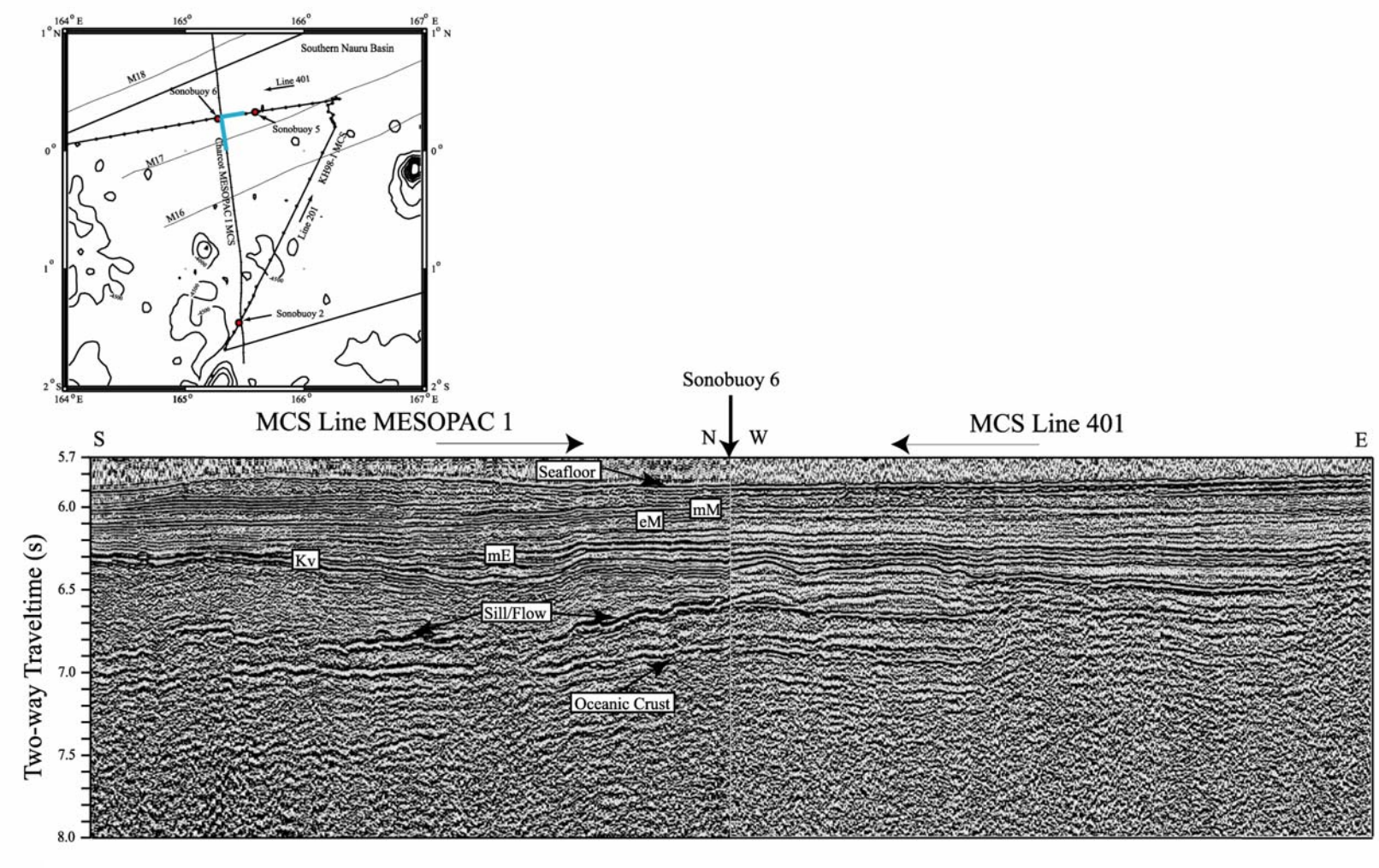

Figure 19. Intersection of MCS Line 401 and MESOPAC 1. An index map shows the location of intersecting MCS lines (thick blue lines). Reflections were identified, modeled, and correlated along both MCS reflection profiles with the addition of velocity analysis from Sonobuoy 6 data.

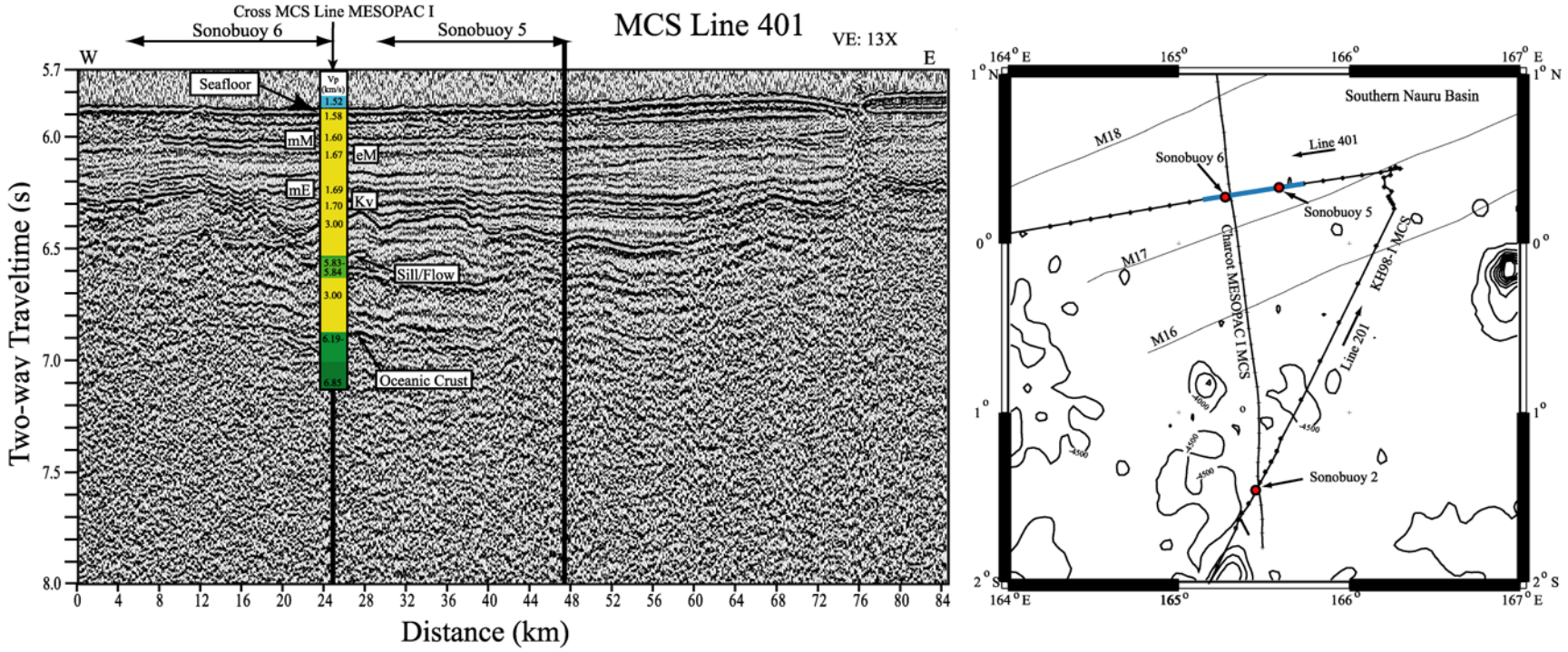

Figure 20. A section of the Line 401 MCS data with the velocities obtained from modeling Sonobuoy 6 shown in the colored column. An index map shows the location of MCS data (thick blue line).Modeling of Sonobuoy 6 allowed for correlation of seismic facies and velocities along Line 401 to the location where Sonobuoy 5 was deployed.

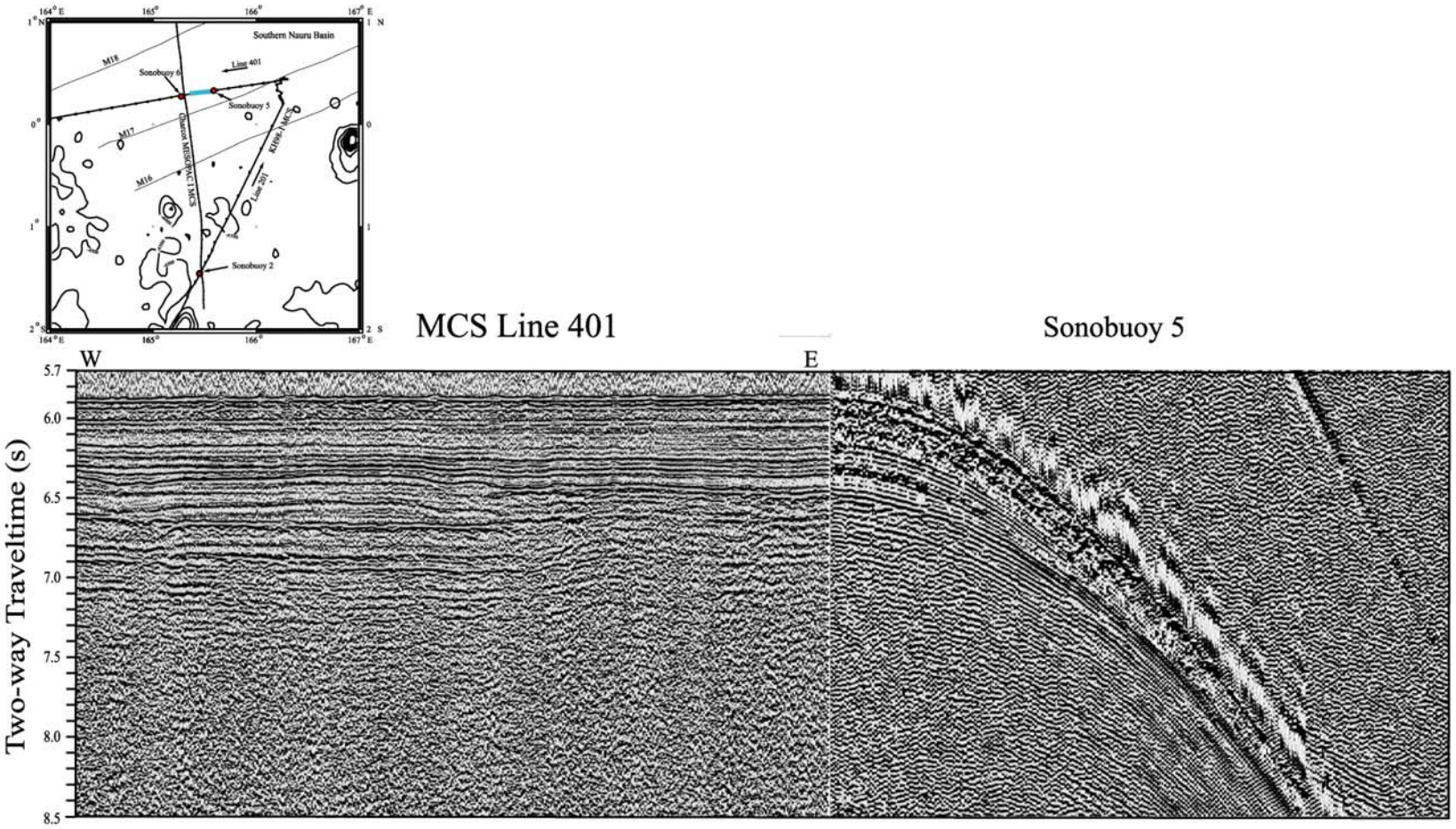

Figure 21. Merged reflection profiles of Sonobuoy 5 and its range over MCS Line 401. An index map shows the location of MCS data (thick blue line) coincident with Sonobuoy 5. Significant reflections can be seen both in the sonobuoy record and coincident reflection profile where Sonobuoy 5 was deployed. Similar to Sonobuoy 6 results, a shorter refracted arrival is tangent to a reflection interpreted as a sill/flow. A deeper reflection is seen below a thin, high velocity sill and low velocity sediments. This deeper reflection is interpreted as oceanic crust.

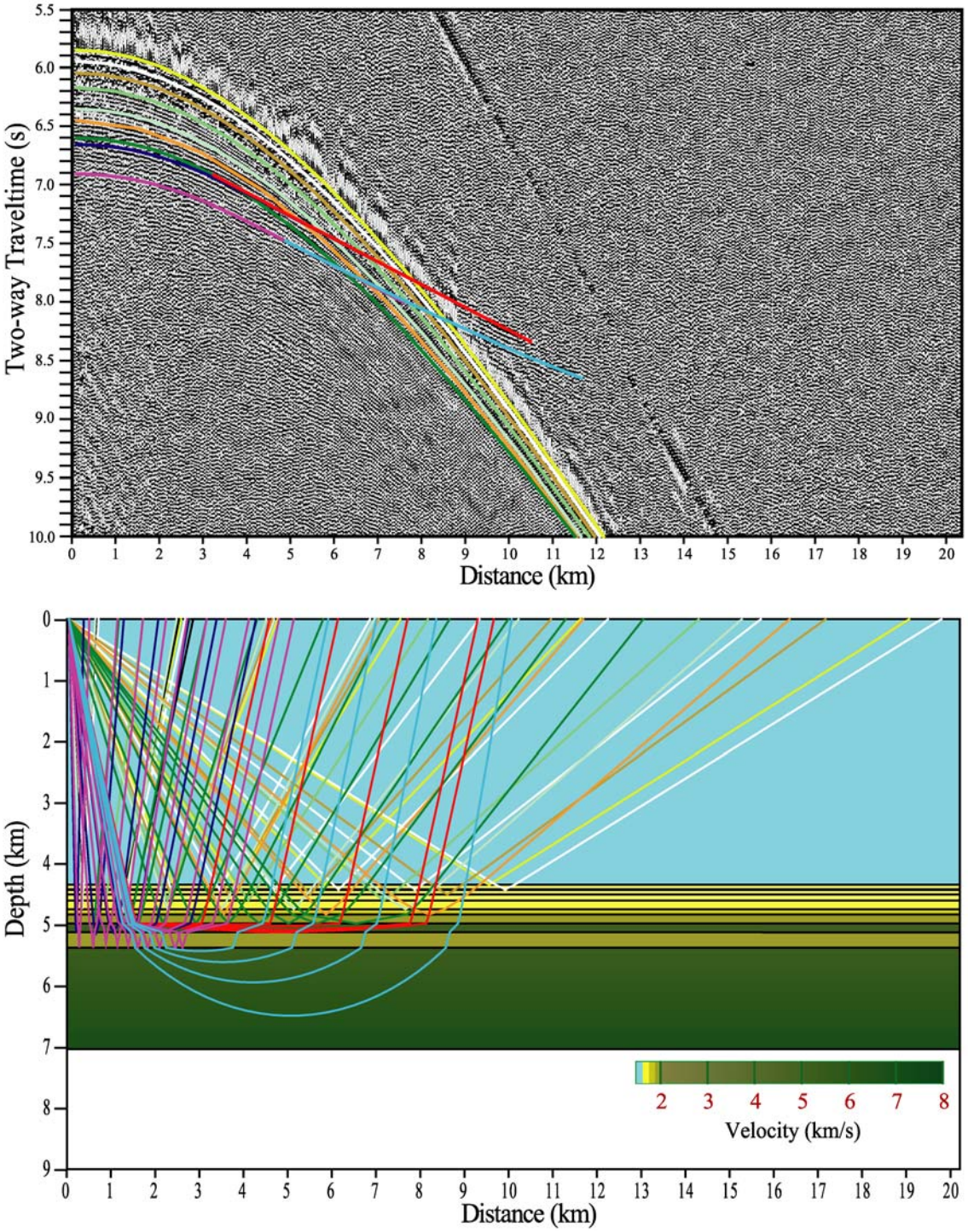

Figure 22. (Top) A comparison of modeled versus observed travel time-range data from Sonobuoy 5. Similar to sonobuoy 6, the refracted arrival returns later than the high amplitude reflection off the top of the Cretaceous volcanogenic layer, indicating deep, previously unsampled material. (Bottom) Ray-traced forward model of Sonobuoy 5 located along MCS Line 401 ~23.5 km east of Sonobuoy 6. Similar to Sonobuoy 6, the forward model requires unusually high velocity gradients in upper oceanic crust.

km range) with a slightly less steep slope than in the Sonobuoy 6 data, indicating a lower interval velocity (~5.100 km/s) and variations in layer thickness and/or velocity gradient (Figure 23). This refraction is tangent to the reflection interpreted as a sill/flow based on its high-amplitude (Shipley et al., 1993). A weak, second arrival refraction was modeled out to 11.90 km range, and is tangent to the deep reflection at 6.89 stwt identified as the top of oceanic crust (Shipley et al., 1993) (Fig 7, Figure 24). Again, the velocities and velocity gradients used to model the refraction are unlike those of Layer 2 crust, and make it difficult to interpret the sonobuoy data imaging arrival from original crust (Figure 22).

Seismic facies from the Shipley et al. [1993] interpretation could be traced to the intersection with MCS Line 201, allowing for more precise arrival picking and modeling of the Sonobuoy 2 data (Figure 25 & 26). A distinct refraction is imaged in the data out to 12.120 km tangent to a reflection at ~6.595 stwt and modeled with velocities typical of Layer 2 oceanic crust (4.65-6.60 km/s) (Figure 27-29). Unlike modeling the refractions in Sonobuoy 5 and 6, the refraction in Sonobuoy 2 is modeled tangent to a lower amplitude, undulating reflection in coincident MCS Line 201 data without the presence of an overlying thin, high-amplitude, high-velocity layer (Figure 30). In addition, tracing the rough reflection along MCS Line 201 to its intersection with MESOPAC I results in its tangency to a reflection interpreted as oceanic crust by Shipley et al. [1993] (Figure 30-32).

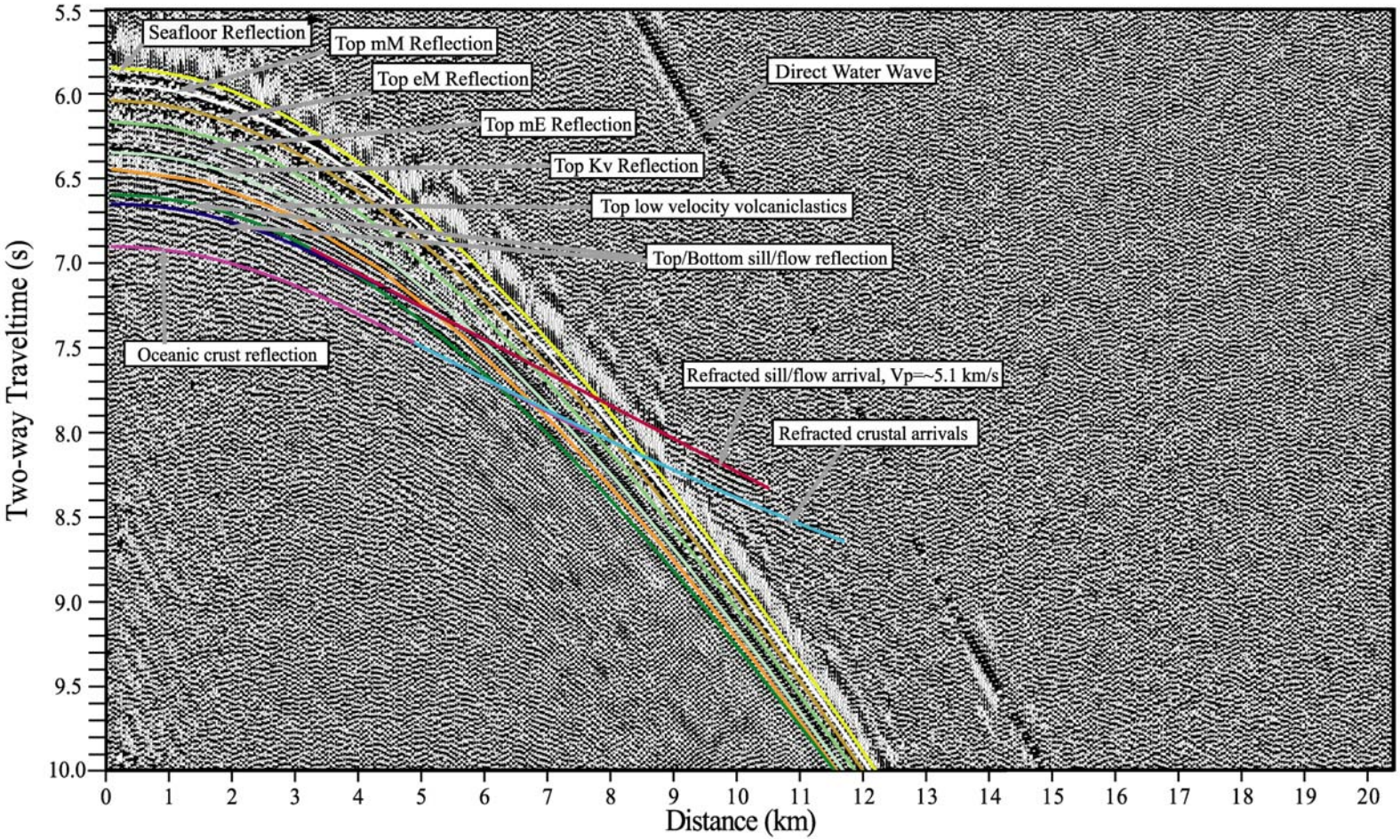

Figure 23. Modeled travel time-range curves on observed data from Sonobuoy 5. Significant reflections identified in MCS data by Shipley et al., [1993] are labeled. Note that refracted arrivals are tangent to reflections identified as sill/flow and oceanic crust.

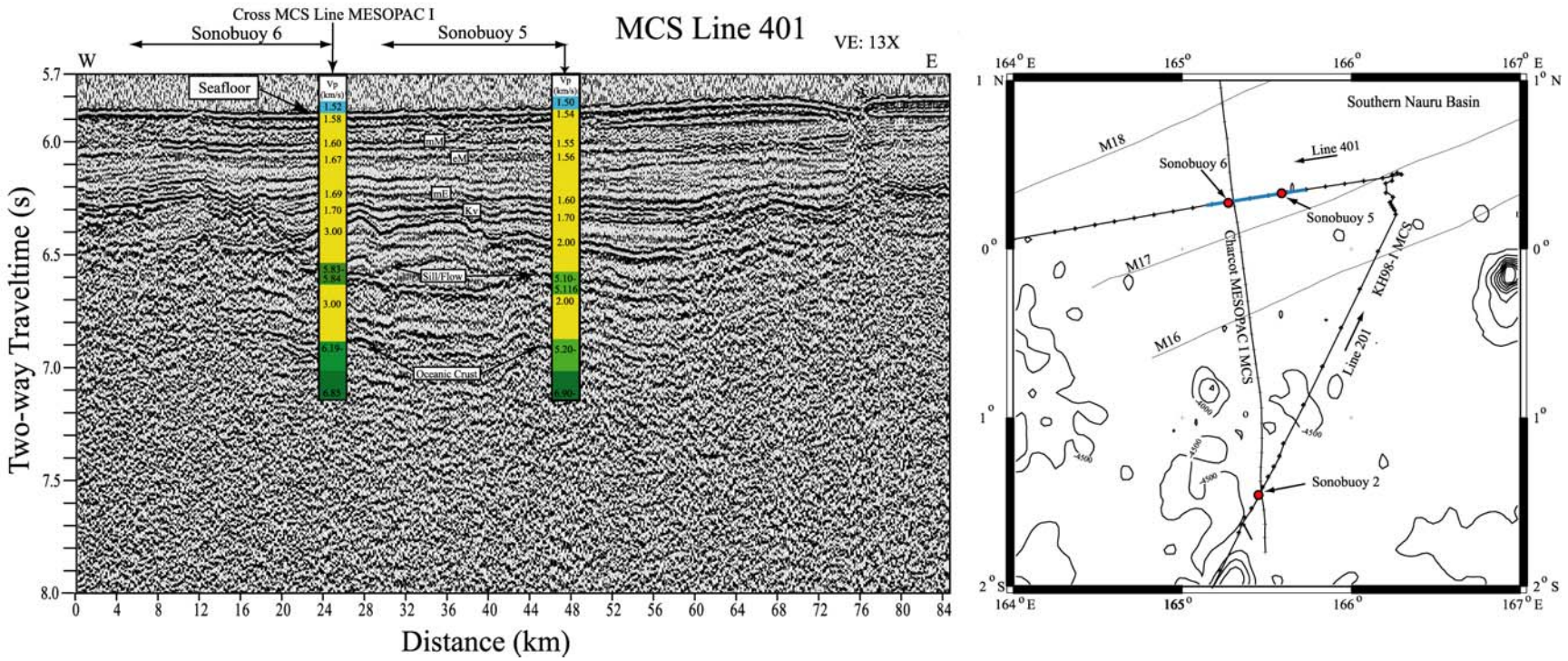

Figure 24. A section of Line 401 MCS data with the velocities obtained from modeling Sonobuoy 6 and 5 shown in the colored columns. The index map shows the location of MCS data (thick blue line). Interval velocities are consistent with the Shipley et al. [1993] interpretation of thin sills/flows within sediments overlying oceanic crust.

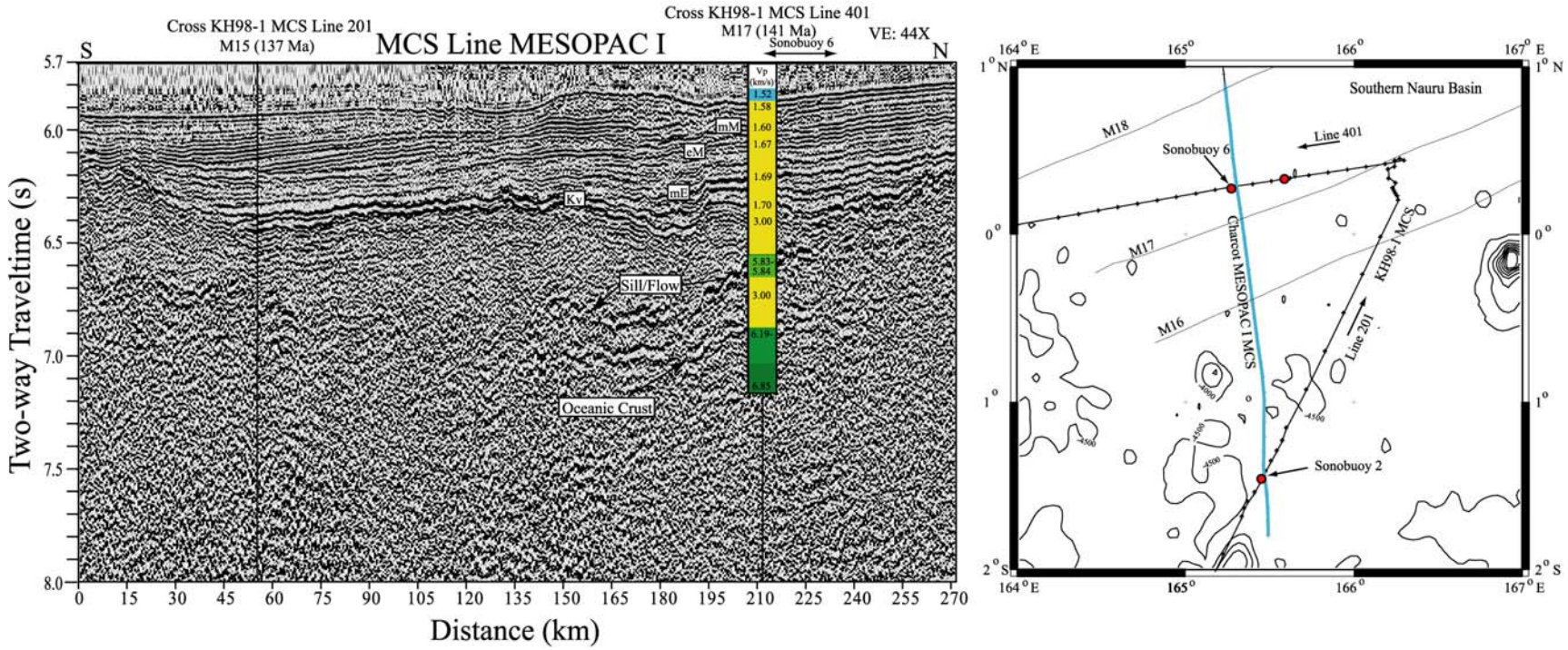

Figure 25. A section of MESOPAC I MCS data with the velocities obtained from modeling Sonobuoy 6 shown in the colored column. The index map shows the location of MCS data (thick blue line). The high amplitude reflection corresponding to high refraction velocities does not appear to extend to the south where MESOPAC I intersects MCS Line 201.

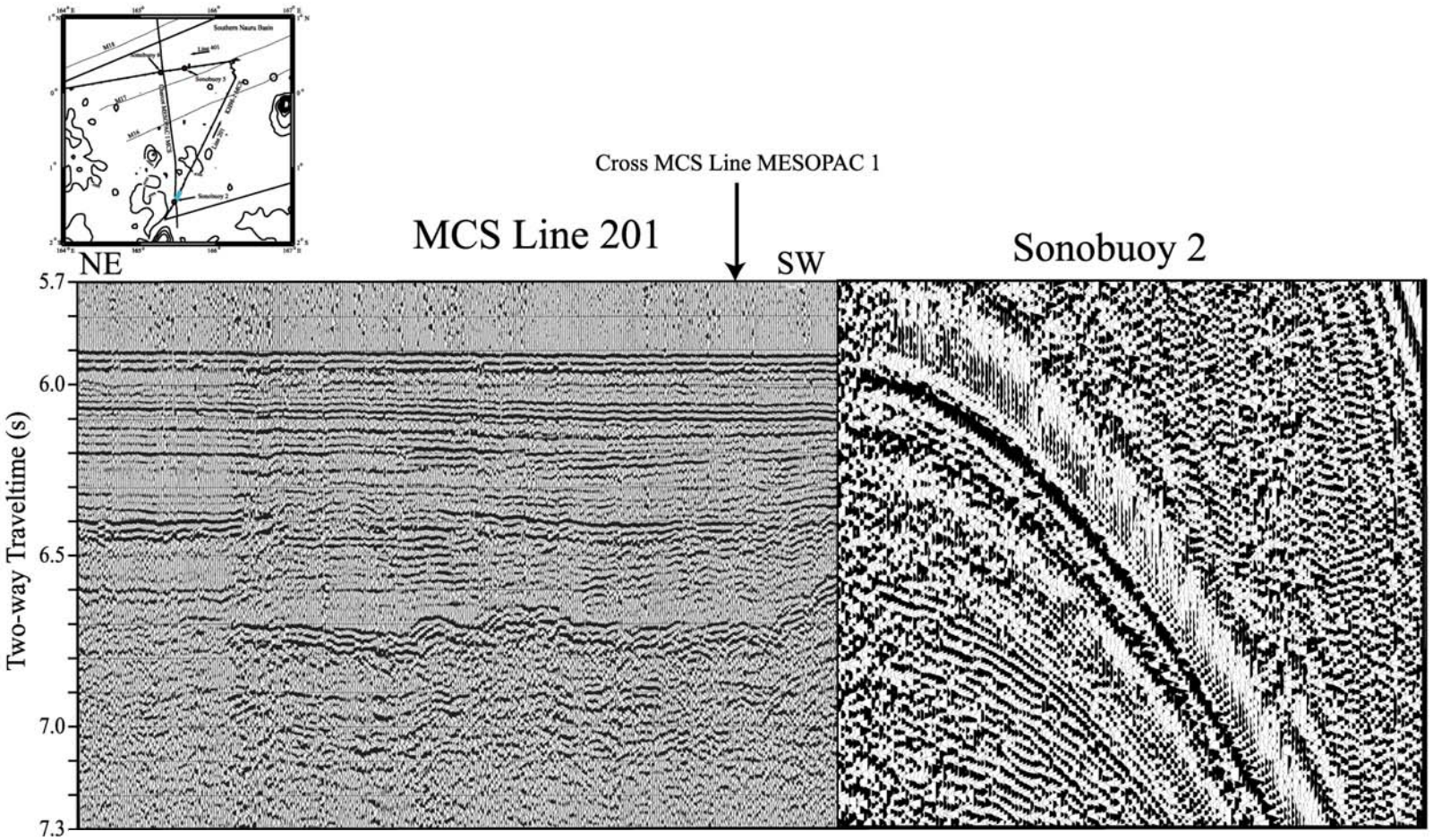

Figure 26. Merged reflection profiles of Sonobuoy 2 and MCS Line 201. An index map shows the location of MCS data (thick blue line) coincident with Sonobuoy 2. A refracted arrival in the T/X record is tangent to a rough reflection surface at ~ 6.6 stwt. This surface denotes the onset of high velocities (4.65 km/s) and is interpreted as the top of Early Cretaceous normal oceanic crust. This data give no indication of a thin sill overlying the original crust.

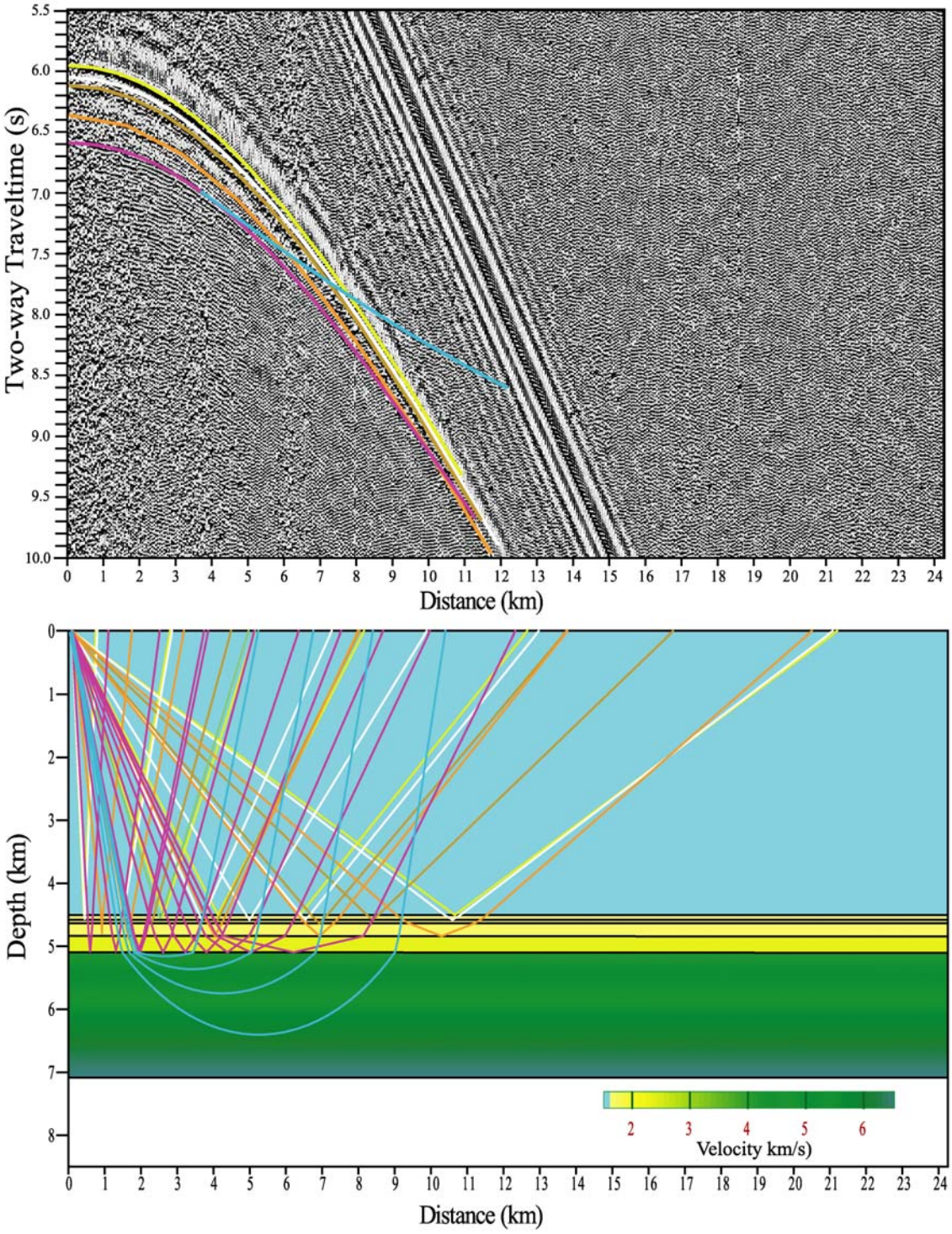

Figure 27. (Top) A comparison of modeled versus observed travel time-range data from Sonobuoy 2. The data indicate a refracted arrival tangent to a reflection (~6.6 stwt) interpreted by Shipley et al [1993] as the top of oceanic crust on MESOPAC I, without the presence of overlying thin sills or flows. (Bottom) Ray traced forward model of Sonobuoy 2 located along MCS Line 201. Modeled crustal velocities and velocity gradients are more fitting for the range of velocities that characterize upper oceanic crust.

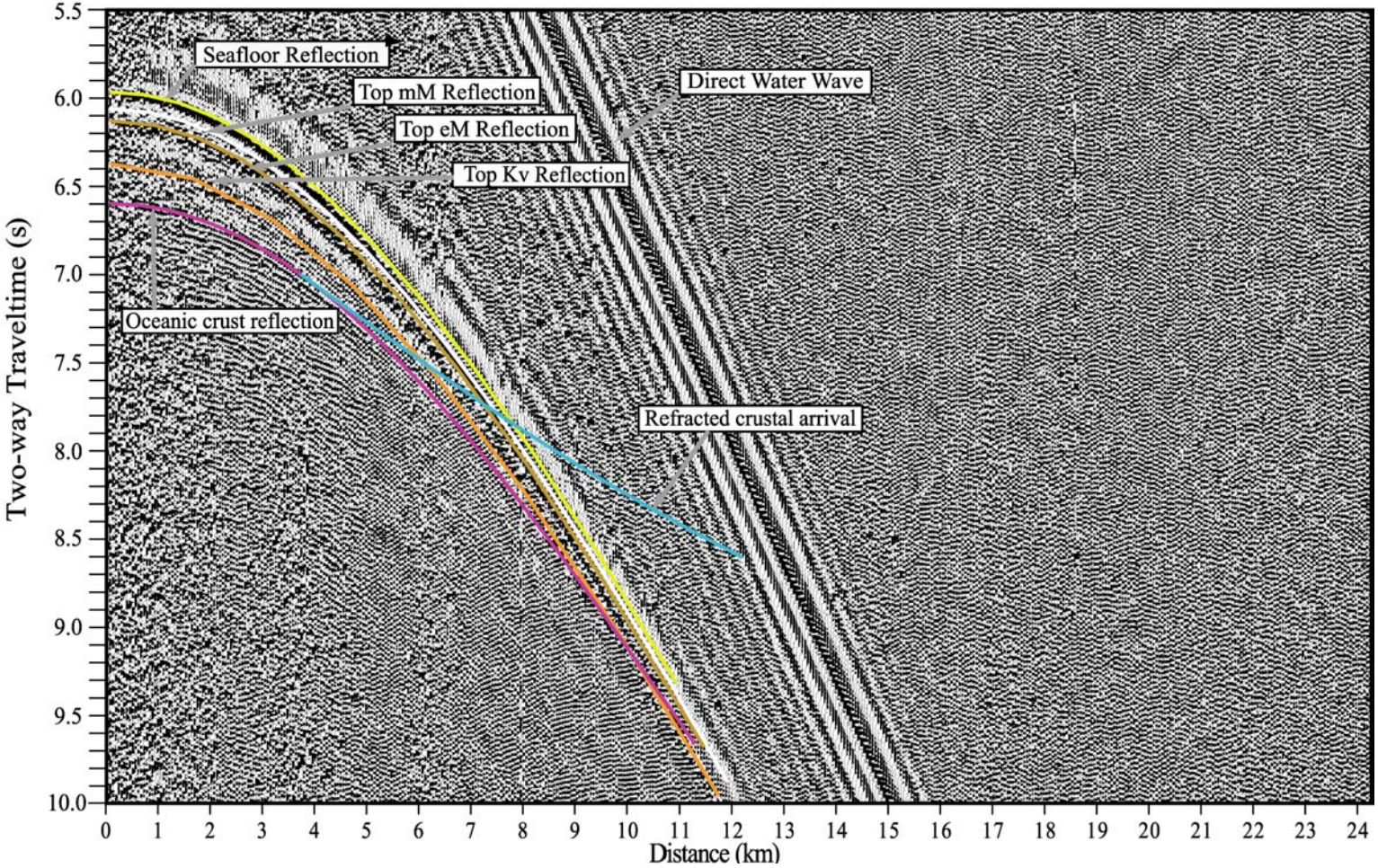

Figure 28. Figure 23. Modeled travel time-range curves on observed data from Sonobuoy 2. Significant reflections identified in MCS data by Shipley et al., [1993] are labeled. Note that a refracted arrival is tangent to a reflection identified as the top of oceanic crust.

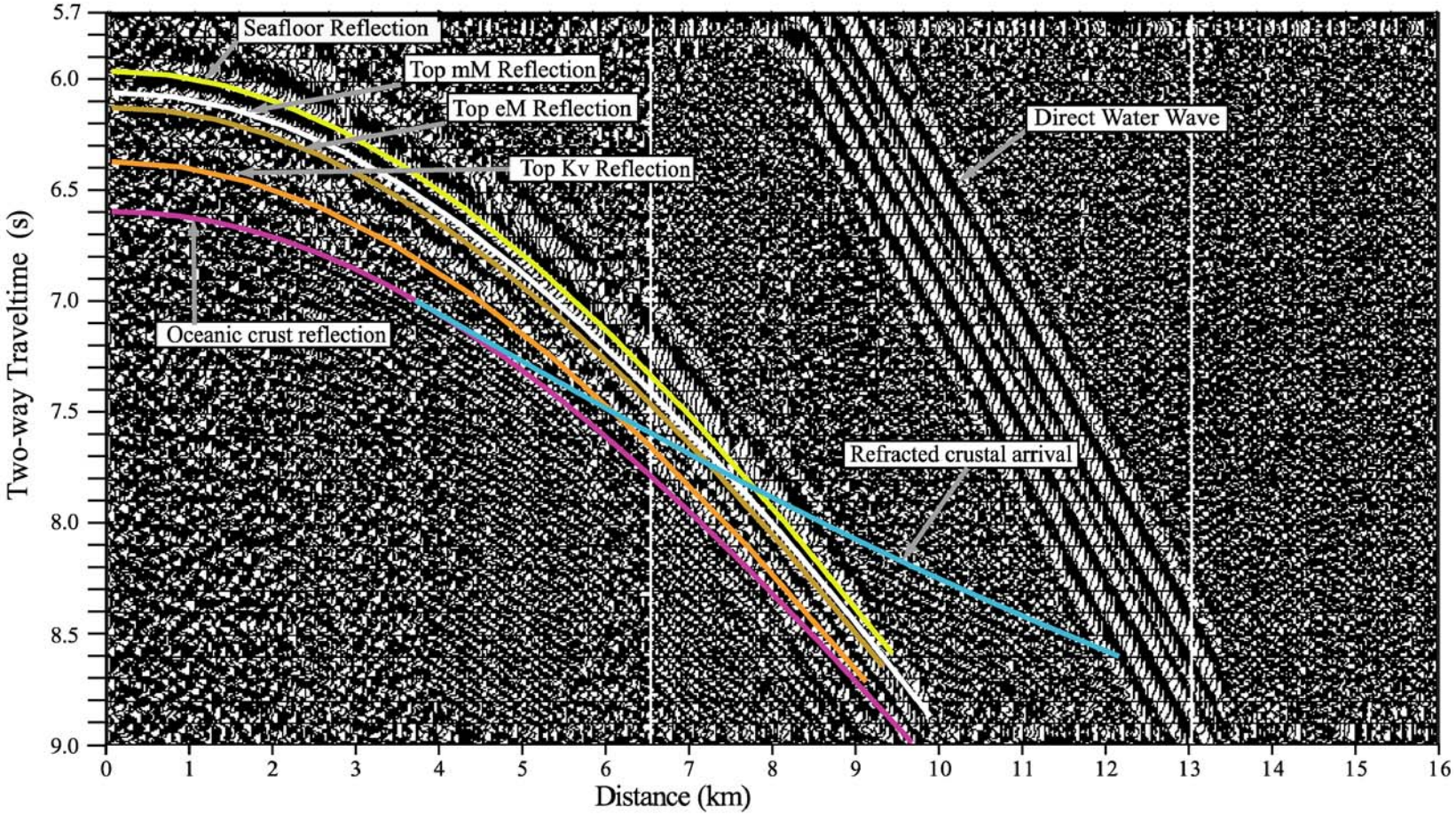

Figure 29. Magnified view of Sonobuoy 2 illustrating the ray traced reflected and refracted arrivals. The refraction modeled out to ~12 km is seen tangent to a reflected arrival at ~6.6 s and interpreted as the reflection off the top of oceanic crust.

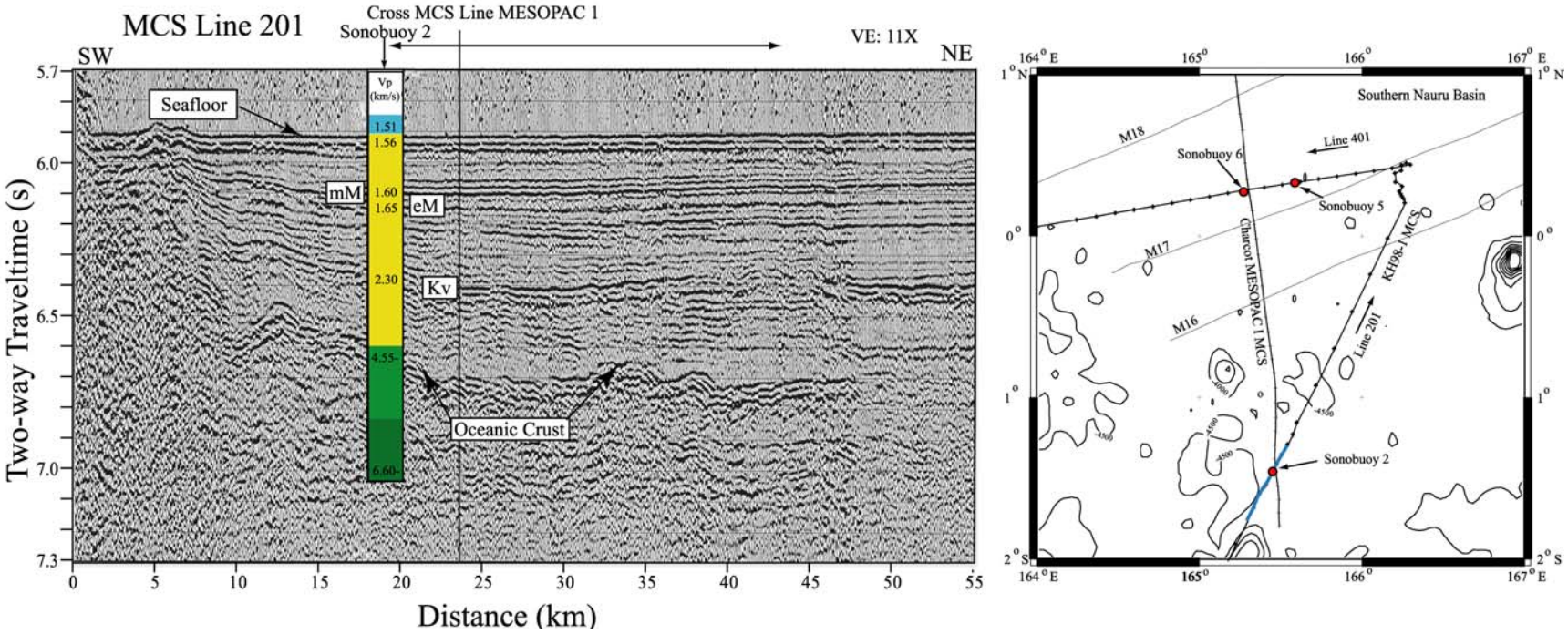

Figure 30. A section of MCS Line 201 data with the velocities obtained from modeling Sonobuoy 2 shown in the colored column. The index map shows the location of MCS data (thick blue line). Reflection facies and velocities from Sonobuoy 2 data could be correlated to the intersection of MCS Line 201 with MCS Line MESOPAC I.

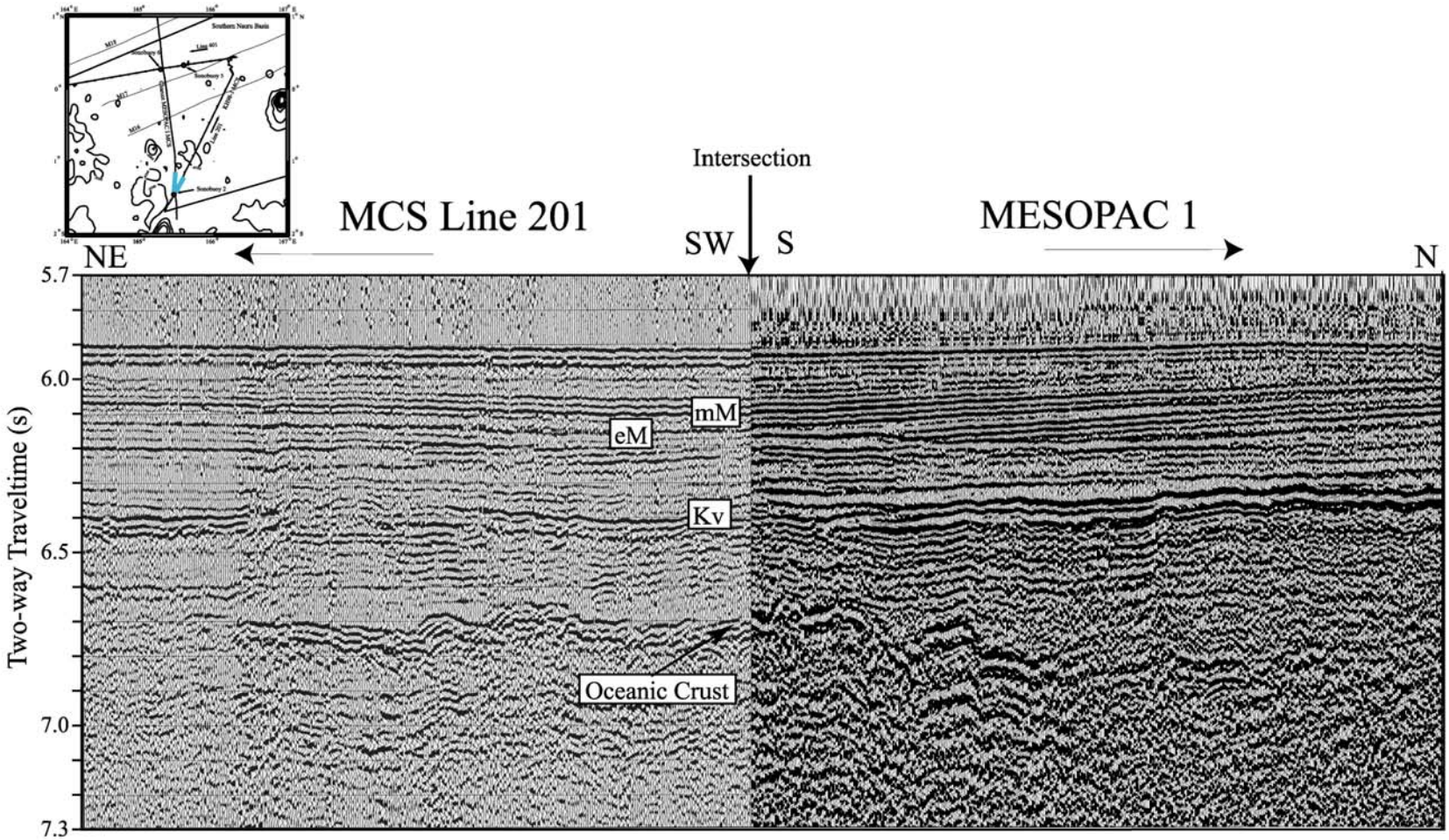

Figure 31. Intersection of MCS Line 201 and MESOPAC 1. An index map shows the location of intersecting MCS lines (thick blue lines). Reflections were correlated along both MCS profiles with the addition of velocity structure from Sonobuoy 2 data collected along Line 201. The undulating reflection at ~6.7 stwt is interpreted as the top of oceanic crust on the MESOPAC 1 profile by Shipley et al. [1993].

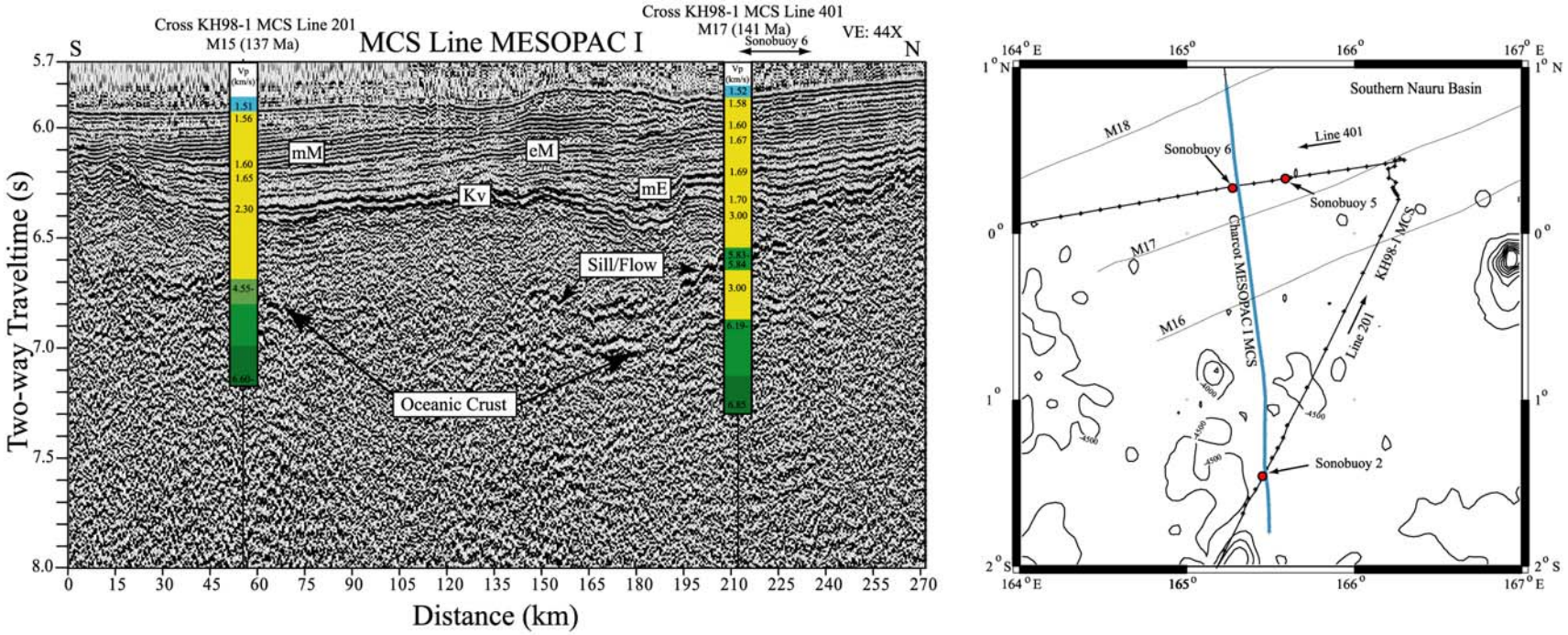

Figure 32. A section of MCS Line MESOPAC I data with the velocities obtained from modeling Sonobuoy 2 and 6 shown in the colored columns. The index map shows the location of MCS data (thick blue line), and the extent of the sill/flow complex in the study area. Interval velocities support the Shipley et al. [1993] interpretation for the presence of thin sills/flows within sediments overlying oceanic crust in the northern part of the study area. Sonobuoy 2 data provide interval velocities supporting the Shipley et al., [1993] interpretation of oceanic crust without overlying thin sills/flows in the southernmost Nauru Basin.

Reflection Data Analysis

With ray-traced velocity-depth models constructed to match observed sonobuoy data (Figure 33), travel time data were converted to depth sections over the range of each sonobuoy along coincident MCS reflection profiles. Two-way travel times were converted to depth at vertical incidence where sonobuoys were located along reflection profiles. Magnification of specific model areas of interest allowed for precise digitizing of individual layer boundaries across the velocity model projected on top of the resultant depth section, based on seismic reflection character.

The results of this study are displayed as depth sections (Figures 34-37) and time sections (Figures 38-40). The cross sections were constructed after modeling the sonobuoy data, then digitizing distinct, coincident reflection surfaces based on individual seismic facies throughout the southern Nauru Basin. Notable horizons include the seafloor, various DSDP Site 462 units, volcanic sills/flows and oceanic crust. The selected horizons are based on lithologies collected at DSDP Site 462, seismic facies interpreted by Shipley et al. [1993], and are constrained with sonobuoy refraction data.

MESOPAC 1 reflection data reveal an undulating, rough, reflection surface that was interpreted as the top of normal oceanic crust (Figures 32 and 38, Shipley et al., 1993). Reflection data from KH98-1 confirm this reflection attribute and are consistent with the Shipley et al., [1993] interpretation (Figures 24 and 39). MCS Line 401 shows oceanic crust of lower relief, most likely due to the near-parallel orientation of the seismic line with respect to magnetic anomaly lineations and ridge spreading direction (Figure 3 and 39). The depths to the top of oceanic crust range from a minimum of ~650 mbsf along MCS Line 201, to a maximum of ~1250 mbsf along MESOPAC 1.

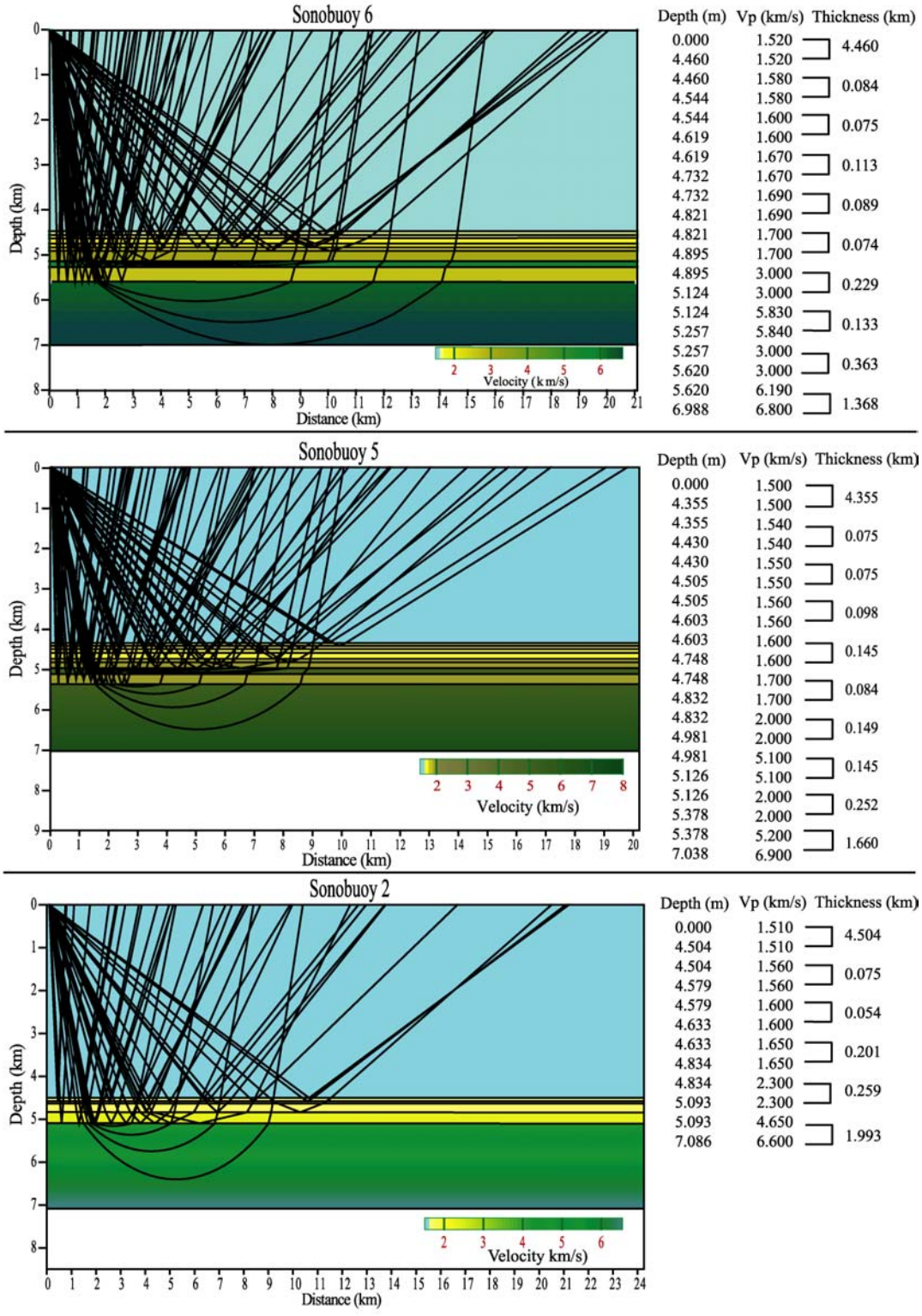

Figure 33. Ray-traced forward models of the three sonobuoys modeled in this study, adjacent to which are tables depicting subsurface depth, p-wave velocity, and individual thickness for each layer.

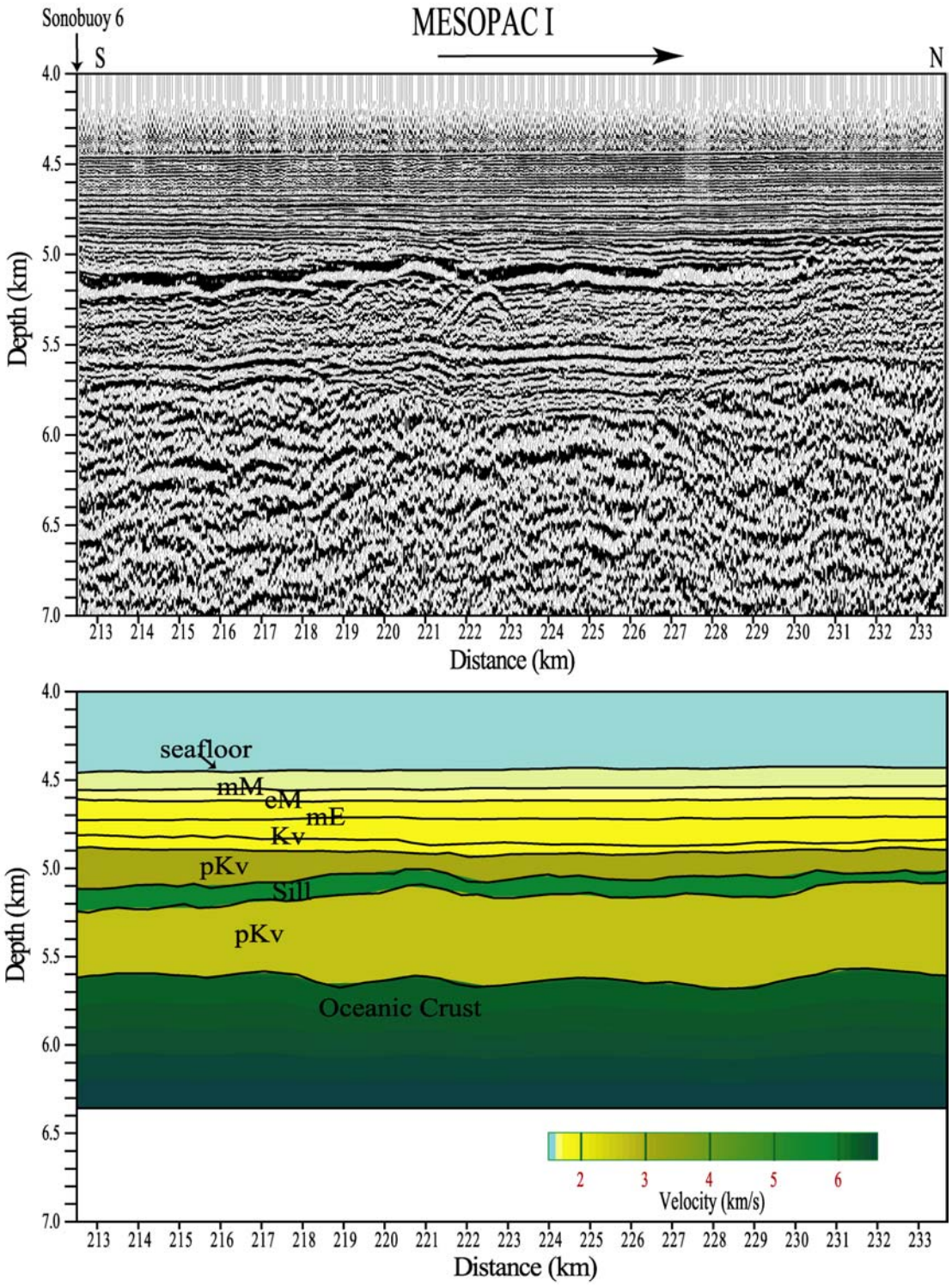

Figure 34. Depth section derived from conversion of MCS Line MESOPAC I two-way travel time data to depth using the velocity model derived from Sonobuoy 6.
The labeled horizons include units recovered at DSDP Site 462 (mM, eM, mE, Kv), and what Shipley et al. [1993] interpret as a thin sill within a low velocity sedimentary package (pKv) overlying oceanic crust.

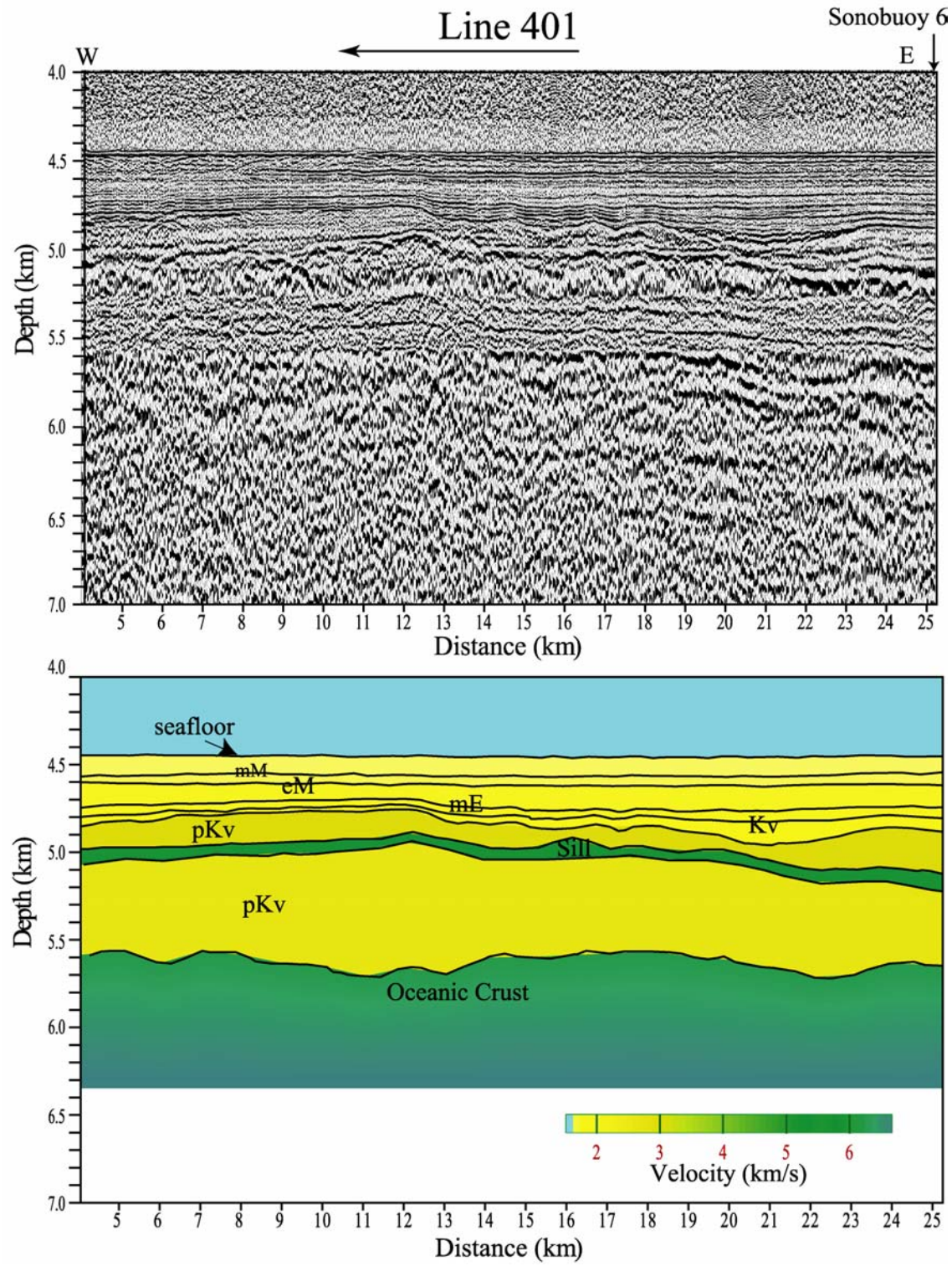

Figure 35. Depth section derived from conversion of MCS Line 401 two-way travel time data to depth using the velocity model derived from Sonobuoy 6. The labeled horizons include units recovered at DSDP Site 462 (mM, eM, mE, Kv), and what Shipley et al. [1993] interpret as a thin sill within a low velocity sedimentary package (pKv) overlying oceanic crust.

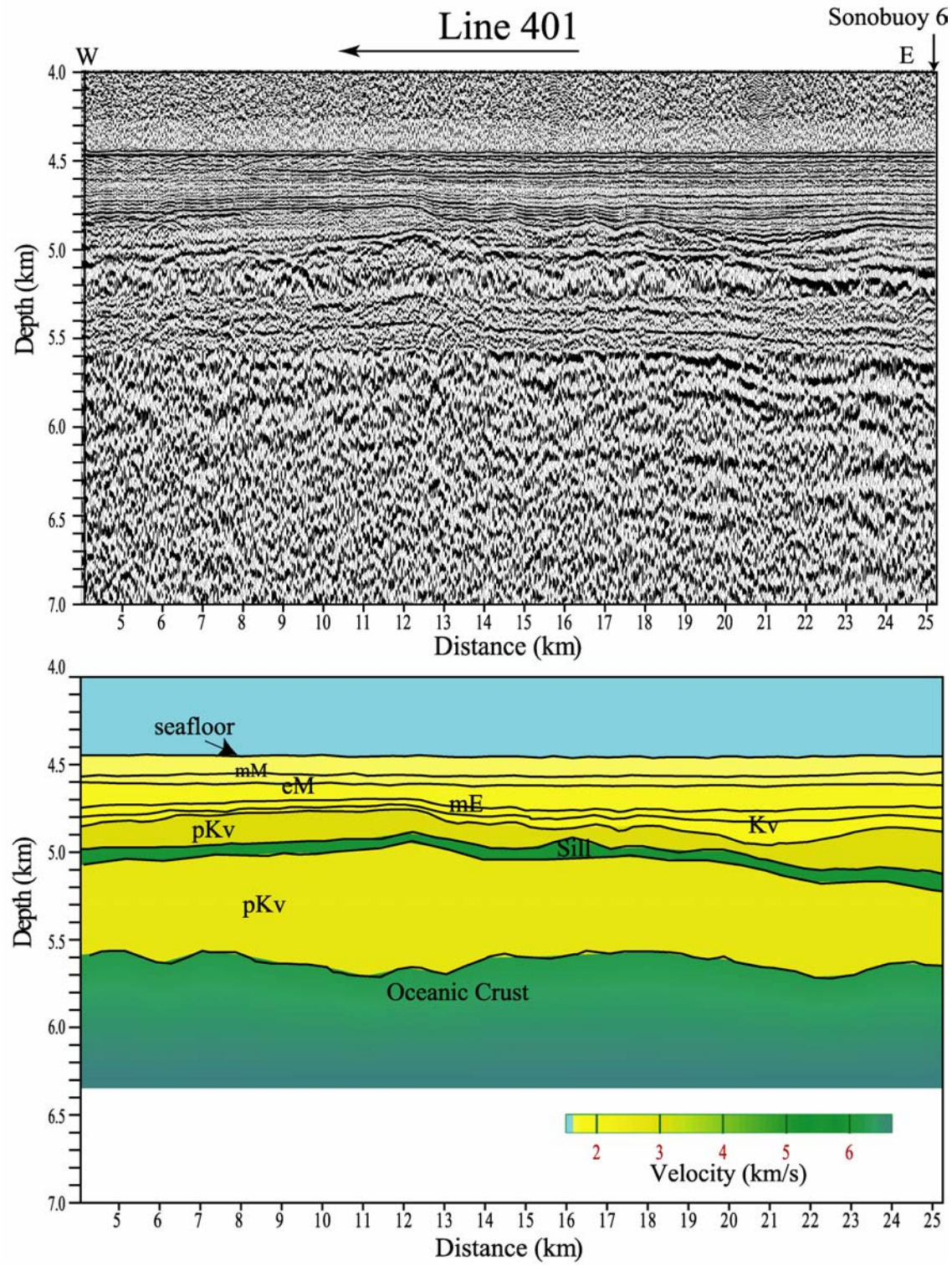

Figure 36. Depth section derived from conversion of MCS Line 401 two-way travel time data to depth using the velocity model derived from Sonobuoy 5. The labeled horizons include units recovered at DSDP Site 462 (mM, eM, mE, Kv), and what Shipley et al. [1993] interpret as a thin sill within a low velocity sedimentary package (pKv) overlying oceanic crust.

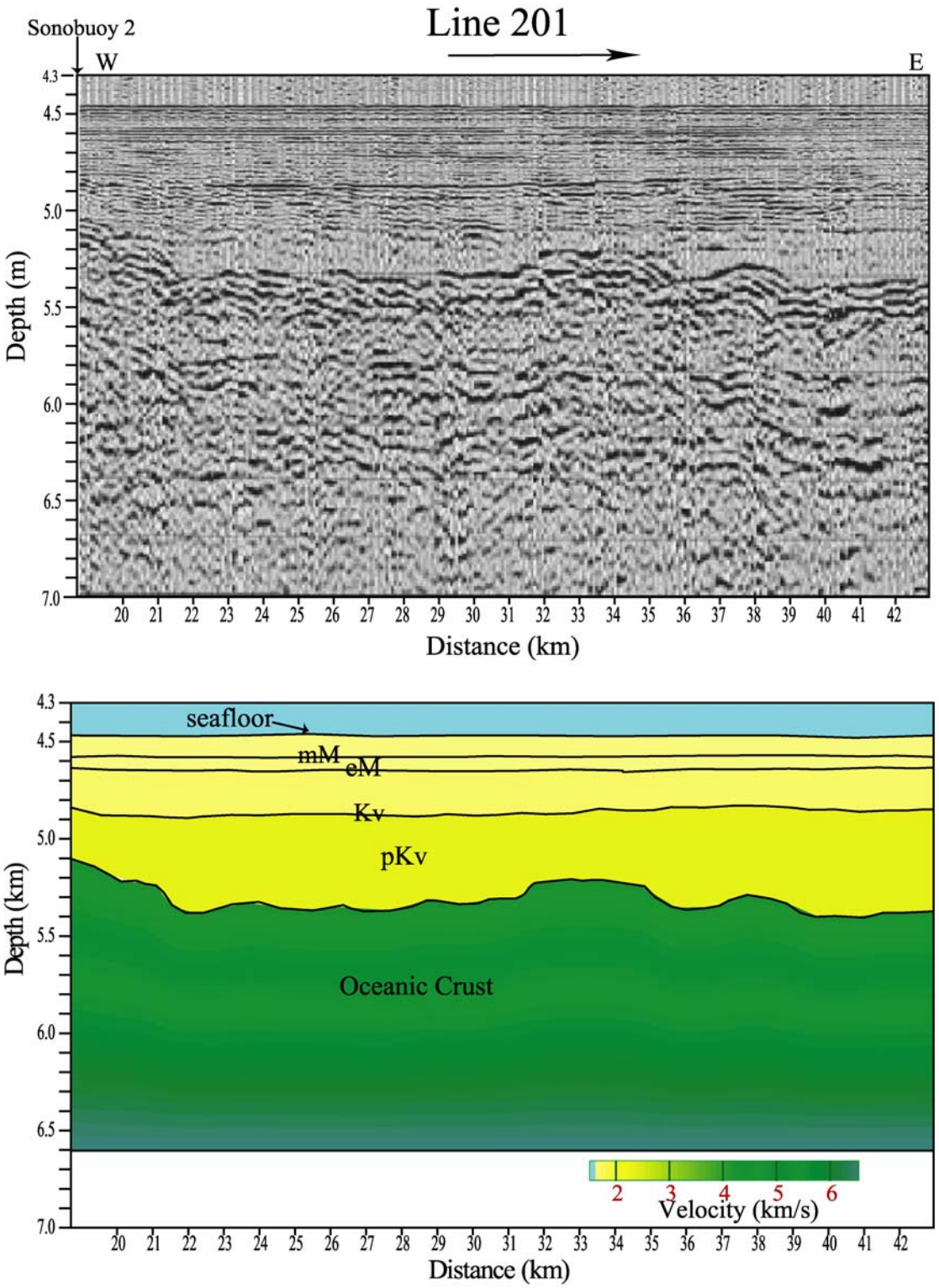

Figure 37. Depth section derived from conversion of MCS Line 201 two-way travel time data to depth using the velocity model derived from Sonobuoy 2. The labeled horizons include units recovered at DSDP Site 462 (mM, eM, Kv), and what Shipley et al. [1993] interpret the top of oceanic crust without overlying thin sills/flows within the thick sedimentary package (pKv).

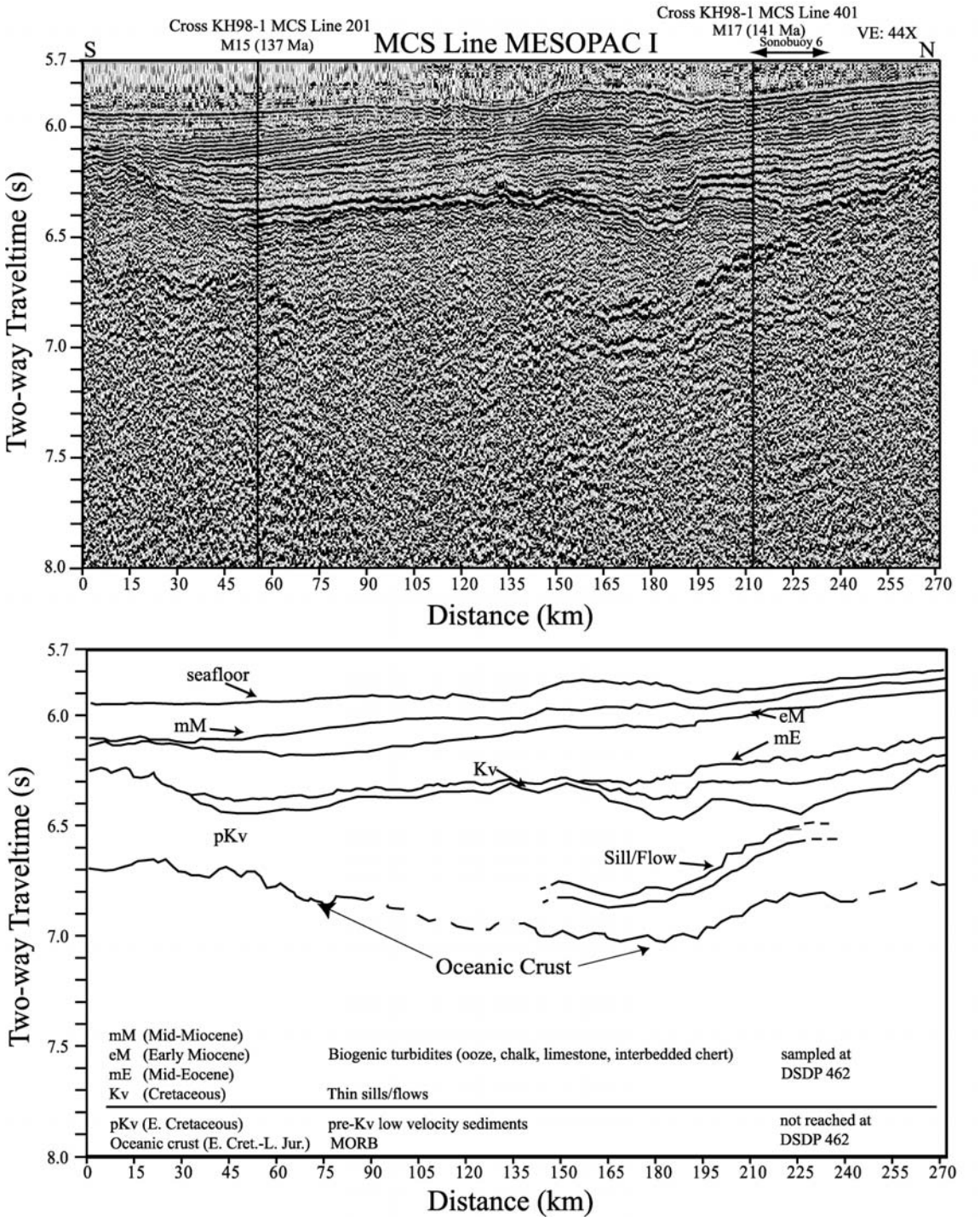

Figure 38. (Top) MESOPAC I MCS profile collected perpendicular to M-series magnetic anomaly lineations in the southern Nauru Basin, with the location of Sonobuoy 6 and intersecting KH98-1 MCS Lines labeled. (Bottom) Line-drawn interpretation based on reflection character and velocity structure obtained from models constructed from Sonobuoy 6 and 2 data, supporting the Shipley et al. [1993] interpretation.

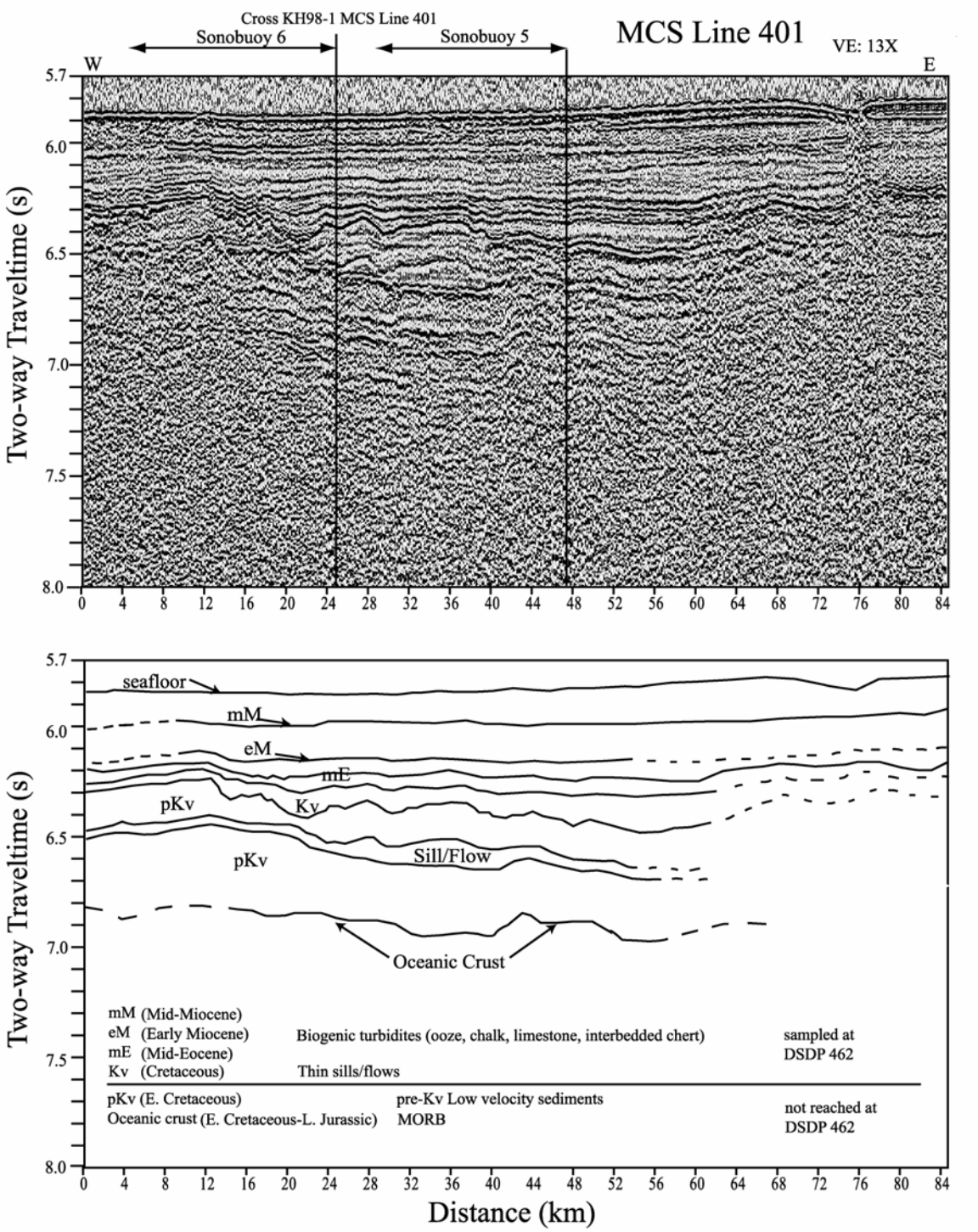

Figure 39. (Top) KH98-1 Line 401 MCS profile collected near parallel to M-series magnetic anomaly lineations in the southern Nauru Basin, with the location of Sonobuoy 5, 6 and MESOPAC 1 MCS line labeled. (Bottom) Line-drawn interpretation based on reflection character and velocity modeling from Sonobuoy 5 and 6. Seismic facies were traced from MESOPAC 1 along MCS Line 401, where forward modeling support the presence of a thin, high velocity sill over lower velocity sediments and oceanic crust.

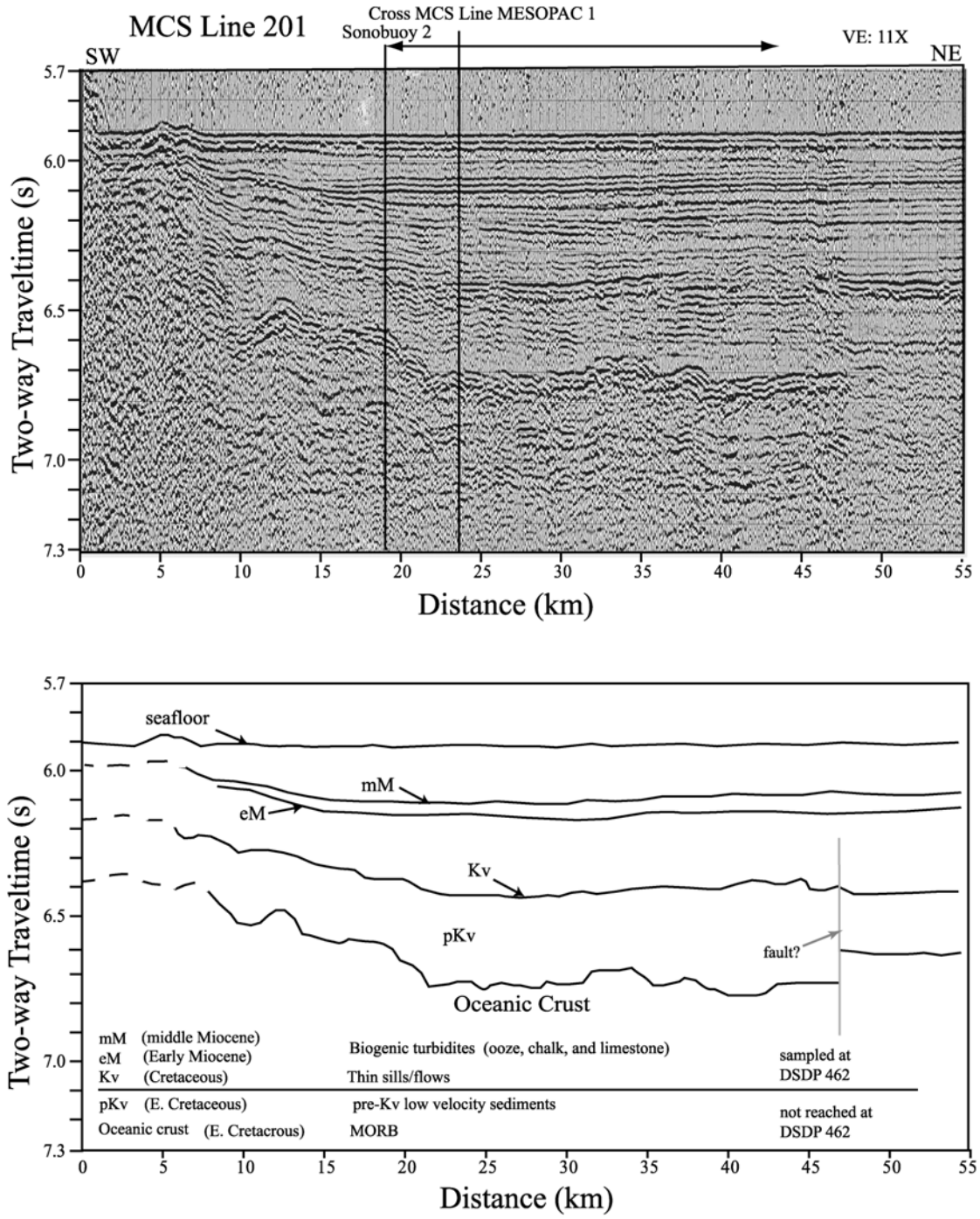

Figure 40. (Top) KH98-1 Line 201 MCS profile collected at an oblique angle to M-series magnetic anomaly lineations in the southern Nauru Basin, with the location of Sonobuoy 2 and intersecting MESOPAC 1 MCS line labeled. (Bottom) Line-drawn interpretation based on reflection character and velocity modeling of Sonobuoy 2 data. In contrast to Sonobuoy 5 and 6, velocity analysis from Sonobuoy 2 does not require modeling a thin, high velocity sill within sediments overlying oceanic crust.

The high-amplitude reflection originally interpreted as a sill/flow by Shipley et al., [1993] is also imaged on MCS Line 401 at ~6.592 stwt, 646 mbsf (Figures 24 and 39). This high-amplitude reflection is not apparent on either MESOPAC 1 or MCS Line 201 in the vicinity of Sonobuoy 2. Instead, a relatively high-relief (100-300 m), "rough" reflection is imaged on both MESOPAC 1 and MCS Line 201 data that is also associated with velocity and velocity gradients characteristic of layer 2 (Figure 30 and 32). These data are consistent with the original interpretation that this reflection represents the top of oceanic crust with no overlying sills or flows in the southernmost region of the Nauru Basin (Figures 3, 38 and 40). The new depth sections indicate that oceanic crust lies at ~ 656 mbsf (Figure 37).

To accurately model the hyperbolic character of crustal reflections in Sonobuoy 5 and 6 travel time-range records, a thick overlying, low velocity layer was required between the thin, high velocity sill and crustal interface (Figures 16 and 22). Depth sections indicate the total thickness of the low velocity sediments ranging from ~430-1000 m where volcanic sills are apparent along MCS Line MESOPAC 1 and MCS Line 401 (Figures 34-36). Where no sills are present, MCS Line 201 depicts this layer thinning to the southwest, with a minimum thickness of 438 m over the range of Sonobuoy 2, and thickening to the northwest (Figure 37). This unit is label pKv in depth sections and line-drawn interpretations.

Velocity modeling of oceanic crust was difficult to determine from T/X data in this study. Primary limitations in modeling oceanic crustal velocities are the absence of high amplitude, long-range refractions that characterize the complete section of normal oceanic crust in T/X records. This is likely due to the presence of the thick sedimentary section, a high velocity sill and a low-velocity zone between the sill and top of crust. Others believe such incoherent refractions may be a result of the minimal velocity contrast across a limestone/basalt boundary

(Larson, 1976) or alternating bands of sediments and volcanics (Houtz, 1976) too incoherent to produce a refraction but strong enough to emit a prominent reflection.

Sill/Flow Thickness

A thin sill/flow is identified within the thick, low-velocity layer by its high-amplitude reflection and high velocity along MCS Line 401 and MESOPAC 1 (Figures 34-36). At vertical incidence, modeling Sonobuoy 6 depicts the sill with a maximum thickness of 132 m where MCS Lines 401 and MESOPAC 1 intersect (Figures 34 and 35). Where Sonobuoy 5 is located along MCS Line 401 the sill is slightly thicker at 159 m, with a maximum thickness of ~204 m between Sonobuoy 5 and 6 (Figure 36). From MESOPAC 1 reflection data, the sill thins to the south and does not appear to extend south of ~0.5° S, where deep reflectors appear rough and are of lower amplitude (Figures 3 and 38), and thins out laterally along MCS Line 401 (Figure 39). A thin sill is not evident along MCS Line 201, where the onset of high velocities corresponds to the top of oceanic crust, predicted as Early Cretaceous age according to magnetic anomaly lineations (Figure 40).

DSDP Site 462 sediments

Seismic facies corresponding to sediments recovered at DSDP Site 462 extend throughout the southern Nauru Basin, and can be traced throughout the three seismic reflection profiles in this study (Figures 38-40). Its high reflection amplitude allows for easy identification of the Cretaceous volcanic unit Kv. The unit does not exceed 100 m thick, except along a small portion of MCS Line 401 (Figure 35), and thins out to the west along MCS Line 401, and to the south along MESOPAC 1 where it terminates in close proximity to the intersection of MESOPAC 1

and MCS Line 201, at ~ 1.5° S (Figure 38). The top of seismic facies Kv was modeled in Sonobuoy 2 data, however the bottom of the unit was not resolvable in T/X data and therefore correct thickness could not be determined. On MCS Line 201, the unit does not exceed 1 stwt, combined with a low velocity (~1.7 km/s), gives an estimate thickness comparable to other DSDP Site 462 sediments. Sequence Kv-mE ranges from ~50-150 m thick over the range of Sonobuoy 5 and 6, thinning to the west along MCS Line 401. The top of mE downlaps onto Kv further north at ~ 0.1° S along MESOPAC 1 and is therefore not imaged on MCS Line 201 (Figure 38). Sequence mE-eM appears fairly uniform in thickness (100-150 m) along MCS Line 401, with MESOPAC 1 data showing an apparent southerly dip direction and thinning (Figures 38 and 39). Sequence eM-mM does not exceed 100 km thick and thins significantly in the southern part of the study area along MESOPAC 1 and MCS Line 201. Both MESOPAC 1 and MCS Line 201 cross sections depict this unit dipping to the south and southwest, downlapping onto unit eM on MCS Line 201 (Figures 38 and 40).

DISCUSSION

Late Jurassic to Early Cretaceous oceanic crust and sediments are identifiable in the southern Nauru Basin. Sonobuoy refraction data are consistent with the Shipley et al. [1993] mapping of the sequence of DSDP Site 462 lithologies in the southern Nauru Basin. In addition, a thin, high-velocity sill/flow unit is imaged within low-velocity rocks overlying oceanic crust in the northern region of the study area. Evidence for these observations are as follows:

1) Oceanic crust is observed in the three MCS profiles based on its high-relief, low-amplitude reflection character, most notably along MESOPAC 1 and MCS Line 201, where data were collected nearly perpendicular to magnetic anomaly lineations. The three sonobuoys image deep

reflections correlated to reflections in the MCS data that are hypothesized to be the top of oceanic crust (Shipley et al., 1993).

The end-member forward model shown in Figure 10 indicates that long-range, first arrival refractions should be produced between 10-40 km range by normal oceanic crust. These long-range refractions are not observed in the sonobuoy data within the southern Nauru Basin, however this does not necessarily imply that the deep reflection in MCS and T/X data is not the top of oceanic crust for the following reasons:

i) Forward modeling does not model amplitude and therefore cannot delineate between amplitudes variances created at the top of a volcanic sill or oceanic crust.

ii) Seismic energy is dissipated by a thick sediment section and a very reflective sill/flow surface, thus minimizing any long-range return energy of the top of oceanic crust.

iii) Other sonobuoy experiments north of this area also fail to show clear crustal arrivals (Wipperman et al., 1981; Shipley et al., 1993)

Imaging deep reflections in both the T/X and MCS profiles indicate subsurface variation in physical/elastic properties (i.e., two different lithologies), combined with reflection character and correlated magnetic anomaly lineations, support the presence of oceanic crust.

2) Forward modeling of sonobuoy 5 and 6 T/X data indicate the presence of a thin, high-velocity layer consistent with a thin sill and/or flow within a lower velocity layer. The prominent refracted arrival cannot be modeled with a velocity gradient, and is tangent to a reflection corresponding to high-amplitude MCS reflections. The sill/flow arrivals precede later arrivals interpreted as normal oceanic crust. Depth conversions estimate the thickness of the sill to be ~100-200 m in the study area.

3) Sonobuoy 5 and 6 do not place definitive velocity constraints on the deep reflections interpreted as the top of oceanic crust, due to the absence of prominent crustal refractions in the two data sets. Weak, longer-range refractions are observed and modeled in the sonobuoy data. The refracted arrivals are modeled with unusually high velocities and cannot be modeled with a large velocity gradient characteristic of Layer 2 oceanic crust. Combined with the lack of long-range return energy and low amplitude arrivals in the data do not allow for reliable velocity constraints, and give inadequate support for the oceanic crust section of the forward models.

4) Reflections from the sill complex and oceanic crust arrive beneath high amplitude seismic facies correlating to a thin Cretaceous volcanic interval (Kv), the deepest material cored at DSDP Site 462. This fact supports the presence of materials in the southern Nauru Basin that were not reached at DSDP Site 462, notably Early Cretaceous-Late Jurassic oceanic crust, and the basalts drilled at DSDP Site 462 were not in fact MORB.

5) Sonobuoy 2 was the only data set where a refracted arrival was observed tangent to a rough acoustic surface along MCS Line 201 without the presence of overlying, high-velocity sills or flows. The refraction was modeled out to ~12 km with velocities and velocity gradients comparable to Layer 2 oceanic crust. However, the lack of long-range crustal refractions (i.e., Layer 3) prevented further velocity and crustal thickness modeling to greater depths. Tracing the rough reflection along both of the intersecting MCS profiles allowed for identification of Late Jurassic-Early Cretaceous oceanic crust within the southernmost Nauru Basin.

Possible Tectonic Setting

Sonobuoy refraction data provide velocity structure to MCS reflection data imaging normal oceanic crust in the southern Nauru Basin. As indicated by M-series magnetic anomaly

lineations M15-M18, oceanic crust within the study area is Berriasian in age, ~137-144 m.y. (Figure 3). Overlying oceanic crust is a thick sequence of low velocity rocks with evident volcanic sill intrusions. The exact ages of the sills are not known, however, they intrude rocks stratigraphically beneath the mid-Cretaceous volcanic unit recovered at DSDP Site 462 (Kv). This particular stratigraphic relationship would place an age of the sills younger than the pre-Kv sediment section. However, without direct sampling it remains uncertain whether or not the sills are directly related in both time and space to the mid-Cretaceous basalt drilled in the northern Nauru Basin.

If in fact, the basalt from DSDP 462 were mid-Cretaceous MORB, the presence of underlying, high-amplitude reflections in MCS profiles would not be geologically impossible, however an intraplate origin for their emplacement is favored. The correlation of Mesozoic magnetic anomaly lineations and deeper, rough reflections imaged in MCS data still provide the most substantial evidence for the presence of Jurassic oceanic crust beneath the mid-Cretaceous igneous basalt.

Velocities obtained from forward modeling of sonobuoy T/X data verify the Shipley et al. [1993] interpretation for thin sills/flows within low velocity sediments overlying Early Cretaceous-Late Jurassic oceanic crust in the southern Nauru Basin. The source for the widespread mid-Cretaceous igneous complex is still speculative, however, MCS reflection and sonobuoy refraction data show evidence for at least three volcanic episodes characterizing the southern Nauru Basin:

i) The formation of Late Jurassic-Early Cretaceous oceanic crust as a result of normal seafloor spreading with age determined by M-series magnetic anomaly lineations;

ii) The eruption of volcanic sheet flows as intraplate flood basalts during the Berremian-Aptian (~115 Ma). These MORB-like flows are hypothesized to have erupted through non-edifice building fissures along the pre-existing Jurassic crust (Larson and Schlanger, 1981). This large volcanic event is presumably associated with the formation of the Ontong Java Plateau and emplacement of the mid-Cretaceous igneous complex as basin filling flood basalts approximately 120 Ma, over top of the original Jurassic crust in an off-ridge tectonic setting;

iii) The intrusion of discontinuous sills during the Cretaceous. The exact age of these sills is undetermined in the southern Nauru Basin, although stratigraphic principles place a maximum age on the intrusions to that of the thick pre-Kv sediment package.

CONCLUSIONS

1) Sonobuoy travel time-range and MCS reflection data collected during KH98-1 provide constraints on the structure of the southern Nauru Basin that are consistent with the interpretations of Shipley et al., [1993].

2) The top of oceanic crust is imaged beneath ~656 m of sedimentary rocks with no evidence of a sill intrusion in the southernmost survey area along MCS Line 201 and MESOPAC 1. M-sequence magnetic anomalies (M15 –16) indicate a Berriasian crustal age of (~137 – 140 Ma).

3) Discontinuous, high-velocity sills ranging from ~100 to 200 m thick intrude the low-velocity sedimentary package along segments of MCS Line 401 and MESOPAC 1 in the northern part of the study area. The sills are mapped beneath the mid-Cretaceous volcanic unit Kv. This relationship contests the hypothesis that the basalts recovered at Site 462 are MORB created at

mid-Cretaceous spreading centers, however, support the existence of deeper, unsampled materials in the Nauru Basin, including original oceanic crust.

4) The detection of volcanic sills/flows in the northern section of the study area intermittent between materials drilled at DSDP Site 462 and a rough surface interpreted as oceanic crust in MCS profiles suggest an off-ridge tectonic setting for emplacement of mid-Cretaceous volcanic material in the southern Nauru Basin, and consistent with the intraplate model of MORB overprinted by later volcanism

REFERENCES

Abrams, L.J., R.L. Larson, T.H. Shipley, and Y. Lancelot, Cretaceous volcanic sequences and Jurassic oceanic crust in the East Mariana and Pigafetta Basins of the western Pacific, in *The Mesozoic Pacific: Geology, Tectonics, and Volcanism*, Geophys. Monogr. Ser., vol. 77, edited by M. S. Pringle, W. W. Sager, W. V. Sliter and S. Stein, pp. 77-103, AGU, Washington, D.C., 1993.

Batiza, R., Trace element characteristics of Leg 61 basalts, *Init. Repts. DSDP, 61*, 689 -696, 1981.

Batiza, R., Larson, R.L., Schlanger, S.O., Shcheka, S.A., and H. Tokuyama, Trace Element abundances in basalts of Nauru Basin, *Nature, 286*, 476-487, 1980.

Cande, S.C., R.L. Larson, and J.L. LaBrecque, Magnetic lineations in the Pacific Jurassic quiet zone, *Earth Planet. Sci. Lett., 41*, 434-440, 1978.

Carlson, R.L., Seismic velocities in the uppermost oceanic crust: age dependence and the fate of layer 2A, *J. Geophys. Res., 103*, 7069-7078, 1998.

Castillo, P.R., R. Batiza and R.J. Stern, Petrology and geochemistry of Nauru Basin igneous complex: large-volume eruptions of MORB-like basalt during the Cretaceous, *Initial Rept. Deep Sea Drill. Proj., 89*, 555-576, 1986.

Castillo, P.R., R.W. Carlson, and R. Batiza, Origin of Nauru Basin igneous complex: Sr, Nd and Pb isotope and REE constraints, *Earth Planet. Sci. Lett., 103*, 200-213, 1991.

Castillo, P.R., and M.S. Pringle, Cretaceous volcanism in the western Pacific sampled at Sites 800 and 802, ODP Leg 129, *Eos, Trans. AGU*, 72, 300, 1991.

Dix, C.H., Seismic velocities from surface measurements, *Geophysics, 20*, 68-86, 1955.

Eldholm, O, Abrams, L.J., Coffin, M.F. and M. Weiderspahn, Sonobuoy Wide-Angle Seismic Velocity Acquisition Program, *KH98-1 Cruise Report*, 1998.

Gradstein, F.M., Agterberg, F.P., Ogg, J.G, Hardenbol, J., van Veen, P., Thierry, J., and Huange, Z., A Mesozoic time scale, *J. Geophys. Res., 99*, 24051-24074, 1994

Green, C.H., Velocity determinations by means of reflection profiles, *Geophysics, 3*, 295-302, 1938.

Handschumacher, D.W, Sager, W.W., Hilde, T.W.C, and D.R. Bracey, Pre-Cretaceous tectonic evolution of the Pacific plate and extension of the geomagnetic polarity reversal time scale with implications for the origin of the Jurassic “Quiet Zone”, *Tectonophysics, 155,* 365-380, 1988.

Janney, P.E., and P.R. Castillo, Basalts from the Central Pacific Basin: Evidence for the Origin of Cretaceous igneous complexes in the Jurassic western Pacific, *J. Geophys. Res., 101*, 2875-2894, 1996.

Kennett, J.P. *Marine Geology*. Prentice-Hall, Englewood Cliffs, New Jersey, 1982.

Lancelot, Y., R.L. Larson, et al., *Proc. ODP, Init. Repts. 129*, College Station, TX (Ocean Drilling Program), 1990.

Larson, R.L., Late Jurassic and Early Cretaceous evolution of the western Pacific Ocean, *J. Geomagnet. Geoelec*., 28, 219-236, 1976.

Larson, R.L., et al., *Initial Reports, Deep Sea Drilling Project, vol. 61*, 885 pp., U. S. Gov. Print. Off., Washington, D. C., 1981.

Larson, R.L., and C.G. Chase, Late Mesozoic evolution of the Western Pacific Ocean, *Geol. Soc. Amer. Bull., 83*, 3627-3644, 1972.

Larson, R.L., and T.W.C. Hilde, A revised time scale of magnetic reversals for the Early Cretaceous and Late Jurassic, *J. Geophys. Res., 80*, 2586-2594, 1975.

Larson, R.L., Y. Lancelot, et al., eds*., Proc. ODP, Sci. Results, 129*, College Station, TX (Ocean Drilling Program), pp. 488, 1992.

Larson, R.L., and S.O. Schlanger, Cretaceous volcanic and Jurassic magnetic anomalies in the Nauru Basin, western Pacific Ocean, *Geology, 9,* 480-484, 1981.

Larson, R.L., and S.O. Schlanger, Geological evolution of the Nauru Basin, and regional implications, *Initial Rept. Deep Sea Drill. Proj., 61*, 841-862, 1981.

Parker, R.L., and S.P. Huestis, The inversion of magnetic anomalies in the presence of topography, *J. Geophys. Res., 79*, 1587-1593, 1974.

Parsons, B. and D. McKenzie, Mantle convection and the thermal structure of the plate, *J. Geophys. Res., 83*, 4485-4496, 1978.

Sager, W.W., C.J. Weiss, M.A. Tivey, and H.P. Johnson, Geomagnetic polarity reversal model of deep-tow profiles from the Pacific Jurassic Quiet Zone, *J. Geophys. Res., 103*, 5269-5286, 1998.

Saunders, A.D, Geochemistry of basalts from the Nauru Basin, Deep Sea Drilling Project Legs 61 and 89: implications for the origin of oceanic flood basalts, *Initial Rept. Deep Sea Drill. Proj., 89*, 499-511.

Shcheka, S., Igneous rocks of Deep Sea Drilling Project Leg 61, *Init. Repts. DSDP, 61,* 633-649, 1981.

Smith, W. H. F. and Sandwell, D. T. Global seafloor topography from satellite altimetry and ship depth soundings. *Science*, 277:195-196, 1997.

Shipley, T.H., L.J. Abrams, Y. Lancelot, and R.L. Larson, Late Jurassic-Early Cretaceous oceanic crust and Early Cretaceous volcanic sequences of the Nauru Basin, western Pacific, in *The Mesozoic Pacific: Geology, Tectonics, and Volcanism*, Geophys. Monogr. Ser., vol. 77, edited by M.S. Pringle, W.W. Sager, W.V. Sliter and S. Stein, pp. 103-119, AGU, Washington D.C., 1993.

Smith, W. H. F. and Sandwell, D. T. Global seafloor topography from satellite altimetry and ship depth soundings. *Science*, 277:195-196,1997.

Tarduno, J.A., W.V. Sliter, L. Kroenke, M. Leckie, H. Mayer, J.J. Mahoney, R. Musgrave, M. Storey, and E.L. Winterer, Rapid formation of Ontong Java Plateau by Aptian mantle plume volcanism, *Science, 254*, 399-403, 1991.

Tokuyama, H., and R. Batiza, Chemical composition of igneous rocks and origin of the Sill and pillow basalt complex of Nauru Basin, Southwest Pacific, *Init. Repts. DSDP, 61*, 673-686, 1981.

Vine, F. J. and D. H. Matthews, Magnetic anomalies over oceanic ridges. *Nature* 199: 947-949, 1963.

Wessel, P. and Smith, W. H. F. New version of the Generic Mapping Tools released. *EOS Trans. AGU*, 76:329, 1995.

White, R.S., D. McKenzie, and R.K. O'Nions, Oceanic crustal thickness from seismic Measurements and Rare Earth Element inversions, *J. Geophys. Res., 97*, 19683-19715, 1992.

Winterer, E.L., et al., *Initial Reports, Deep Sea Drilling Project, vol. 17*, 930 pp, U. S. Gov. Print. Off., Washington, D. C., 1973.

Wipperman, L. K., R. L. Larson, and D. M. Hussong, The geological and geophysical Setting near site 462, *Init. Repts. DSDP, 61*, 763-770, 1981.

Zelt, C. A. and R. M. Ellis, Practical and efficient ray tracing in two-dimensional media for rapid traveltime and amplitude forward modelling, *Canadian Journal of Exploration Geophysics, 24*, 16-31, 1988.

Zelt, C. A., and R. B. Smith, Seismic traveltime inversion for 2-D crustal velocity structure, *Geophys. J. Int., 108*, 16-34, 1992.

Zelt, C. A., Modelling strategies and model assessment for wide-angle seismic traveltime Data, *Geophys. J. Int., 139*, 183-204, 1999.

APPENDIX A

Appendix A. Procedure for constructing a velocity model in SeisWide for ray traced forward modeling.

1. Click on New Model icon, enter number of model layers and save both velocity and model files.

2. Use the Edit dialogue bow to adjust boundary nodes and velocities for individual layers. Save both files frequently to eliminate model adjustments made.
   **Note the digitized values in the lower right hand corner of the display when editing model.
   **The modeler can zoom in considerably on boundary nodes for more concise modeling.
   **Boundary nodes can pinch out, but not cross

3. In the Modeling dialogue menu, select the Ray Trace command and click Auto to generate an automated ray tracing parameters (.in). The .in file can be edited in the text box to adjust variable inputs for ray tracing.
   **For a detailed explanation of all the parameters for ray parameter file, refer to RayInvr.txt file .\RayInvr\Doc directory as written by Dr. Colin Zelt.
   **Essential parameters are already in the .in file. Entering other parameters in the script sequence causes errors or will have no response in the program. Simple edits of the automated file will produce sufficient ray tracing results.
   **Enter ishot=0.001 in the .in file seems to work best. One can easily go back and change ishot=0.000 for model display purposes but will get erroneous travel time curve plots over observed data.

4. After ray tracing is performed, an .out file is generated displaying detailed information on the rays traced through the model. This file is not intended for editing, but just to be used for general information about the modeling process, and is stored in the main SeisWide directory.
   **Unless an error message is given, skip showing the ray tracing details.

5. Click Veiw|Velocity Color Map to edit common display parameters, such as axis values and velocity color values.
   **When editing velocity color values, choose colors first then edit velocity values. The velocity values have a tendency to refer back to the default values if edited first.

6. In the File command menu, final models can be exported as a high-resolution bitmaps or copied and pasted in most graphic editing programs.
   **When exporting model, copying and pasting into editing programs works best. This enables you to edit individual ray path colors, and text fonts.
   **If export model as a bitmap, X-Y pixel values of 4000x2000 is adequate.

**I found that sometimes you have to export as a monochrome bitmap first before a full color bitmap could be exported properly.

7. The modeler should click Edit|Display Tune-up to adjust the model display before copying or exporting as bitmap.

APPENDIX B

How to display seismic sections and compare observed versus modeled data in Seiswide.

1. First select Process|SEGY Conversion|UNIX to PC Batch, to ensure a new Segy file is in PC format.
   **A new file will automatically be generated with "PC" appended to the end in the folder the original SEGY data was stored.

2. To display some of the SEGY header information, run View|Segy Info. If the numbers are displayed correctly, it is most likely that SeisWide can use this file.

3. To display trace header information select Dump More Trace Info button, which shows for every Trace Number, FFID, SP (shot point), CDP, Offset, tmin, tmax, sDepth (depth of source in km), sLat, sLong (value divided by 36,000, which normally means latitude and longitude in degrees), and dDepth, gLat, gLong for group receivers.

4. First, display seismic sections trace-by-trace, select View|Time Section by Trace. When the dialogue bow appears, enter the PC-converted SEGY file.
   **The correct trace values should automatically be entered into the proper boxes.
   **Click Ok and the time section should soon appear in the display.
   **Now one can go back to View|Time Section by Trace to edit any display parameter the user wishes. I found it convenient to display all Trace header information at first to compare sonobuoy data to coincident MCS data.

5. To display the segy section by offset or (model) distance, must first input correct distance information stored in the segy header: (a) for an MCS reflection profile, run Processing menu|Associate km to Trace; (b) for wide-angle sections, offsets should already be stored in the binary headers (in field segy.offset).
   **I had to enter appropriate offset/distance values in the Processing menu|Associate km to Trace|Increment (in km) for Successive Traces box for viewing both sonobuoy and MCS data. (e.g., if 45.28 m/shot, enter 0.04528).
   **Click Ok and the distance/offset for the last trace should be given in meters.

6. Now, to display a time section in km, select View menu|Time Section by km, and a dialog box will appear. You do not have to enter all the information in this dialog box before you can display something. Most of the information in this dialog box has defaults, and once you enter a file name for a time section, you may get your view right away even without entering any further information.
   **SeisWide will tell you if the values enter into the dialogue box will hang up the program (e.g. trace step too dense, or gain adjustments are needed)

7. Numerous processing commands can be applied in the Processing command window.
   **The Select Water Wave for Sonobuoy Data and Associate km to Sonobuoy Traces Commands do not work, however the Processing menu|Associate km

to Trace|Increment (in km) for Successive Traces can be applied to sonobuoy data for correct offset values.

8. To overlay computed rays from a particular velocity model on a sample of wide-Angle data, click the View|Time Section by km button, then the Time or Depth Section tab, and check the Overlay computed Rays box.
   **Pressing Control + T will also overlay modeled travel times and saves time.
   **Having both the velocity model and time section open simultaneously allows for rapid adjustments in model ray tracing and displaying travel time curves.

9. Once a velocity model is generated that accurately fits to the observed data it is easy to convert MCS travel-time sections to depth sections.
   Click Porcessing|Time-Depth Conversions|For Segy Data. When the dialogue box appears, enter the correct time and velocity files and input a new name for the generated depth section.
   **It is important to remember to input the correct values for the range (Xmin, Xmax) which the model covers over the coincident wide-angle date (Trace1, Trace2). The depth intervals. for processing should not have to be edited and can always be adjusted after the depth section is created.
   **You will have to go back and resize the model to the proper range values before converting the time section to depth.
   **You should save the resized model and velocity file as different names to keep those ray traced models used in overlying travel time curves to wide-angle data, and those models with ranges coincident over coincident reflection data. If not, you will get frequent errors when trying to overlay travel time curves over wide-angle data if model distance and wide-angle offsets don't match.

10. After the depth section is generated, click View|Both Velocity+Depth Sections to edit model nodes and digitize model boundaries to trace reflected arrivals. Don't forget to frequently save both the proper velocity and model files to avoid losing adjustments made to the model.
    **Remember you can view the converted depth sections, velocity sections, and depth+velocity sections separately for exporting to graphics editing softwares.

APPENDIX C

The following is a list of files used in the modeling process and stored on the appended Digital Video Disk.

SeisWide Modeling files:

1) SeisWide Package
    a. SeisWideDist4.6.4.zip- zipped SeisWide package
    b. SeisWideDist4.6.4- unzipped folder containing all SeisWide files necessary for ray trace forward modeling
    c. Click SeisWide.exe to run main program

See SeisWide > SeisWide4.6.4 > RayInvrDoc > Doc > RAYINVR.txt for detailed description of all subdirectories created while ray tracing and ray tracing parameters

Please refer to Appendices A and B for the sequence of steps necessary for displaying and modeling the appended seismic data

See also SeisWide > SeisWide4.6.4 > SEISWIDE.HLP to access the SeisWide Applications help topics

After running SeisWide.exe, the following are data files for each velocity model, time and depth section

.

1) Sonobuoy 6 Files
   → Found in CD Drive > Thesis Data > Sonobuoy_6_Data folder
    a. sb6-filter-agc500.sgy- raw SEGY traveltime-range data, must be converted to PC format
    b. sb6-filter-agc500PC.sgy- time section converted to PC format, necessary to view in SeisWide command Veiw|Time Section by km
    c. sb6-filter-agc500-model.SEI- brings up the 1-D velocity model
    d. sb6-filter-agc500.SEI- brings up the time section model
    e. sb6-agc-filter-500_velocity.bin- velocity file name (SeisWide binary format)
    f. sb6-agc-filter-500_velocity.bin_r.in- ray tracing parameter file
    g. sb6-agc-filter-500_velocity_MPAC1range.bin- sonobuoy 6 velocity file with the correct range over MESOPAC1
    h. sb6-agc-filter-500_velocity_Line401range.bin- sonobuoy 6 velocity file with the correct range over Line 401

2) Sonobuoy 5 Files
   → Found in CD Drive > Thesis Data > Sonobuoy_5_Data folder
    a. sb5-filter-agc500.sgy- raw SEGY traveltime-range data, must be converted to PC format
    b. sb5-filter-agc500PC.sgy- time section converted to PC format, necessary to view in SeisWide command Veiw|Time Section by km
    c. Sonobuoy_5-model.SEI- brings up the 1-D velocity model

d. Sonobuoy_5-km.SEI- brings up the time section model
e. sonobuoy_5_velocity.bin- velocity file name (SeisWide binary format)
f. sonobuoy_5_velocity.bin_r.in- ray tracing parameter file
g. sonobuoy_5_velocity_line401-range.bin- sonobuoy 5 velocity file with the correct range over Line 401

3) Sonobuoy 2 Files
→ Found in CD Drive > Thesis Data > Sonobuoy_2_Data folder
a. sb2-filter-agc500.sgy- raw SEGY traveltime-range data, must be converted to PC format
b. sb2-filter-agc500PC.sgy- time section converted to PC format, necessary to view in SeisWide command Veiw|Time Section by km
c. Sonobuoy2-model.SEI- brings up the 1-D velocity model
d. Sonobuoy2-km.SEI- brings up the time section model
e. sonobuoy_2-velocity.bin- velocity file name (SeisWide binary format)
f. sonobuoy_2-velocity.bin_r.in- ray tracing parameter file
g. sb2.bmp- contains bitmap file with better refraction display
h. Sonobuoy2-km10-12.SEI- SeisWide model with correct offset display
i. sonobuoy_2-velocity-line201range.bin- sonobuoy 2 velocity file with the correct range over Line 201

4) MESOPAC I Files
→ Found in CD Drive > Thesis Data > MPAC1 Data folder
a. meso1-6000.decon.sgy- raw SEGY MCS data, must be converted to PC format
b. meso1-6000.deconPC.sgy- time section converted to PC format
c. MESOPAC1.SEI- brings up time section with correct range applied
d. meso1-6000.deconPC-depth.sgy- converted time section to depth; to be used with 4(b) and 1(g) when running Processing|Time-Depth Conversion|For Segy Data
e. MESOPAC1-sb6_range-vel-depth.SEI- SeisWide display of velocity file overlain on converted depth section

5) Line 401 File
→ Found in CD Drive > Thesis Data > Line_401 Data folder
a. ln401-agc-filter-spw.sgy- raw SEGY MCS data, must be converted to PC format
b. ln401-agc-filter-spwPC-correct.sgy- time section converted to PC format
c. Line_401-time.SEI- brings up time section with correct range applied
d. ln401-agc-filter-spwPC-sb5depth.sgy- converted time section to depth, to be used with 5(b) and 2(g) when running Processing|Time-Depth Conversion|For Segy Data

e. Line_401-time_sb5_vel-depth.SEI- SeisWide display of velocity file overlain on converted depth section
f. Line_401-time_sb6_vel-depth.SEI- converted time section to depth; to be used with 5(b) and 1(g) when running Processing|Time-Depth Conversion|For Segy Data
g. Line_401-time_sb6_vel-depth.SEI- SeisWide display of velocity file overlain on converted depth section

6) Line 201 Files
→ Found in CD Drive > Thesis Data > Line_201 Data folder
   a. ln201-agc-filter-spw.sgy- raw SEGY MCS data, must be converted to PC format
   b. ln201-agc-filter-spwPC.sgy- time section converted to PC format
   c. MCS_Line-201-sgy.SEI- brings up time section with correct range applied
   d. SPWLine201-true.bmp- bitmap image of Line 201; dumped from Seismic Processing Workshop and used to import into SeisWide since original SEGY data was not the best display in SeisWide (I had trouble with the parameter adjustment to view the data adequately)
   e. MCS_Line-201.SEI- brings up the bitmap display in SeisWide with the correct range applied
   f. ln201-agc-filter-spwPC-depth.sgy- converted SEGY data to depth; used with 6(a) and 3(i) when running Processing|Time-Depth Conversion|For Segy Data
   g. MCS_Line-201-sb2-depth.SEI- SeisWide display of velocity file overlain on converted depth section

7) Sonobuoy 22 Files
→ Found in CD Drive > Thesis Data > Sonobuoy_22_Data folder
   a. sb22-crop.bmp- bitmap of sonobuoy 22 to be imported into SeisWide
   b. Sonobuoy_22_Raw.SEI- Seiswide display of sonobuoy 22 bitmap with the correct range
   c. Sonobuoy_22_Model.SEI- the 1-D velocity model for ray tracing
   d. sonobuoy_22_velocity.bin- velocity file name (SeisWide binary format)
   e. sonobuoy_22_velocity.bin_r.in- ray tracing parameter file

8) Sonobuoy 8 Data
→ Found in CD Drive > Thesis Data > Sonobuoy_8_Data folder
   a. sb8-crop.bmp- bitmap of sonobuoy 8 to be imported into SeisWide
   b. Sonobuoy_8_Raw.SEI- Seiswide display of sonobuoy 8 bitmap with the correct range
   c. Sonobuoy_8_Model.SEI- the 1-D velocity model for ray tracing

d. sonobuoy_8_velocity.bin- velocity file name (SeisWide binary format)
e. sonobuoy_8_velocity.bin_r.in- ray tracing parameter file

APPENDIX D

Traveltime, range, velocity and depth values obtained from the T^2-X^2 Method.

SEE FOLLOWING GRAPHS

Sonobuoy 6 Data

Distance (m)	Seafloor reflection (s)	X^2	T^2
0.053	5.901	0.002809	34.821801
0.487	5.906	0.237169	34.880836
0.915	5.927	0.837225	35.129329
1.417	5.965	2.007889	35.581225
1.866	6.01	3.481956	36.1201

2.489	6.104	6.195121	37.258816
3.156	6.236	9.960336	38.887696
3.695	6.344	13.653025	40.246336
4.108	6.448	16.875664	41.576704
4.55	6.57	20.7025	43.1649
4.932	6.681	24.324624	44.635761
5.382	6.814	28.965924	46.430596
5.802	6.979	33.663204	48.706441
6.266	7.149	39.262756	51.108201
6.641	7.314	44.102881	53.494596

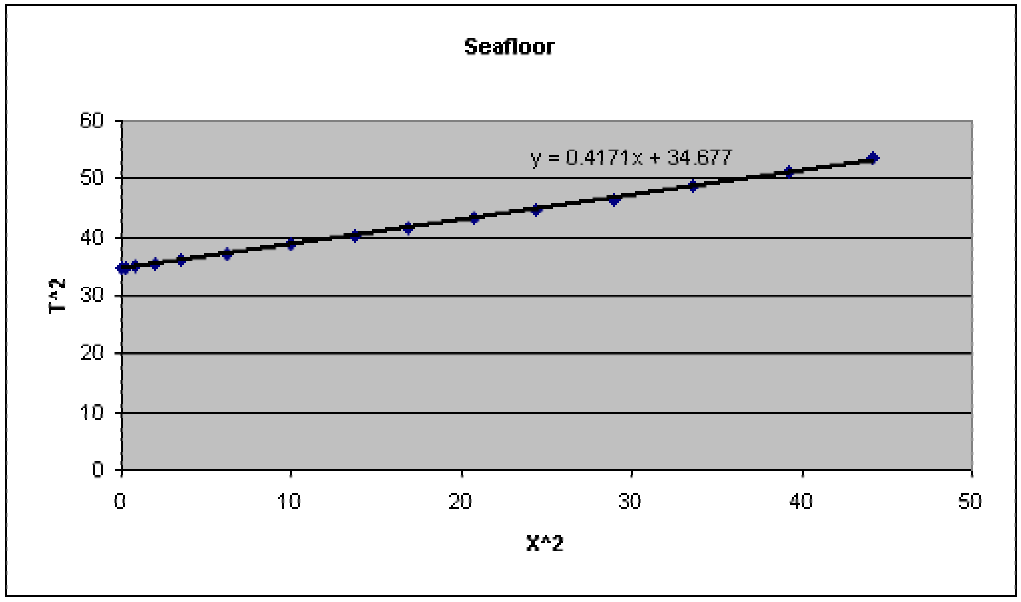

Vrms1 (km/s)	sqrt(1/slope)	1.548
t_{01}-reflection (s)		5.888

Distance (m)	**Top eM reflection (s)**	**X^2**	**T^2**
0.074	6.006	0.005476	36.072036
0.407	6.006	0.165649	36.072036
0.852	6.028	0.725904	36.336784
1.296	6.044	1.679616	36.529936
1.685	6.092	2.839225	37.112464

2.037	6.135	4.149369	37.638225
2.463	6.2	6.066369	38.44
2.815	6.259	7.924225	39.175081
3.148	6.324	9.909904	39.992976
3.444	6.383	11.861136	40.742689
3.796	6.474	14.409616	41.912676
4.074	6.544	16.597476	42.823936
4.37	6.631	19.0969	43.970161
4.611	6.695	21.261321	44.823025
4.926	6.787	24.265476	46.063369

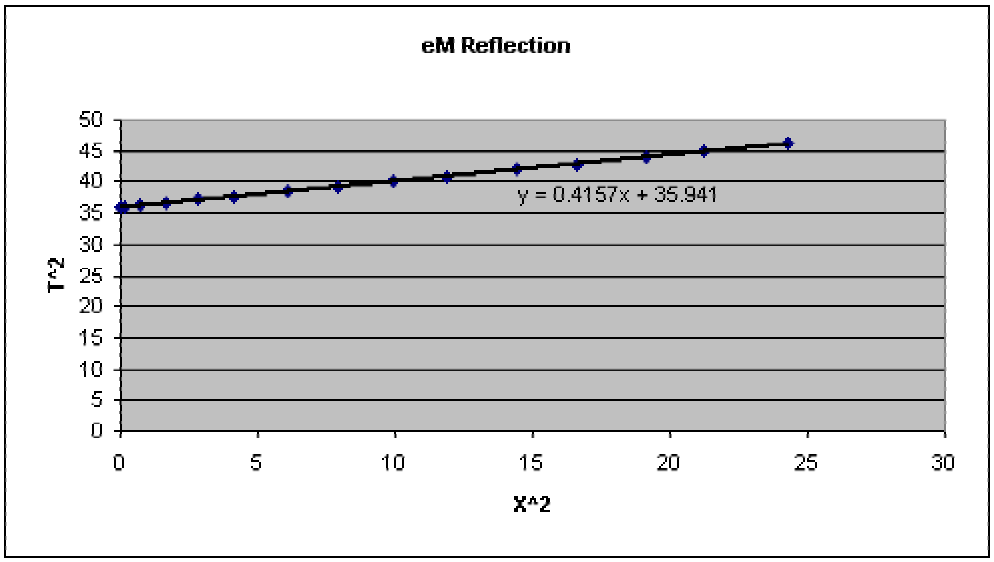

Vrms2 (km/s)	sqrt(1/slope)	1.55
t_{02}-reflection (s)		5.996

Distance (m)	**Top mE reflection (s)**	**X^2**	**T^2**
0.13	6.2	0.0169	38.44
0.63	6.211	0.3969	38.576521
1.074	6.232	1.153476	38.837824
1.5	6.259	2.25	39.175081

1.889	6.291	3.568321	39.576681
2.204	6.329	4.857616	40.056241
2.574	6.378	6.625476	40.678884
2.907	6.437	8.450649	41.434969
3.222	6.501	10.381284	42.263001
3.556	6.566	12.645136	43.112356
3.87	6.641	14.9769	44.102881
4.148	6.711	17.205904	45.037521
4.389	6.781	19.263321	45.981961
4.778	6.884	22.829284	47.389456
5.037	6.97	25.371369	48.5809

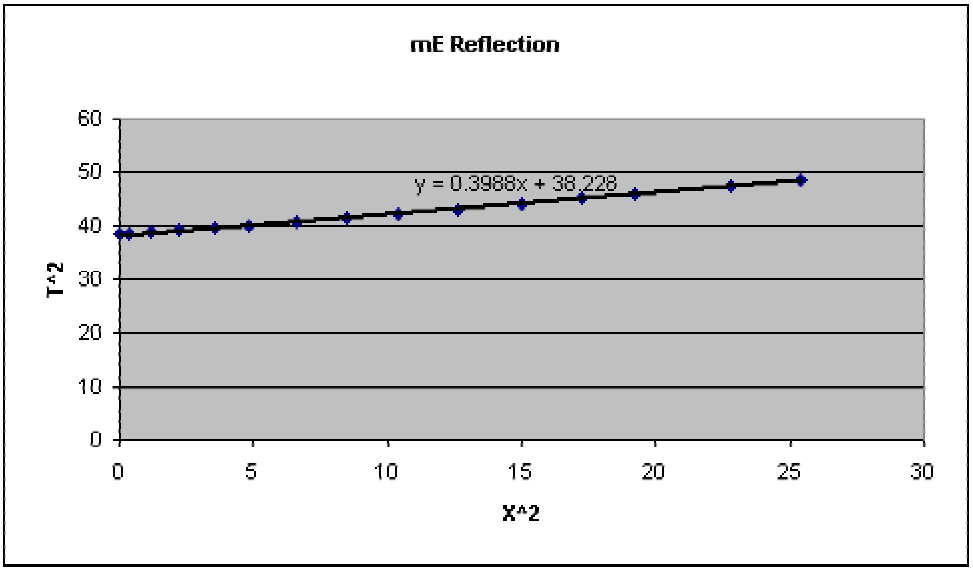

	Vrms (km/s)	sqrt(1/slope)	1.58
	t_{03}-reflection (s)		6.182

Distance (m)	**Top K reflection (s)**	**X^2**	**T^2**
0.037	6.297	0.001369	39.652209
0.481	6.302	0.231361	39.715204
0.87	6.297	0.7569	39.652209
1.315	6.324	1.729225	39.992976

1.667	6.356	2.778889	40.398736
2.093	6.415	4.380649	41.152225
2.426	6.464	5.885476	41.783296
2.778	6.517	7.717284	42.471289
3.074	6.577	9.449476	43.256929
3.37	6.647	11.3569	44.182609
3.667	6.706	13.446889	44.970436
4.093	6.803	16.752649	46.280809
4.426	6.889	19.589476	47.458321
4.741	6.97	22.477081	48.5809

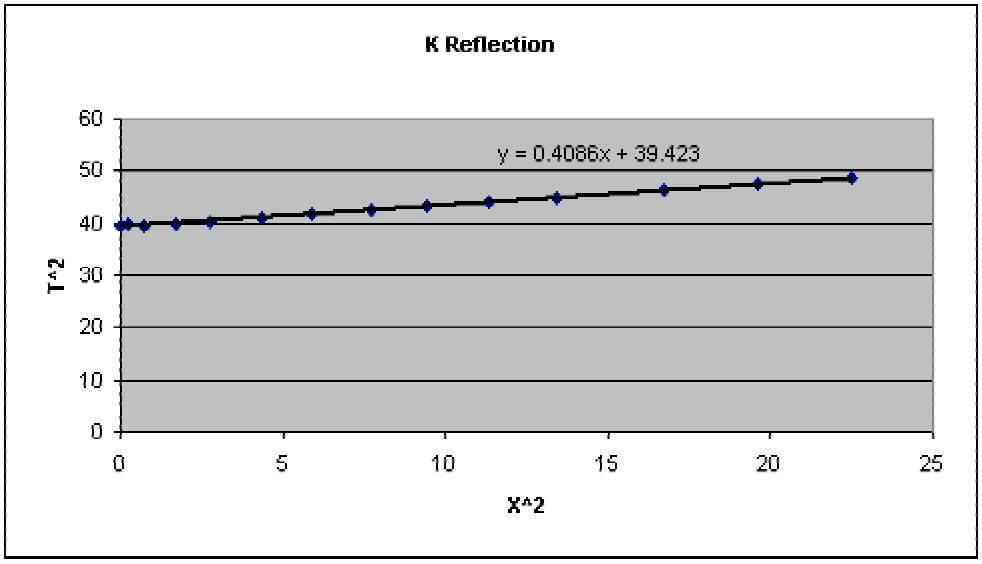

Vrms (km/s)	sqrt(1/slope)	1.57
t_{04}-reflection (s)		6.28

Distance (m)	**Top LVsed (s)**	**X^2**	**T^2**
0.093	6.41	0.008649	41.0881
0.574	6.41	0.329476	41.0881
1.074	6.426	1.153476	41.293476

1.537	6.453	2.362369	41.641209
1.907	6.491	3.636649	42.133081
2.278	6.528	5.189284	42.614784
2.63	6.593	6.9169	43.467649
3.037	6.668	9.223369	44.462224
3.352	6.738	11.235904	45.400644
3.722	6.814	13.853284	46.430596
3.963	6.873	15.705369	47.238129
4.222	6.932	17.825284	48.052624
4.519	6.997	20.421361	48.958009

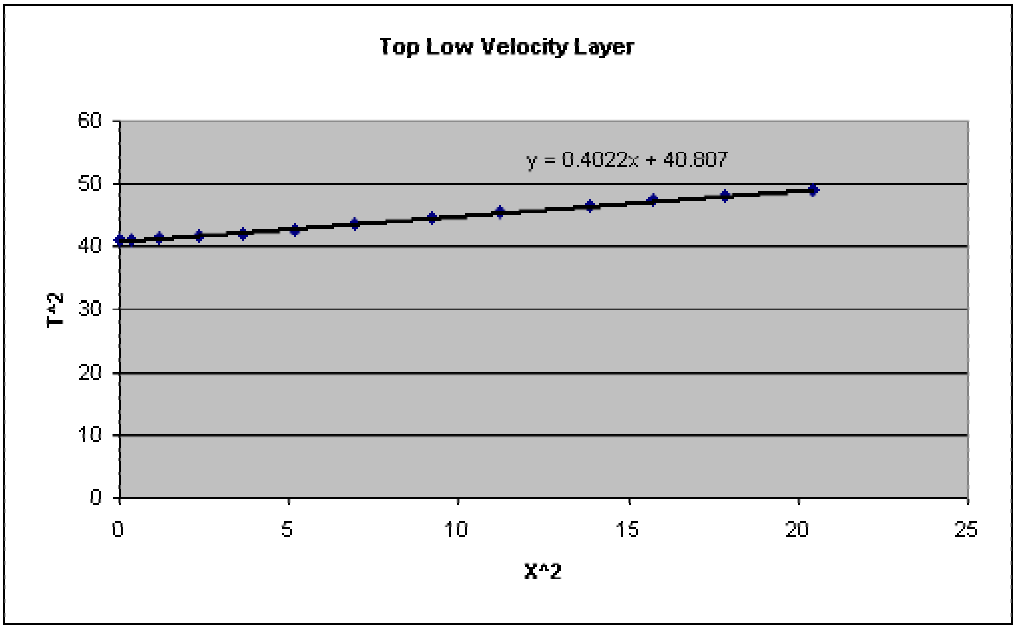

	Vrms5 (km/s)	sqrt(1/slope)	1.58
	t_{05}-reflection (s)		6.388

Distance (m)	**Top sill (s)**	**X^2**	**T^2**
0.038	6.557	0.001444	42.994249
0.457	6.564	0.208849	43.086096

0.697	6.568	0.485809	43.138624
1.177	6.583	1.385329	43.335889
1.507	6.611	2.271049	43.705321
1.792	6.634	3.211264	44.009956
2.114	6.67	4.468996	44.4889
2.459	6.712	6.046681	45.050944
2.759	6.75	7.612081	45.5625
3.058	6.809	9.351364	46.362481
3.358	6.858	11.276164	47.032164
3.628	6.912	13.162384	47.775744
3.92	6.967	15.3664	48.539089
4.183	7.016	17.497489	49.224256
4.385	7.07	19.228225	49.9849
4.73	7.138	22.3729	50.951044
4.977	7.197	24.770529	51.796809

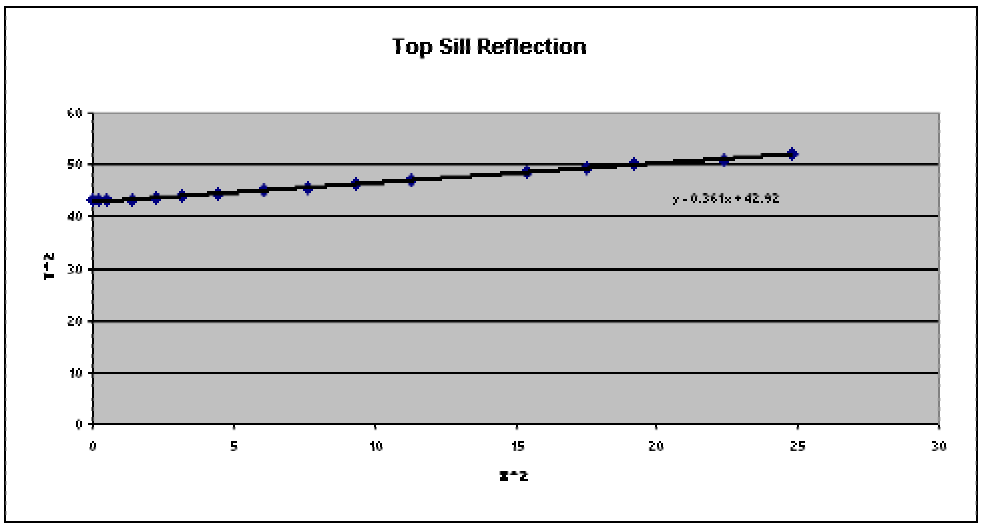

	Vrms6 (km/s)	sqrt(1/slope)	1.663
	t_{06}-reflection (s)		6.551

Distance (m)	**Top sed2 (s)**	**X^2**	**T^2**
0.03	6.592	0.0009	43.454464

0.54	6.601	0.2916	43.573201
0.945	6.613	0.893025	43.731769
1.327	6.639	1.760929	44.076321
1.672	6.665	2.795584	44.422225
2.009	6.693	4.036081	44.796249
2.346	6.726	5.503716	45.239076
2.646	6.771	7.001316	45.846441
3.006	6.835	9.036036	46.717225
3.291	6.882	10.830681	47.361924
3.621	6.938	13.111641	48.135844
3.898	6.992	15.194404	48.888064
4.213	7.056	17.749369	49.787136
4.483	7.12	20.097289	50.6944
4.797	7.176	23.011209	51.494976
5.015	7.24	25.150225	52.4176
5.307	7.31	28.164249	53.4361

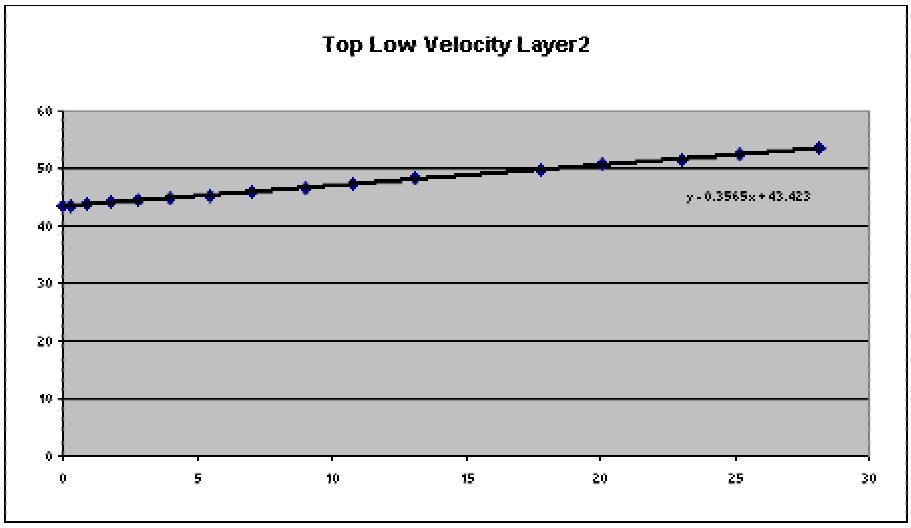

	Vrms7 (km/s)	sqrt(1/slope)	1.674
	t_{07}-reflection (s)		6.59

Distance (m)	**Top oceanic crust (s)**	**X^2**	**T^2**

0.022	6.844	0.000484	46.840336
0.322	6.846	0.103684	46.867716
0.6	6.856	0.36	47.004736
0.847	6.856	0.717409	47.004736
1.222	6.865	1.493284	47.128225
1.544	6.889	2.383936	47.458321
1.836	6.907	3.370896	47.706649
2.144	6.931	4.596736	48.038761
2.376	6.95	5.645376	48.3025
2.668	6.976	7.118224	48.664576
2.931	7.002	8.590761	49.028004
3.193	7.042	10.195249	49.589764
3.455	7.084	11.937025	50.183056
3.643	7.124	13.271449	50.751376
3.905	7.174	15.249025	51.466276
4.197	7.228	17.614809	52.243984
4.422	7.265	19.554084	52.780225

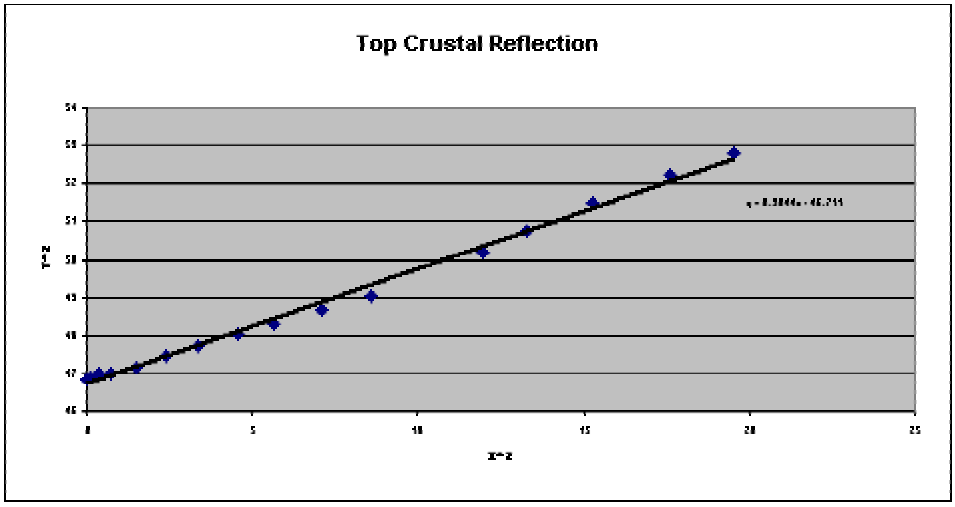

Vrms8 (km/s)	sqrt(1/slope)	1.815
t_{08}-reflection (s)		6.834

Distant (m)	Sill refraction (s)	X^2	T^2
8.215	7.696	67.486225	59.228416
8.523	7.748	72.641529	60.031504
8.763	7.795	76.790169	60.762025
9.047	7.842	81.848209	61.496964
9.28	7.887	86.1184	62.204769
9.58	7.927	91.7764	62.837329
9.879	7.993	97.594641	63.888049
10.179	8.04	103.612041	64.6416
10.442	8.087	109.035364	65.399569
10.719	8.134	114.896961	66.161956
10.951	8.177	119.924401	66.863329
11.244	8.224	126.427536	67.634176
11.483	8.262	131.859289	68.260644
11.716	8.302	137.264656	68.923204
11.986	8.342	143.664196	69.588964

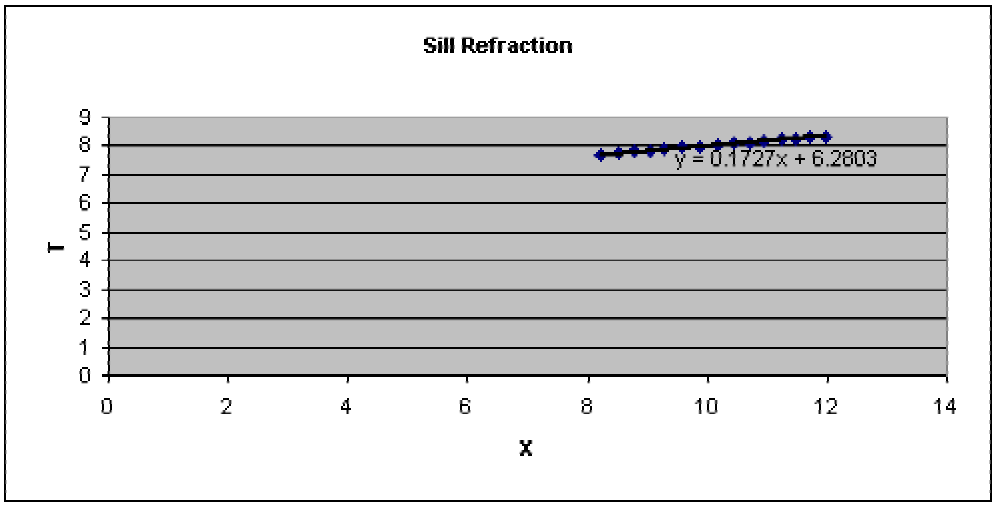

V (km/s) 1/slope 5.7903

Distance (m)	Crustal Refraction	X^2	T^2
8.583	7.913	73.667889	62.615569
8.916	7.964	79.495056	63.425296
9.176	8.007	84.198976	64.112049
9.472	8.05	89.718784	64.8025
9.759	8.104	95.238081	65.674816
10.064	8.155	101.284096	66.504025
10.398	8.207	108.118404	67.354849
10.777	8.268	116.143729	68.359824
11.083	8.317	122.832889	69.172489
11.435	8.373	130.759225	70.107129
11.74	8.425	137.8276	70.980625
12.092	8.478	146.216464	71.876484
12.444	8.527	154.853136	72.709729
12.907	8.6	166.590649	73.96
13.333	8.672	177.768889	75.203584
13.759	8.742	189.310081	76.422564
14.074	8.801	198.077476	77.457601

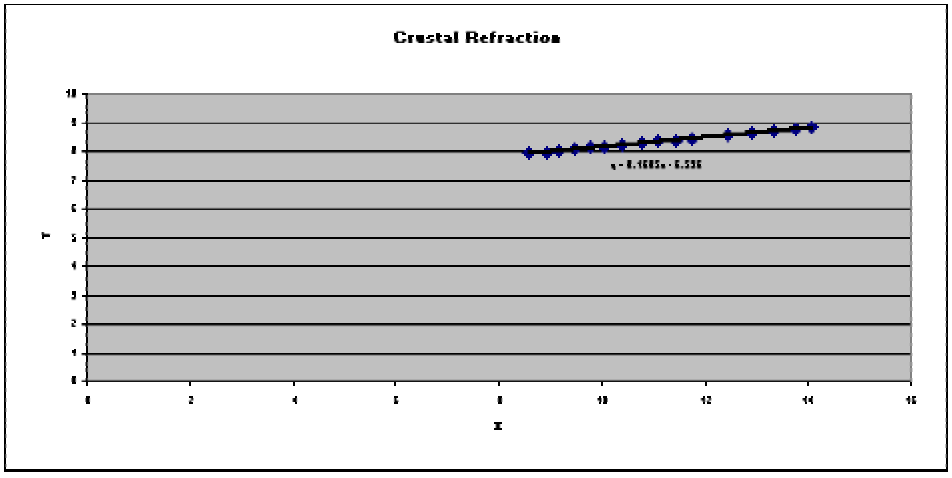

V (km/s)	1/slope	6.2305

Use Dix Equation with Vrms and t0n to calculate Interval Velocity (Vint)

	t_{0n}-reflection (s)	Vrms (km/s)
n=1	5.888	1.548
n=2	5.996	1.55
n=3	6.182	1.584
n=4	6.28	1.575
n=5	6.388	1.58
n=6	6.551	1.663
n=7	6.59	1.674
n=8	6.834	1.815

Thickness=	$h_n = ((t_0 - t_{0n-1})/2) * V_{int-n}$	h_n	Vint (km/s)
	h_0 (km)	4.534	1.54
	h_1 (km)	0.0896	1.66
	h_2 (km)	0.217	2.33
	h_3 (km)	0.0627	1.8
	h_4 (km)	0.1	1.85
	h_5 (km)	0.298	3.65
	h_6 (km)	0.111	5.709
	h_7 (km)	0.497	4.07
	h_8 (km)		6.2305-

Sonobuoy 5 Data

Distance from shot (m)	Seafloor reflection (s)	X^2	T^2
0.054	5.871	0.002916	34.468641
0.522	5.88	0.272484	34.5744
1.043	5.911	1.087849	34.939921
1.619	5.965	2.621161	35.581225
2.212	6.056	4.892944	36.675136
2.725	6.15	7.425625	37.8225
3.183	6.247	10.131489	39.025009
3.606	6.353	13.003236	40.360609
4.047	6.453	16.378209	41.641209
4.388	6.553	19.254544	42.941809
4.793	6.68	22.972849	44.6224
5.261	6.84	27.678121	46.7856
5.611	6.974	31.483321	48.636676
5.98	7.107	35.7604	50.509449

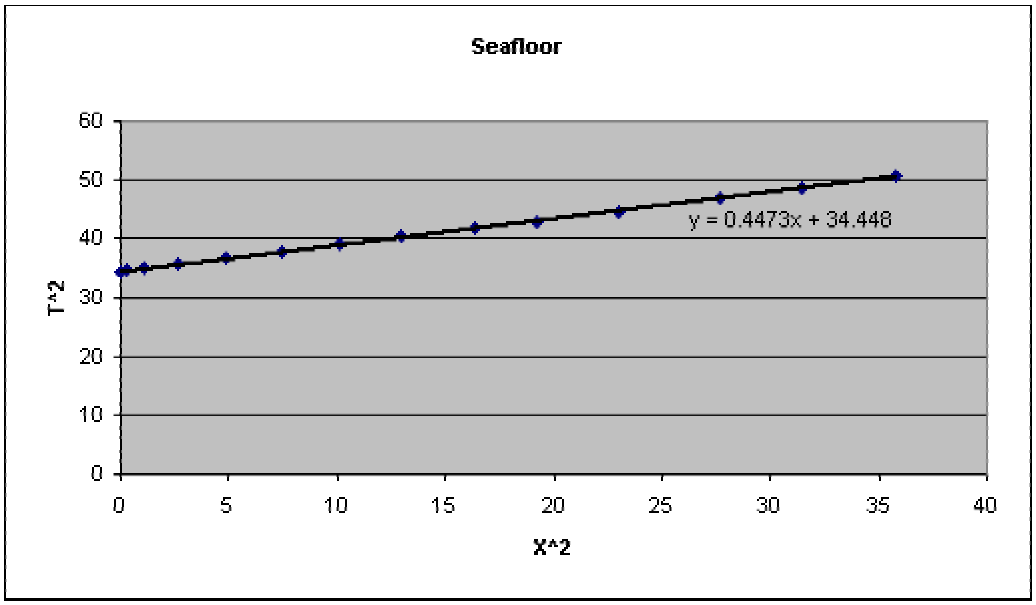

Vrms1 (km/s)	sqrt(1/slope)	1.495
t_{01}-reflection (s)		5.873

Distance from shot (m)	Top eM reflection (s)	X^2	T^2
0.072	6.038	0.005184	36.457444
0.45	6.038	0.2025	36.457444
0.935	6.065	0.874225	36.784225
1.583	6.119	2.505889	37.442161
2.176	6.194	4.734976	38.365636
2.842	6.313	8.076964	39.853969
3.399	6.442	11.553201	41.499364
3.759	6.528	14.130081	42.614784
4.101	6.631	16.818201	43.970161
4.478	6.738	20.052484	45.400644
4.802	6.819	23.059204	46.498761
5.126	6.943	26.275876	48.205249
5.413	7.029	29.300569	49.406841
5.701	7.126	32.501401	50.779876

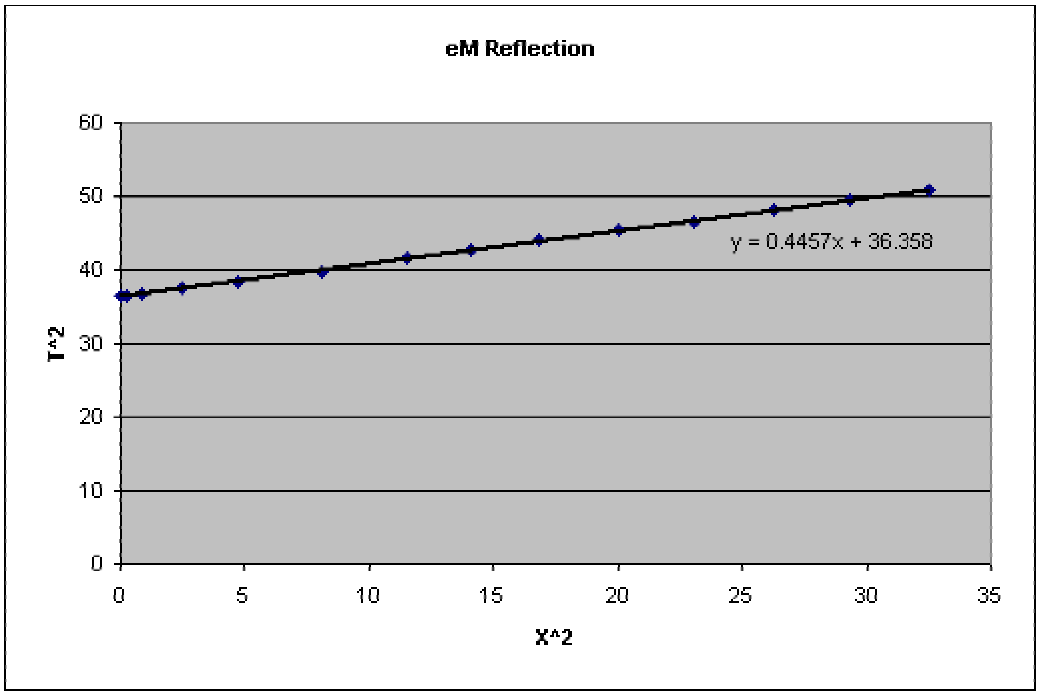

Vrms2 (km/s)	sqrt(1/slope)	1.499
t_{02}-reflection (s)		6.03

Distance from source (m)	Top mE reflection (s)	X^2	T^2
0.108	6.189	0.011664	38.303721
0.683	6.2	0.466489	38.44
1.097	6.238	1.203409	38.912644
1.619	6.281	2.621161	39.450961
2.014	6.351	4.056196	40.335201
2.554	6.437	6.522916	41.434969
3.021	6.496	9.126441	42.198016
3.561	6.625	12.680721	43.890625
3.993	6.722	15.944049	45.185284
4.388	6.808	19.254544	46.348864
4.694	6.916	22.033636	47.831056

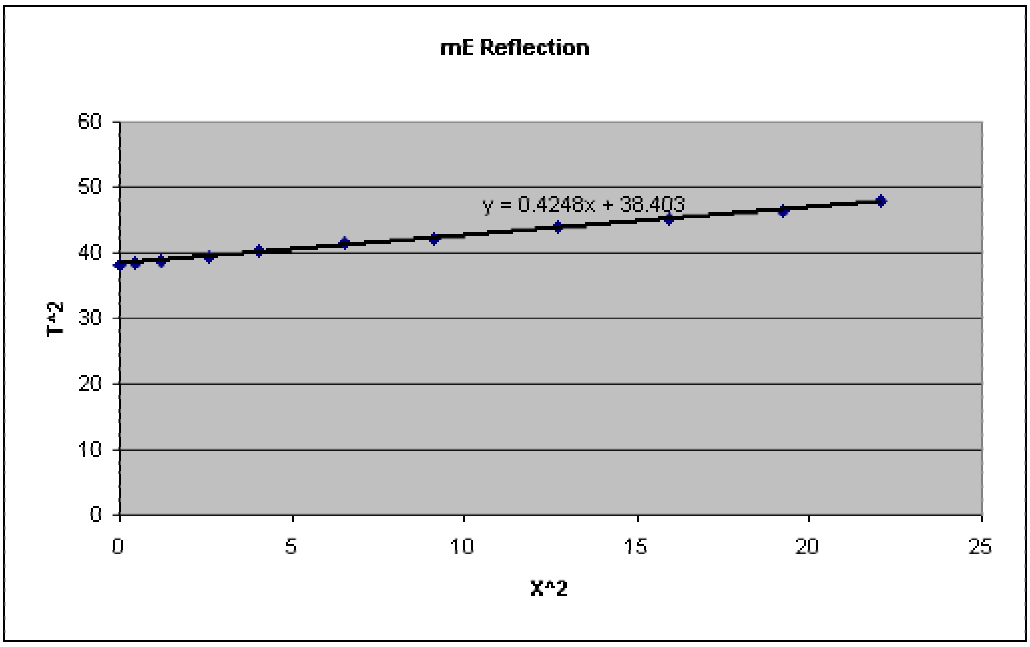

Vrms (km/s)	1.534
t_{03}-reflection (s)	6.19

Distance from source (m)	Top K reflection (s)	X^2	T^2
0.036	6.329	0.001296	40.056241
0.378	6.334	0.142884	40.119556
0.827	6.356	0.683929	40.398736
1.259	6.394	1.585081	40.883236
1.709	6.426	2.920681	41.293476
2.122	6.491	4.502884	42.133081
2.464	6.534	6.071296	42.693156
2.878	6.609	8.282884	43.678881
3.237	6.663	10.478169	44.395569
3.561	6.749	12.680721	45.549001
3.867	6.824	14.953689	46.566976

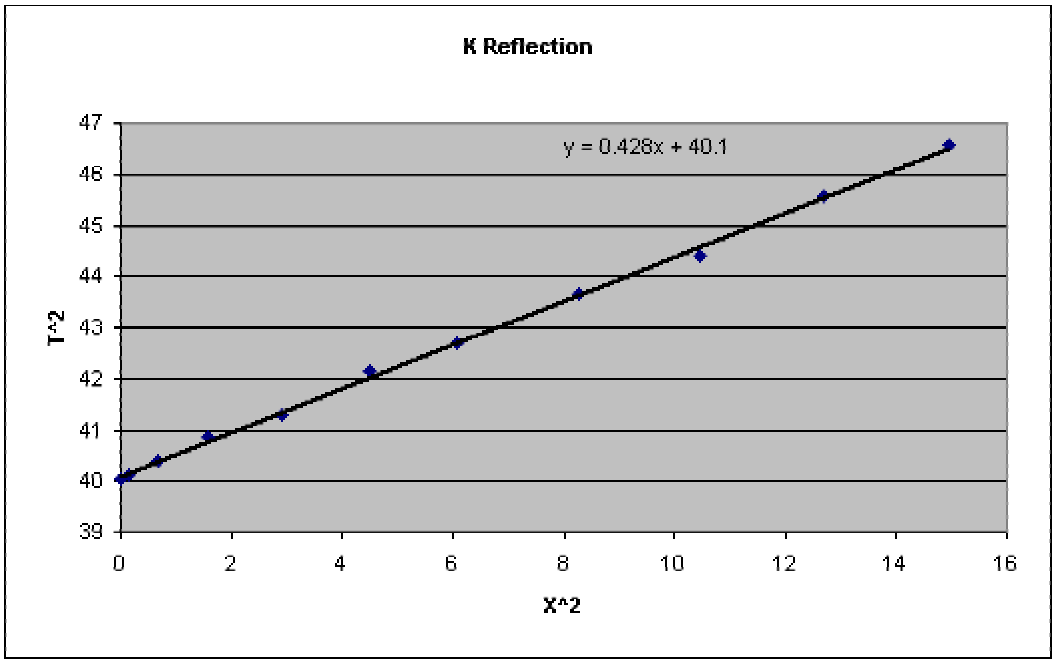

Vrms (km/s)	sqrt(1/slope)	1.538
t_{04}-reflection (s)		6.33

Distance from shot (m)	Top LVsed (s)	X^2	T^2
0.054	6.453	0.002916	41.641209
0.576	6.448	0.331776	41.576704
1.007	6.485	1.014049	42.055225
1.403	6.512	1.968409	42.406144
1.852	6.555	3.429904	42.968025
2.284	6.604	5.216656	43.612816
2.68	6.679	7.1824	44.609041
3.057	6.733	9.345249	45.333289
3.453	6.803	11.923209	46.280809
3.867	6.889	14.953689	47.458321
4.119	6.959	16.966161	48.427681
4.496	7.04	20.214016	49.5616
4.82	7.126	23.2324	50.779876

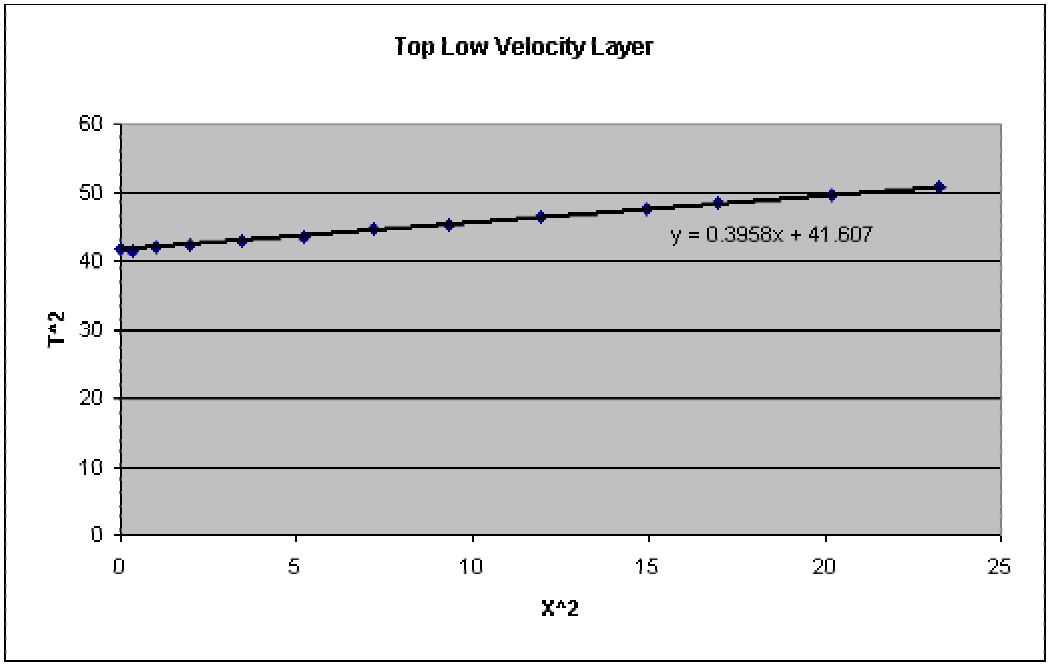

Vrms5 (km/s)	sqrt(1/slope)	1.59
t_{05}-reflection (s)		6.45

Distance from shot (m)	Top sill (s)	X^2	T^2
0.018	6.604	0.000324	43.612816
0.441	6.607	0.194481	43.652449
0.962	6.628	0.925444	43.930384
1.295	6.655	1.677025	44.289025
1.79	6.7	3.2041	44.89
2.365	6.773	5.593225	45.873529
2.743	6.825	7.524049	46.580625
3.237	6.925	10.478169	47.955625
3.624	7	13.133376	49
4.029	7.076	16.232841	50.069776
4.487	7.173	20.133169	51.451929
5.009	7.288	25.090081	53.114944

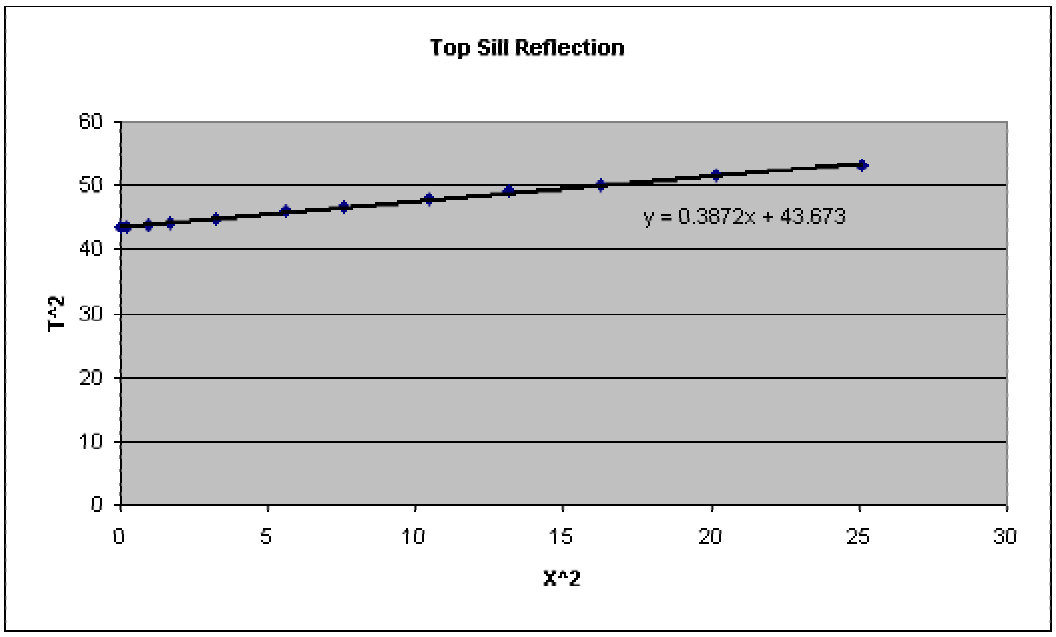

Vrms6 (km/s)	sqrt(1/slope)	1.607
t_{06}-reflection (s)		6.609
Vint6 (km/s)		5.189

Distance from shot (m)	Top sed2 (s)	X^2	T^2
0.036	6.652	0.001296	44.249104
0.414	6.655	0.171396	44.289025
0.81	6.682	0.6561	44.649124
1.295	6.719	1.677025	45.144961
1.736	6.755	3.013696	45.630025
2.14	6.806	4.5796	46.321636
2.518	6.858	6.340324	47.032164
2.896	6.912	8.386816	47.775744
3.237	6.967	10.478169	48.539089
3.543	7.04	12.552849	49.5616
3.813	7.082	14.538969	50.154724
4.02	7.137	16.1604	50.936769
4.361	7.209	19.018321	51.969681

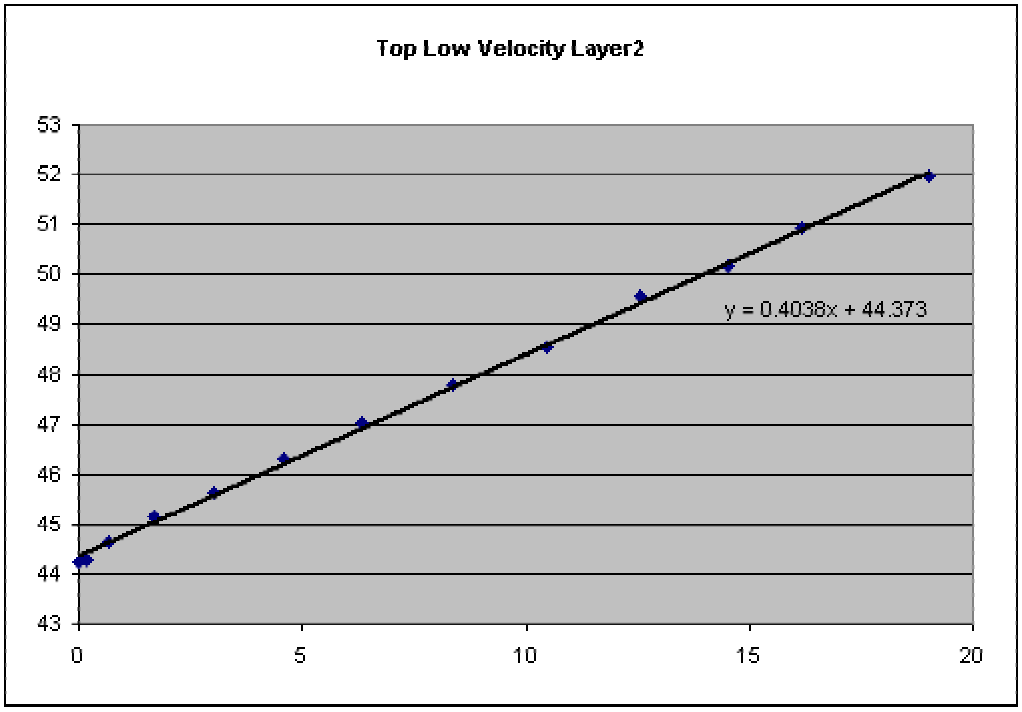

Vrms7 (km/s)	1.574
t_{07}-reflection (s)	6.661

Distance from shot (m)	Top oceanic crust (s)	X^2	T^2
0.054	6.884	0.002916	47.389456
0.719	6.9	0.516961	47.61
1.349	6.932	1.819801	48.052624
1.852	6.964	3.429904	48.497296
2.446	7.029	5.982916	49.406841
2.932	7.083	8.596624	50.168889
3.417	7.158	11.675889	51.236964
3.759	7.217	14.130081	52.085089
4.262	7.298	18.164644	53.260804

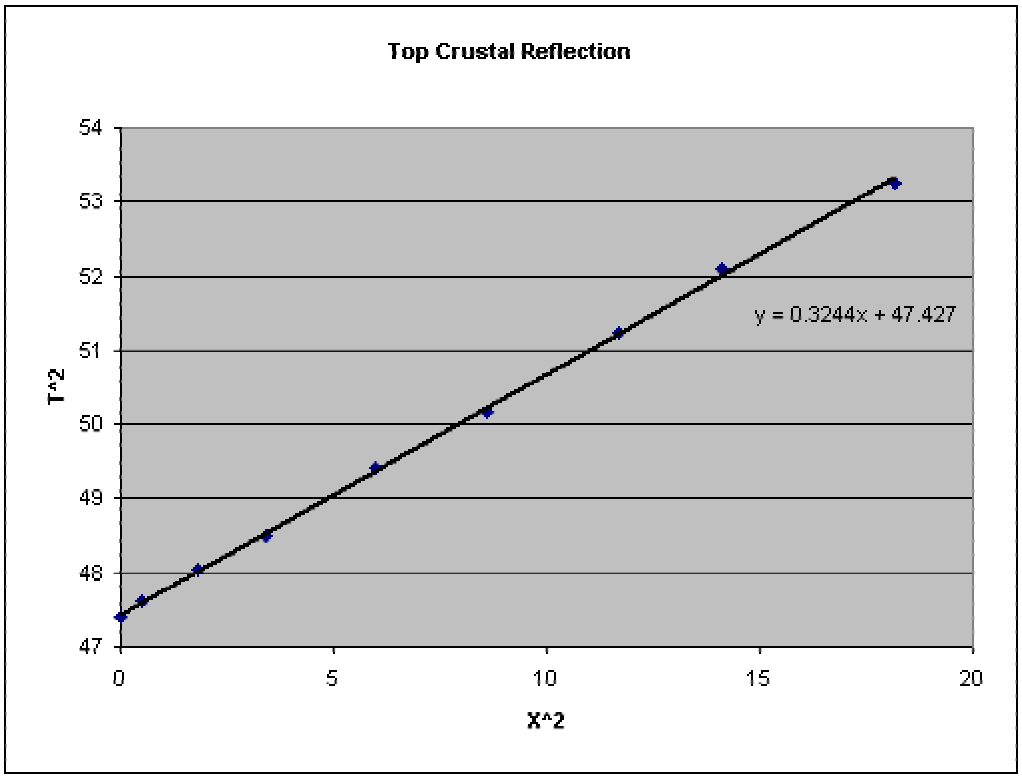

Vrms8 (km/s)	sqrt(1/slope)	1.76
t_{08}-reflection (s)		6.887

Distant from shot (m)	Sill refraction (s)	X^2	T^2
8.831	8.015	77.986561	64.240225
9.056	8.057	82.011136	64.915249
9.227	8.099	85.137529	65.593801
9.55	8.154	91.2025	66.487716
9.784	8.205	95.726656	67.322025
9.973	8.242	99.460729	67.930564
10.324	8.299	106.584976	68.873401

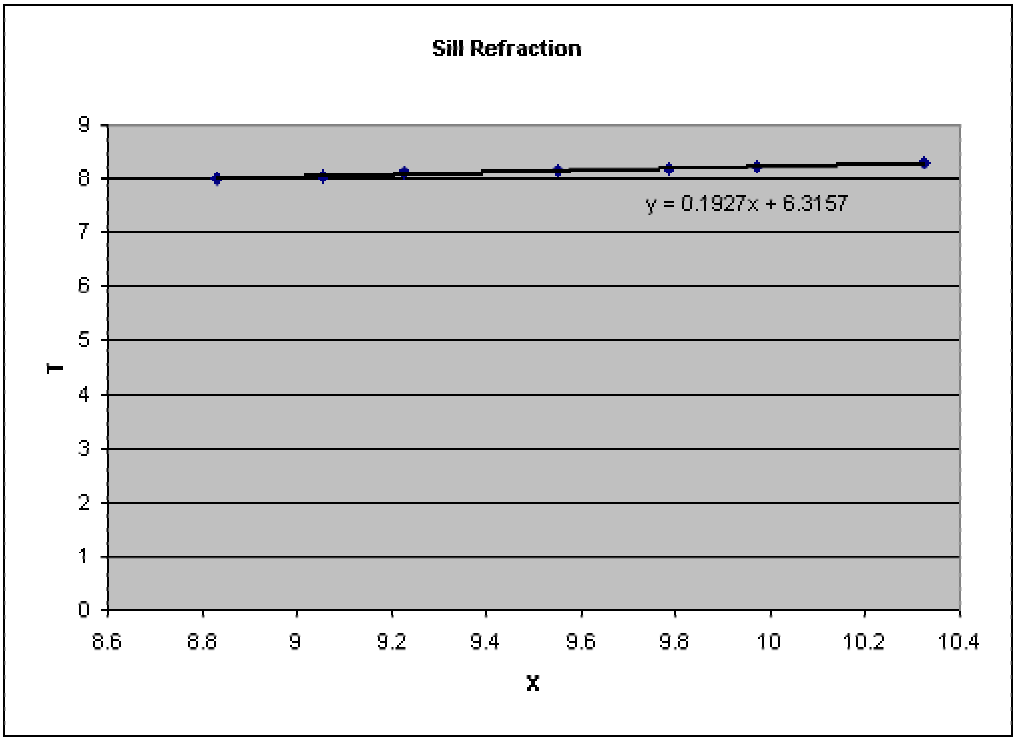

V (km/s) 1/slope 5.189

Distance from shot (m)	Crustal Refraction	X^2	T^2
9.127	8.251	83.302129	68.079001
9.415	8.302	88.642225	68.923204
9.703	8.357	94.148209	69.839449
9.928	8.402	98.565184	70.593604
10.189	8.442	103.815721	71.267364
10.341	8.478	106.936281	71.876484

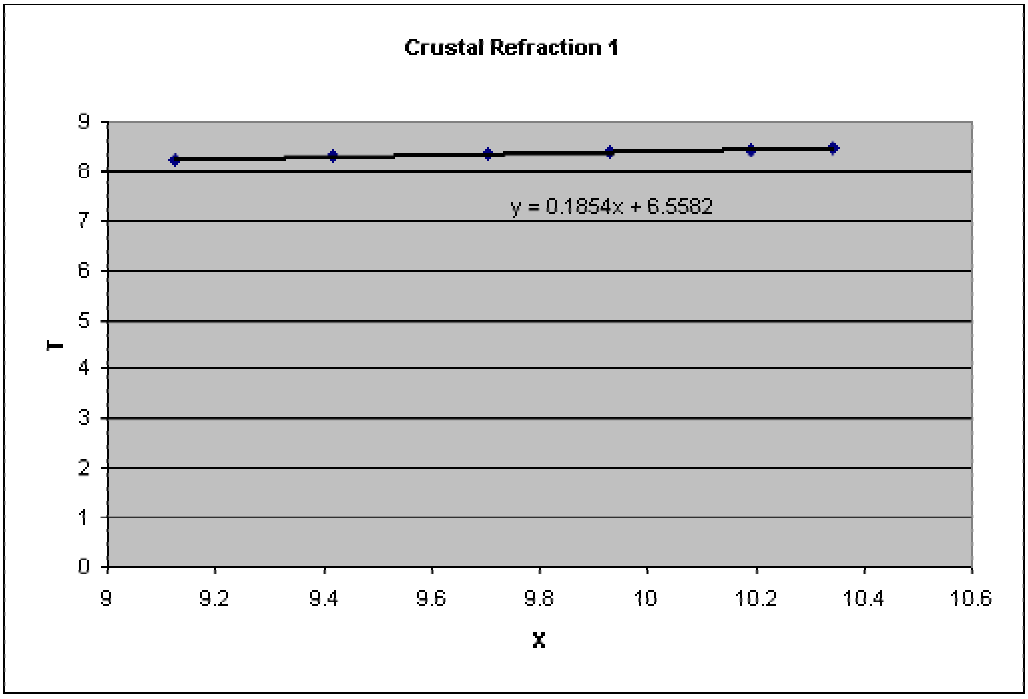

V (km/s) 1/slope 5.394

Use Dix Equation with Vrms and t_{0n} to calculate Interval Velocity (Vint)

	t_{0n}-reflection (s)	Vrms (km/s)	
	n=1	5.873	1.495
	n=2	6.032	1.499
	n=3	6.169	1.483
	n=4	6.317	1.498
	n=5	6.448	1.572
	n=6	6.609	1.607
	n=7	6.661	1.574
	n=8	6.887	1.589
Thickness=	$h_n = ((t_0 - t_{0n-1})/2) * V_{int-n}$	h_n (km)	Vint (km/s)
	h_0 (km)	4.39	1.495
	h_1 (km)	0.129	1.62
	h_2 (km)	0.034	1.60
	h_3 (km)	0.15	2.027
	h_4 (km)	0.21	3.207
	h_5 (km)	0.427	2.65
	h_6 (km)	0.135	5.189
	h_7 (km)	0.224	1.98
	h_8 (km)		5.394-

Sonobuoy 2 Data

Distance from shot (m)	Seafloor reflection (s)	X^2	T^2
0.128	5.942	0.016384	35.307364
0.62	5.948	0.3844	35.378704
1.134	5.985	1.285956	35.820225
1.732	6.045	2.999824	36.542025
2.267	6.112	5.139289	37.356544
2.716	6.203	7.376656	38.477209
3.208	6.312	10.291264	39.841344
3.743	6.433	14.010049	41.383489
4.235	6.566	17.935225	43.112356
4.77	6.723	22.7529	45.198729
5.219	6.863	27.237961	47.100769
5.689	7.026	32.364721	49.364676

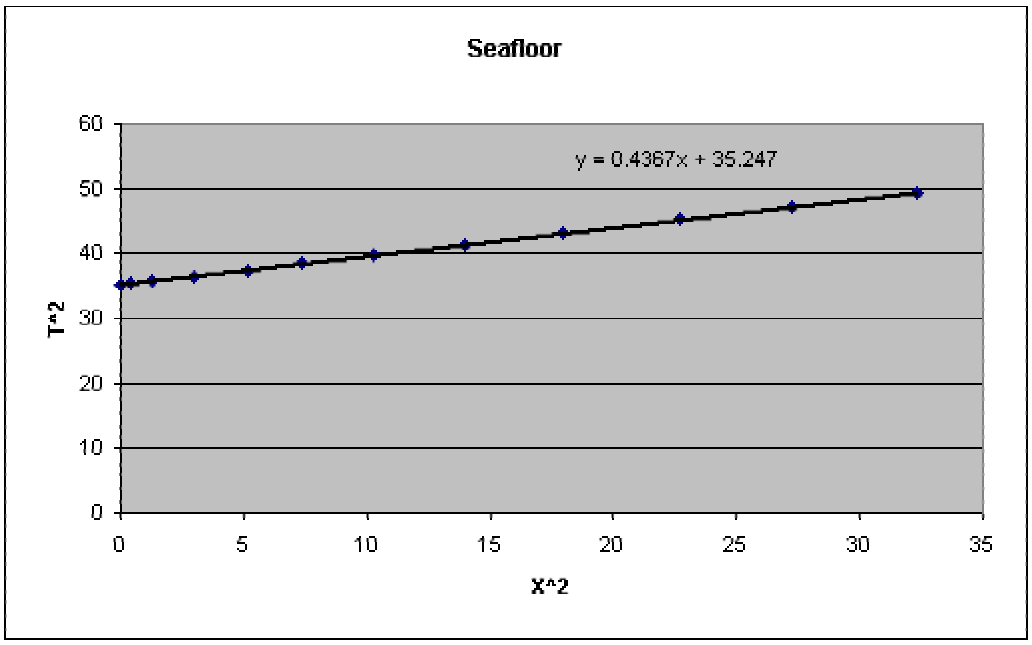

Vrms1 (km/s)	1.513
t_{01}-reflection (s)	5.934

Distance from shot (m)	Top mM reflection (s)	X^2	T^2
0.107	6.112	0.011449	37.356544
0.642	6.124	0.412164	37.503376
1.176	6.16	1.382976	37.9456
1.668	6.203	2.782224	38.477209
2.182	6.275	4.761124	39.375625
2.781	6.372	7.733961	40.602384
3.358	6.475	11.276164	41.925625
3.936	6.608	15.492096	43.665664
4.449	6.748	19.793601	45.535504
4.941	6.887	24.413481	47.430769
5.283	7.002	27.910089	49.028004

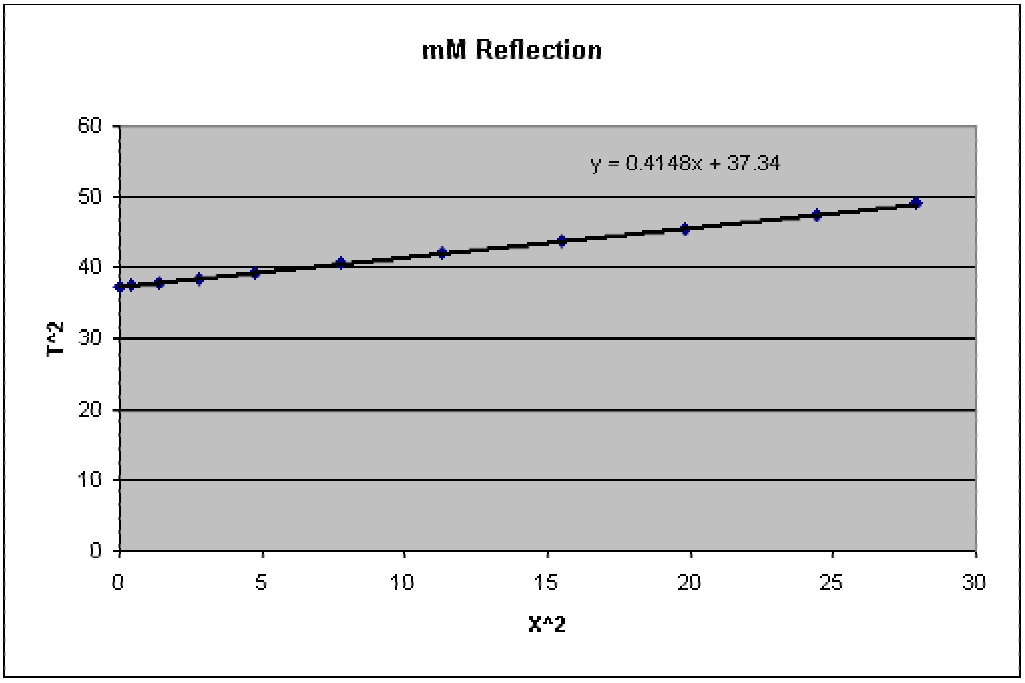

Vrms2 (km/s)	1.553
t_{02}-reflection (s)	6.112

Distance from source (m)	Top crust reflection (s)	X^2	T^2
0.045	6.588	0.002025	43.401744
0.6	6.612	0.36	43.718544
1.139	6.64	1.297321	44.0896
1.724	6.682	2.972176	44.649124
2.204	6.729	4.857616	45.279441
2.773	6.814	7.689529	46.430596
3.268	6.894	10.679824	47.527236
3.733	6.974	13.935289	48.636676
4.123	7.073	16.999129	50.027329
4.617	7.182	21.316689	51.581124
4.917	7.262	24.176889	52.736644
5.157	7.342	26.594649	53.904964

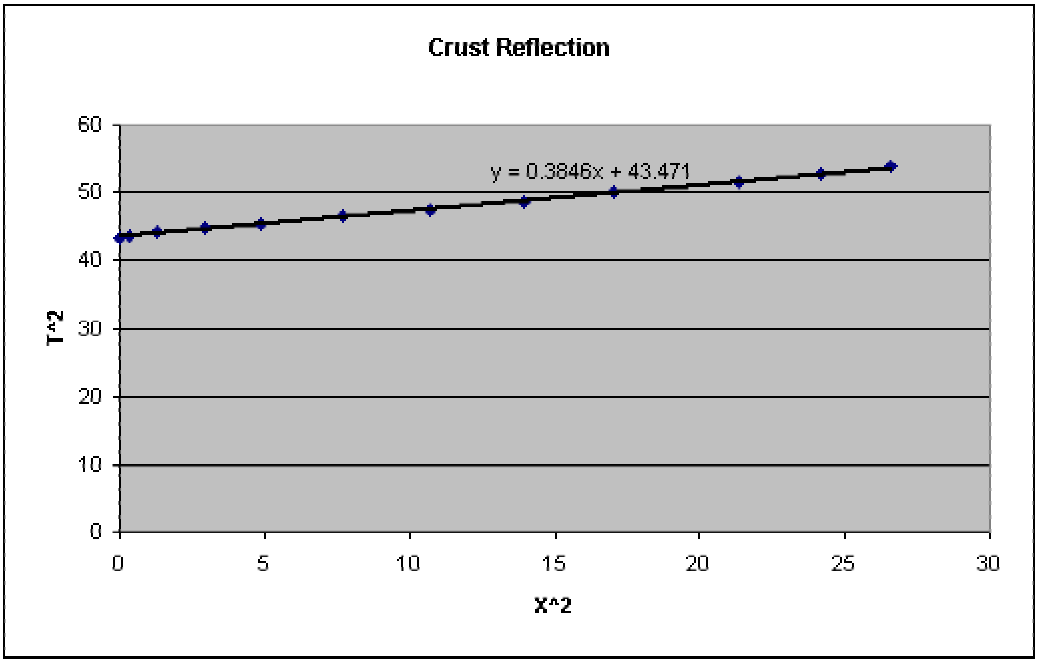

Vrms (km/s)	1.613
t_{03}-reflection (s)	6.593

Distant from shot (m)	Crustal refraction (s)	X^2	T^2
8.889	8.081	79.014321	65.302561
9.199	8.134	84.621601	66.161956
9.552	8.187	91.240704	67.026969
9.905	8.254	98.109025	68.128516
10.272	8.32	105.513984	69.2224
10.653	8.387	113.486409	70.341769
11.062	8.449	122.367844	71.385601
11.414	8.494	130.279396	72.148036
11.753	8.543	138.133009	72.982849

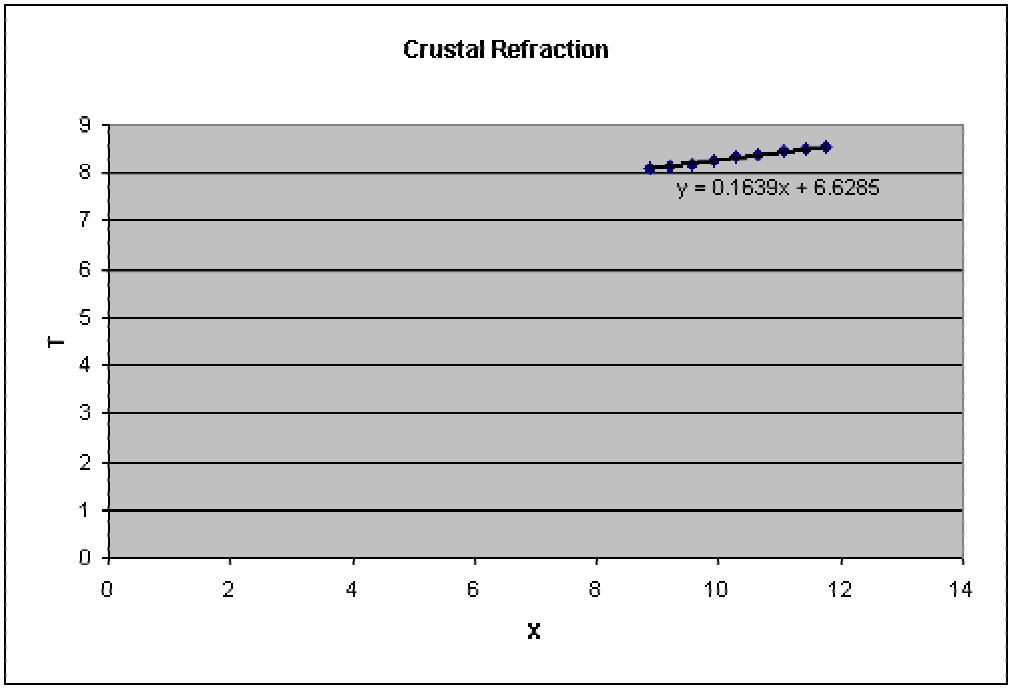

V (km/s) 6.101

Use Dix Equation with Vrms and t0n to calculate Interval Velocity (Vint)

	t_{0n}-reflection (s)	Vrms (km/s)	Vint (km/s)
n=1	5.934	1.513	2.553
n=2	6.112	1.553	2.247
n=3	6.593	1.613	6.101-

Thickness=	$h_n = ((t_0 - t_{0n-1})/2) * V_{int-n}$	h_n	Vint (km/s)
	h_0 (km)	4.489	1.513
	h_1 (km)	0.227	2.553
	h_2 (km)	1.081	2.247
	h_3 (km)		6.101-